UNIVERSIDADE ESTADUAL DE CAMPINAS
FACULDADE DE ENGENHARIA MECÂNICA
E INSTITUTO DE GEOCIÊNCIAS

RICARDO DANTAS GADELHA DE FREITAS FILHO

DISSOLUTION OF CARBONATE ROCKS IN HIGH PRESSURE CO_2/BRINE SYSTEMS: EFFECTS ON POROSITY AND PERMEABILITY

DISSOLUÇÃO DE ROCHAS CARBONÁTICAS EM SISTEMAS DE CO_2/SALMOURA EM ALTA PRESSÃO: EFEITOS NA POROSIDADE E PERMEABILIDADE

CAMPINAS
2017

RICARDO DANTAS GADELHA DE FREITAS FILHO

DISSOLUTION OF CARBONATE ROCKS IN HIGH PRESSURE CO_2/BRINE SYSTEMS: EFFECTS ON POROSITY AND PERMEABILITY

DISSOLUÇÃO DE ROCHAS CARBONÁTICAS EM SISTEMAS DE CO_2/SALMOURA EM ALTA PRESSÃO: EFEITOS NA POROSIDADE E PERMEABILIDADE

Dissertation presented to the Mechanical Engineering Faculty and Geosciences Institute of the University of Campinas in partial fulfillment of the requirements for the degree of Master in Petroleum Sciences and Engineering in the area of Exploitation/Reservoirs and Management.

Dissertação apresentada à Faculdade de Engenharia Mecânica e Instituto de Geociências da Universidade Estadual de Campinas como parte dos requisitos exigidos para a obtenção do título de Mestre em Ciências e Engenharia de Petróleo na área de Reservatórios e Gestão.

Orientador: Prof. Dr. Osvair Vidal Trevisan

Este exemplar corresponde à versão final da Dissertação defendida pelo aluno Ricardo Dantas Gadelha de Freitas Filho e orientada pelo Prof. Dr. Osvair Vidal Trevisan.

_____

Assinatura do Orientador

CAMPINAS

2017

Agência(s) de fomento e nº(s) de processo(s): Não se aplica.

Ficha catalográfica
Universidade Estadual de Campinas
Biblioteca da Área de Engenharia e Arquitetura
Luciana Pietrosanto Milla - CRB 8/8129

F884d

Freitas Filho, Ricardo Dantas Gadelha, 1989-
Dissolution of carbonate rocks in high pressure CO2/brine systems : effects on porosity and permeability / Ricardo Dantas Gadelha de Freitas Filho. – Campinas, SP : [s.n.], 2017.

Orientador: Osvair Vidal Trevisan.
Dissertação (mestrado) – Universidade Estadual de Campinas, Faculdade de Engenharia Mecânica.

1. Dissolução. 2. Dióxido de carbono. 3. Rochas carbonáticas. 4. Permeabilidade. 5. Porosidade. I. Trevisan, Osvair Vidal,1952-. II. Universidade Estadual de Campinas. Faculdade de Engenharia Mecânica. III. Título.

Informações para Biblioteca Digital

Título em outro idioma: Dissolução de rochas carbonáticas em sistemas de CO2/salmoura em alta pressão : efeitos na porosidade e permeabilidade
Palavras-chave em inglês:
Dissolution
Carbon dioxide
Carbonate rocks
Permeability
Porosity
Área de concentração: Reservatórios e Gestão
Titulação: Mestre em Ciências e Engenharia de Petróleo
Banca examinadora:
Osvair Vidal Trevisan [Orientador]
Rosângela Barros Zanoni Lopes Moreno
Denis José Schiozer
Leonardo José do Nascimento Guimarães
Data de defesa: 18-08-2017
Programa de Pós-Graduação: Ciências e Engenharia de Petróleo

UNIVERSIDADE ESTADUAL DE CAMPINAS
FACULDADE DE ENGENHARIA MECÂNICA
E INSTITUTO DE GEOCIÊNCIAS

DISSERTAÇÃO DE MESTRADO ACADÊMICO

DISSOLUTION OF CARBONATE ROCKS IN HIGH PRESSURE CO_2/BRINE SYSTEMS: EFFECTS ON POROSITY AND PERMEABILITY

Autor: Ricardo Dantas Gadelha de Freitas Filho
Orientador: Prof. Dr. Osvair Vidal Trevisan

A Banca Examinadora composta pelos membros abaixo aprovou esta Dissertação:

Prof. Dr. Denis José Schiozer
FEM / UNICAMP

Profa. Dra. Rosângela Barros Zanoni Lopes Moreno
FEM / UNICAMP

Prof. Dr. Leonardo José do Nascimento Guimarães
UFPE / Recife

A Ata da defesa com as respectivas assinaturas dos membros encontra-se no processo de vida acadêmica do aluno.

Campinas, 18 de agosto de 2017.

To Fernanda and Maria Cecília, with my deepest love.

ACKNOWLEDGEMENTS

It is been quite a journey writing this dissertation and throughout its ups and down many people helped me and deserve to be acknowledged. Family, Friends and Colleagues that have helped me during these hard years I would like to thank you all.

Specially, I thank first my mother Adriana and my father Ricardo for bringing me to this world, raising me and giving me the strength when I was lacking.

Prof. Dr. Osvair Vidal Trevisan, I thank you for the discussions and guidance during this process. I am grateful for Dr. Ronaldo Gonçalves dos Santos, Dra. Erika Tomie Koroishi Blini, Dr. Eddy Ruidiaz Muñoz, Dr. Nilo Ricardo Kim and Washington Carlton Botine for the help with the planning and execution of the experiments presented in this work.

I would also like to thank all of the team in the Laboratory of Miscible Recovery Methods at Cepetro – UNICAMP. More specifically I thank the COIN team for giving me the motivation I needed to finish this text.

I thank my friend Fernando for all his help during this final step.

Finally, I acknowledge Repsol Sinopec Brasil for the funding of this work though the project "Study of phase behavior petroleum/CO_2 and molecular diffusion of CO_2 in carbonate rocks", which is greatly appreciated.

.

RESUMO

Descobertas recentes no pré-sal brasileiro revelaram quantidades significativas de petróleo associadas a grandes quantidades de CO_2 em reservatórios carbonáticos. O CO_2 produzido não pode ser liberado para a atmosfera devido ao efeito estufa. Injeção de Água Alternada com Gás CO_2 é um método conhecido de Recuperação Melhorada de Petróleo utilizado para aumentar a recuperação de campos de óleo e pode ser aplicado nos campos do pré-sal. O CO_2 injetado pode interagir com os fluidos no reservatório e mudar as propriedades da rocha carbonática. Quando o CO_2 dissolve na água, forma o ácido carbonico, causando a dissolução dos minerais carbonáticos na rocha (principalmente calcita e dolomita). Isto pode causar mudanças nas propriedades de escoamento na rocha, principalmente a porosidade e permeabilidade, e o seu impacto não foi quantificado nas condições do pré-sal brasiliero (9.000 psi e 64^{o}C). Tendo isso em mente, este trabalho experimental tem como objetivo principal o de avaliar como a porosidade e permeabilidade de rochas carbonáticas mudam devido à exposição de CO_2 e água em condições próximas às dos reservatórios do pré-sal. Um objetivo secondário também foi definido como o de delinear as melhores práticas para a medição de porosidade e permeabilidade em condições de laboratório. O primeiro objetivo foi alcançado através de dois estudos experimentais em reatores: o primeiro, projetado para avaliar como a permeabilidade e porosidade de amostras de coquina e dolomita varia em sistemas de água fresca/CO_2, com variação de pressão (até 9.000 psi) e temperatura constante; o segundo, para avaliar a variação das mesmas propriedades nas mesmas amostras de rocha, em sistemas de salmoura/CO_2 em alta pressão (9.000 psi), temperatura constante e salmoura de salinidade variável. Foi concluído que a taxa dissolução diminiu com o tempo, aumenta com a pressão e porosidade inicial. Também foi constatado que a taxa de dissolução é inversamente proporcional com a salinidade da salmoura. A taxa de dissolução de coquina é maior que a da dolomita. Foi observado que a despressurização do reator de alta pressão poderia causar diminuições na porosidade e permeabilidade da rocha. O procedimento experimental proposto no segundo estudo experimental diminuiu este efeito. Em geral, quando a taxa de dissolução aumenta, a porosidade e permeabilidade das rochas aumentam também. O segundo objetivo foi alcançado comparando os valores de permeabilidade à gás e líquido medidos em laboratório de amostras de coquina e dolomita, assim como, avaliando medidas de porosidade e permeabilidade à gás de amostras de coquina, dolomita e arenito. Foi visto que, com o aparato experimental utilizado, não foi possível realizar a análise de

Klinkenberg para converter permeabilidade à gás em permeabilidade à liquido. Também foi visto que a diminuição de permeabilidade com o aumento do diferencial de pressão utilizado na medade é mais evidente em rochas carbonáticas e que a permeabilidade média a gás da mesma amostra, medida nas mesmas condições, pode ser utilizada para avaliar a variação da permeabilidade da amostra.

Palavras Chave: Dissolução de Rochas Carbonáticas, Dióxido de Carbono, Rochas Carbonáticas, Permeabilidade, Porosidade, Pré-sal, Alta Pressão.

ABSTRACT

Recent discoveries in brazilian pre-salt fields revealed significant quantities of oil associated with high quantities of CO_2 in carbonate reservoirs. The produced CO_2 may not simply be liberated in the atmosphere due to the Greenhouse Effect. Water alternating Gas (WAG) injection together with CO_2 is a well know Enhanced Oil Recovery (EOR) Method used to increase recovery in oil fields and may be applied in the pre-salt fields. The injected CO_2 will interact with the fluids in the reservoir and change the carbonate rocks properties. When CO_2 dissolves in water, it forms carbonic acid, causing the dissolution reaction of the carbonate minerals in the rock (mainly calcite and dolomite). This will change the rock flow properties, mainly porosity and permeability, and its impact has not been fully quantified in pre-salt conditions (9,000 psi and 64^oC). Therefore, this experimental work has the main objective of evaluating how permeability and porosity of carbonate rocks changes due to exposure of CO_2 and water at conditions close to that of the pre-salt reservoirs. A secondary objective was also defined as to delineate the best practices for measuring porosity and permeability in laboratory conditions. The first objective was achieved by two batch dissolution experimental studies: the first one, designed to evaluate how the permeability and porosity of coquina and dolomite outcrop rocks varies in fresh water/CO_2 systems, with increasing pressure (up to 9,000 psi) at constant temperature (64^oC); and the second, to evaluate the variation of the same properties for the same rock types, in high pressure (9,000 psi) brine/CO_2 systems at constant temperature and varying brine salinity. It was concluded that dissolution rate decreases with time, it increases with the pressure and with initial porosity. Also, dissolution rate is inversely proportional with brine salinity. Coquina's dissolution rate is higher than Dolomite's. It was found that the depressurization of the high pressure vessel could cause decreases in porosity and permeability of the rock. The experimental procedure proposed in the second experimental study decreased this effect. In general, as the dissolution rate increases, the permeability and porosity of the rocks increases as well. The secondary objective was achieved by comparing gas permeability and liquid permeability measured in laboratory of coquina and dolomite rock samples and assessing gas porosity and permeability measurement of coquina, dolomite and sandstone samples. It was found that with the used experimental set-up it was not possible to perform Klinkenberg's analysis to convert gas permeability into liquid permeability. It was also found that the decrease in permeability with increase in measuring pressure differential is more evident in

carbonate rocks and the average gas permeability of the same sample, measured at the same conditions can be used to evaluate the variation of the sample's permeability.

Key Word: Carbonate Rock Dissolution, Carbonate Rocks, Permeability, Porosity, Pre-salt, High Pressure.

LISTA DE ILUSTRAÇÕES

LISTA DE TABELAS

,

SUMÁRIO

1. INTRODUCTION

Recent discoveries in Brazilian pre-salt carbonate reservoirs revealed significant quantities of oil at very high pressure conditions (≈ 9,000 psi). One of the main issues the development of these fields is related to the high proportions of CO_2 present together with the oil, that cannot be released in the atmosphere for environment reasons, mainly the greenhouse gas effect. One alternative to that is the reinjection of the CO_2 together with water in the reservoir, with the added benefit of ensuing an efficient Enhanced Oil Recovery Method (EOR).

In terms of physical displacement and pressure maintenance of the reservoir, CO_2 is a very good candidate to be injected in the reservoir because it has sufficient low viscosity, similar to many organic solvent, and density similar to the oil at reservoir conditions. However, it is important to take into account the interactions of this gas with the liquid phases (oil and water) present in these reservoirs. Specifically, when CO_2 dissolves in water, it forms carbonic acid, decreasing pH and, in the case of carbonate reservoir rocks, it will also cause the dissolution of the calcite present in the rock.

The dissolution of carbonate rocks can cause changes in the rock properties, mainly porosity and permeability, which are the fundamental properties for reservoir studies, and therefore, quantifying these changes is very. The main objective of the present work is to evaluate how permeability and porosity of carbonate rocks changes due to the exposure of CO_2 and water at conditions close to that of the pre-salt reservoirs (9,000 psi and 64^{o}C). A secondary objective was also defined as to delineate the best practices for measuring porosity and permeability in laboratory conditions.

Chapter COMPARISONS OF GAS AND LIQUID PERMEABILITY and REPEATABILITY ASSESSMENT OF GAS PERMEABILITY AND POROSITY MEASUREMENT address the secondary objective. The first is the study of the conversion of gas permeability to liquid of eight samples of coquina and dolomite. Klinkenberg's analysis was performed in measured gas permeability values to obtain a calculated liquid permeability which was compared with measured liquid permeability. The second mentioned chapter was performed to access the repeatability of gas porosity and permeability in coquina, dolomite and sandstone sample.

The main objective of this work was addressed by DISSOLUTION OF CARBONATE ROCKS: EFFECTS OF PRESSURE and DISSOLUTION OF CARBONATE ROCKS: EFFECTS OF SALINITY. Chapter 5 presents an experimental study performed to determine the effects of dissolution carbonate rocks in high pressure fresh water/CO_2 systems. It comprised of ten batch dissolution experiments with coquina and dolomite samples at pressures up to 9,000 psi and fixed temperature at 64^{o}C. Chapter 6 presents another experimental study performed to determine the effects of dissolution of carbonate rocks in high pressure Brine/CO_2 systems. It involved four batch dissolution experiments with coquina and dolomite, at fixed pressure and temperature (9,000 psi and 64^{o}C) and different brine salinity (35,000 ppm and 200,000 ppm).

2. BIBLIOGRAPHICAL REVIEW

This chapter presents a bibliographical review of the main concepts used in the dissertation. The concepts of permeability and porosity will be first discussed together with the methods most used to quantify these properties in the laboratory. In sequence, the current literature on dissolution of carbonate rocks and how it can affect the permeability and porosity of carbonate rocks are reviewed.

2.1. Porosity

Porosity is the measure of the available space in a rock for fluid (gas or liquid) storage. It is defined as the ratio of the void space volume in the rock to the bulk volume of the rock (Amyx et al, 1960). The definition is expressed by

$$\phi = \frac{V_p}{V_t} \tag{2.1}$$

where ϕ is the porosity of the rock, V_p is the pore (void) volume of the rock and V_t is the total (bulk) volume of the rock. It is important to recall that the total volume of the rock (V_t) is the sum of the pore volume of the rock (V_p) with the grain volume of the rock (V_g).

For reservoir studies it is also important to define effective porosity, which is ratio of the interconnected void space of the rock to the bulk of the rock (Amyx et al, 1960). The most valuable for reservoir studies is the effective porosity, because it represents the space occupied by mobile fluids.

2.1.1. Porosity Measurement

To calculate the porosity of a rock it is necessary to measure two of three parameters (total rock volume V_t, the rock grain volume V_g and rock pore volume V_p). The bulk volume can be determined by measuring the dimensions of a uniformly shaped rock sample, or by observing the volume of fluid displaced by the rock, making sure the fluid does not penetrates into the pore space of the rock (e.g. by coating the sample with resin or a similar substance, or by previously saturating the sample with the fluid used for the measurement).

The grain volume is usually calculated from the dry weight of the sample and the sample's grain density. To determine the pore volume, usual methods consider the volume of fluid that is ether extracted from the rock, or inserted into it (Amyx et al, 1960).

In the petroleum industry it is common to use a gas porosimeter, such as the Ultra-Pore 300 from Core Lab Instruments, to measure porosity. This equipment is an industry standard that uses the Boyle's Law method to determine the pore or grain volume from the expansion of a known mass of an inert gas (e.g. nitrogen or helium) into a calibrated sample holder. Figure 2.1 depicts a schematic of the gas porosimeter set to measure grain volume.

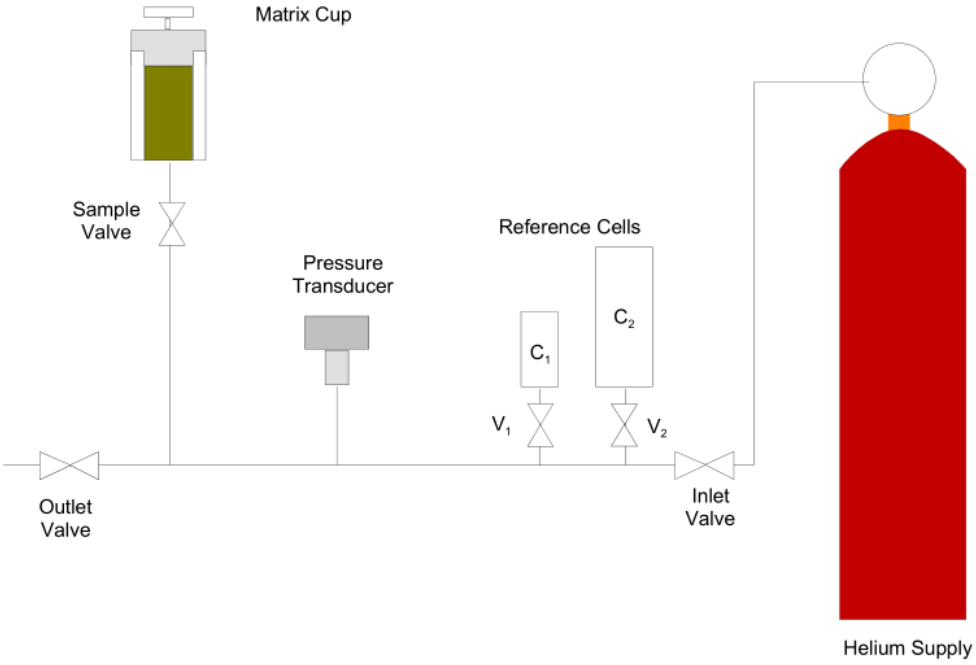

Figure 2.1. Schematic of a gas porosímeter used for grain volume measurements (from the Ultra-Pore 300 operations manual).

The equation used to calculate the grain volume (V_g) is derived from Boyle's Law for a given mass of gas at the same temperature, as:

$$P_1 V_1 = P_2 V_2 \tag{2.2}$$

where, P_1 and V_1 are the initial pressure and volume of the gas and, P_2 and V_2 are the expanded pressure and temperature conditions of the gas.

The Ultra-Pore 300, for example, initially, will pressurize the reference cells, with a total volume of V_{Ref}, by admitting gas into it and recording its pressure value P_1. In the

second step, the equipment will connect the Matrix cup, which has a volume V_{Matrix_Cup}, with the sample already inside of it, to the system, and record the pressure P_2. Therefore:

$$P_1 V_{Ref} = P_2 (V_{Ref} + V_{Matrix\_Cup} - V_g) \quad (2.3a)$$

$$V_g = \left(V_{Matrix\_Cup} + V_{Ref}\right) - \frac{P_1}{P_2} V_{Ref} \quad (2.4b)$$

2.1.2. Precision of Porosity Measurement

The precision of the usual methods employed to measure porosity has been evaluated by Dotson et al (1951). The authors described a core sample porosity-check program where the measurement of ten selected natural and synthetic core samples were performed by a number of laboratories, and each one employed its own method (or methods) of measurement, including Boyle's Law method, water saturation and liquid saturation. They found that the average deviation of porosity from the mean or average values for the group of samples was ±0.5 porosity per cent with the exception of a friable, high-permeability, sandstone sample, for which the deviating from the mean porosity value was ±1.0 porosity per cent.

Another interesting finding of this study was that in general, the gas methods gave slightly higher values, on the average, than liquid saturation methods. This may be partially due to the presence of adsorbed gases in the Boyle's Law Method or to lack of complete saturation of the samples in the liquid saturation methods, or a combination of both (Dotson et al, 1951). Bustin et al (2008) also identified that the porosity value can vary depending on the gas used (helium, methane, argon…), being Helium the one with the lowest adsorption of those presented. Argon and Methane can significantly adsorb on the pore wall resulting in an overestimation of the grain density and therefore has to be corrected by integrating the pore wall adsorption.

Although accurate core porosity measurements are important in all rock types, this accuracy becomes critical in low porosity rocks such as thigh gas sands and source rocks. The growing concern that the current routine core analysis may not be sufficiently reliable in low porosities motivated the works of Luffel and Howard (1987) and Bihan et al (2014) to investigate the porosity measurement of low porosity rocks.

Luffel and Howard (1987) performed a quality check study of the routine core porosity measurement on 242 core plugs of tight gas sand and concluded that: with proper

attention and quality control, measuring porosity at ambient conditions, ether using gas (Boyle's method) or resaturating the sample with water, can be made with errors less than ±0.2 % to ±0.4 %. Furthermore, the quality control measures involve the use of 1-1/2" diameter cores, repeat measurements on 10 to 20% of samples, comparison of porosity with other rock properties and so on.

It can be seen that current methods of core porosity measurements using the fluid displacement method are fully defined conceptually and most of the recent works found in the literature addresses methods to increase the accuracy of these measurements as they are needed for samples with very low pore volumes.

2.2.Permeability

Another key parameter for the success of a reservoir engineering project is the ability of the rock to conduct fluids. This is called permeability and it is formally defined as a property of the porous medium and as a measure of the capacity of the medium to conduct fluids (Amyx et al, 1960). The Darcy's law is used to calculate the permeability of a porous medium and its generalized form is given as:

$$v_s = -\frac{k}{\mu}\left(\frac{dP}{ds}\frac{\rho g}{1.0133}\frac{dz}{ds} * 10^{-6}\right) \tag{2.5}$$

where, s is distance in direction of flow in cm and is always positive; v_s is the volume flux across a unit area of the porous medium in unit time along flow path s in cm/sec; z is the vertical coordinate, considered positive downward, in cm; ρ is the density of the fluid in gm/cc; g is the acceleration of gravity, 980.665 cm/sec^2; dP/ds is the gradient along s at the point to which v_s refers in atm/cm; μ is the viscosity of the fluid in centipoises and k is the permeability of the medium in darcys (Amyx et al, 1960).

The generalized form of Darcy's law can be simplified for the case of rectilinear steady state flow in porous media which is generally used for permeability measurements of core samples. Consider a block of a porous medium as in Figure 2.2. Here Q, the volume rate of flow, is uniformly distributed over the inflow face of area A. By considering the block 100 percent saturated with an incompressible fluid and is horizontal, then $dz/ds = 0$, $dP/ds = dP/dx$ and Eq. (2.4) reduces to (Amyx et al, 1960):

$$v_x = -\frac{k}{\mu}\frac{dP}{dx} =$$

$$\frac{Q}{A} = -\frac{k}{\mu}\frac{dP}{dx} \tag{2.6}$$

by separating the differential variables and integrating between 0 and L in x and P_1 and P_2, it is obtained the following equation:

$$Q = \frac{kA(P_1 - P_2)}{\mu L} \tag{2.7}$$

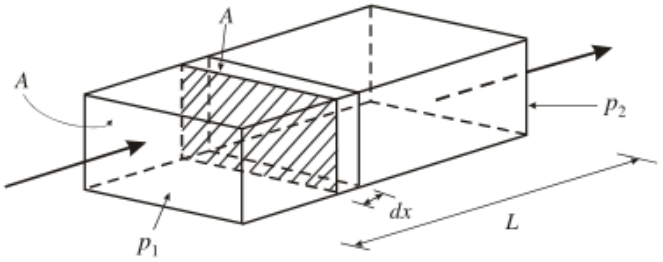

Figure 2.2. Schematic for rectilinear flow of fluids (from Rosa et al., 2006)

Equation 2.6 is extensively used in calculations of flow in porous medium, as well as for measuring the permeability for core samples. It is important to note that the following approximations were used to derive said equation: isothermal, laminar and steady flow; incompressible and homogeneous fluid, and its viscosity does not change with pressure; and a homogeneous porous medium which does not react with the fluid (Rosa et al., 2006).

If a compressible fluid flows through the porous medium, the generalized form of Darcy's law (Eq. 2.4) is still valid. However, for steady flow, instead of the volume rate of flow being constant through the system, it is the mas flow rate that is constant. Therefore, the integrated form of the equation differs. Moreover, considering the linear and steady flow of ideal gases, Eq. (2.4) becomes (Amyx et al, 1960):

$$\rho v_x = -\frac{k_a}{\mu}\rho\frac{dP}{dx} \tag{2.8}$$

where, k_a is the gas permeability. Since $v_x = Q/A$,

$$\rho\frac{Q}{A} = -\frac{k_a}{\mu}\rho\frac{dP}{dx}$$

and $\rho_b Q_b = \rho Q = constant$, where the subscript "b" stands for base conditions, Q and Q_b are defined at flowing temperature and $\rho = \rho_b(P/P_b)$. Therefore,

$$\rho_b Q_b = -\frac{k_a A}{\mu}\rho\frac{dP}{dx}$$

$$\frac{\rho_b Q_b}{A} = -\frac{k_a}{\mu}\rho_b \frac{P}{P_b}\frac{dP}{dx}$$

$$\frac{P_b Q_b}{A} = -\frac{k_a}{\mu}P\frac{dP}{dx}$$

separating variables and integrating,

$$\frac{P_b Q_b}{A}L = \frac{k_a}{\mu}\frac{(P_1^2 - P_2^2)}{2}$$

finally,

$$Q_b = \frac{k_a A}{2\mu L}\frac{(P_1^2 - P_2^2)}{P_b} \tag{2.9}$$

Equation (2.8) is very useful for measuring permeability using gas as it will be shown latter.

2.2.1. Permeability Measurement

This section focus on the permeability measurements made on core plugs. To perform this measurement, a core-holder as the one shown in Figure 2.3 is usually used. First, the sample is mounted in the core-holder and a confining pressure is applied in the rubber tubing. A fluid is then injected at the inlet until a steady flow is achieved. The inlet and outlet pressures are measured (P_1 and P_2, respectively), together with the flow rate Q.

If a liquid is used as the displacement fluid, the flow rate is considered equal through the core-holder and the following equation, obtained from Eq. (2.6), can be used to calculate the liquid permeability of the core-plug.

$$k = \frac{Q\mu L}{A(P_1 - P_2)} \tag{2.10}$$

If, however, a gas is used, the flow rate is measured in the outlet of the core-holder and the following equation, modified from Eq. (2.8), is used to calculate the gas permeability of the sample.

$$k_a = \frac{2Q\mu L P_2}{A(P_1^2 - P_2^2)} \tag{2.11}$$

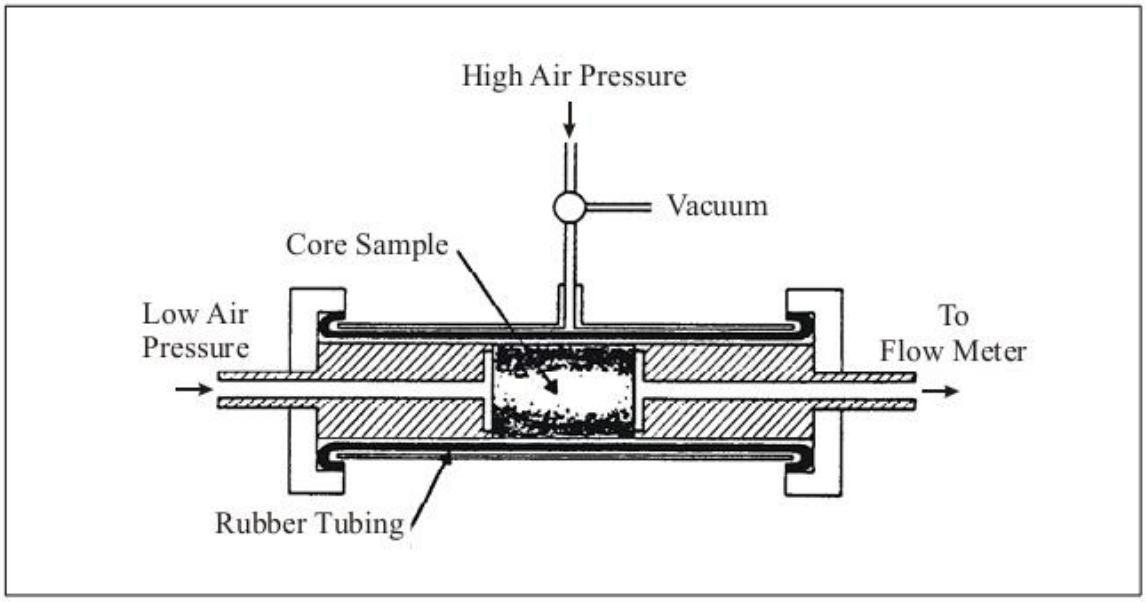

Figure 2.3. Core-holder used to measure the permeability of core-plugs (Torsaeter e Abtahi, 2003).

The liquid permeability measurements performed in this dissertation took place using a core-holder like the one shown in Figure 2.3, connected to a pump and a back pressure, and Eq. 2.9 was used to calculate the permeability of the samples. To measure gas permeability, the Ultra-Perm 300 from Core Lab Instruments, which is an industry standard permeabilimeter, was used connected to a core-holder similar to the one shown in Figure 2.3 and Eq. (2.10) was used to calculate gas permeability.

2.2.2. Factors Affecting Permeability Measurements

When measuring permeability of core plugs, it is important to exercise certain precautions in order to obtain accurate results. The first precaution that must be taken is to make sure that the conditions of viscous flow are being satisfied and therefore Darcy's law may be applied. When liquid is being used as the measuring fluid, care must be taken that it does not react with the solids in the core sample. Also, corrections must be applied for the change in permeability because of the change in confining pressure of the sample. When gas is the testing fluid, it is important to make sure that the value is corrected for gas slippage effect (Amyx et al, 1960).

The requirement that the permeability be determined for conditions of viscous flow is best satisfied by obtaining data at several flow rates and plotting the results as shown

in Figure 2.4 for uncompressible fluids and Figure 2.5 for ideal gases. For conditions of viscous flow, the data should render a straight line, passing through the origin. Turbulence is indicated by curvature of the plotted points (Amyx et al, 1960). This is derived from the fact that Darcy's law should only apply to viscous flow, and therefore the relationship of flow rate and pressure difference should follow Eq. (2.6) for liquid flow and Eq. (2.8) for ideal gas.

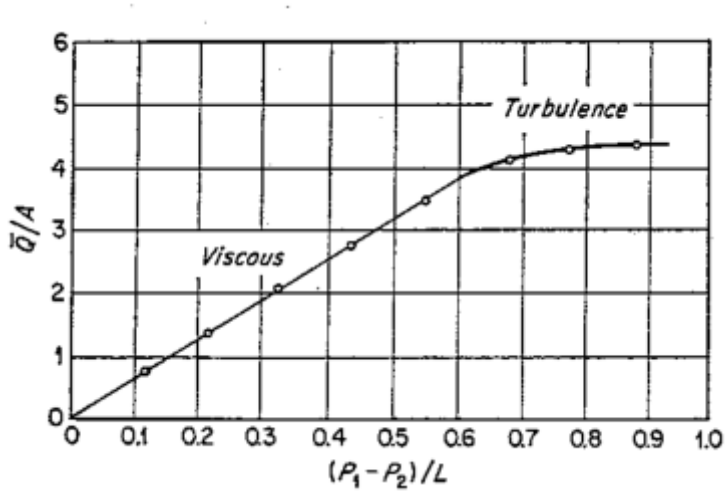

Figure 2.4. Determination of viscous and turbulent flow for uncompressible fluids (from Amyx et al, 1960).

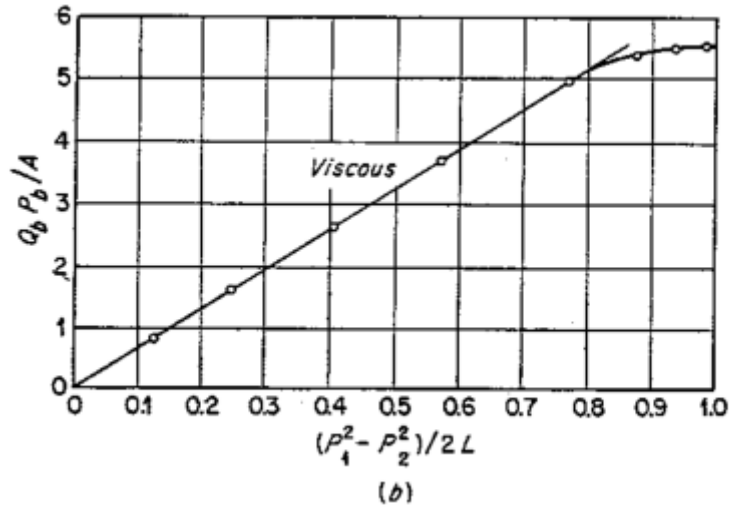

Figure 2.5. Determination of viscous and turbulent flow for ideal gases (from Amyx et al, 1960).

Effects of reactive liquids on permeability are very important to take into account when using liquids to measure permeability. For instance, while water is commonly considered to be nonreactive in the ordinary sense, the occurrence of swelling clays in many

reservoir rock materials results in water being the most frequently occurring reactive liquid in connection with permeability determinations. Reactive liquids alter the internal geometry of the porous medium, making it so that using these types of liquids do not vitiate Darcy's law, but rather results in a new porous medium with a permeability determined by the new internal geometry (Amyx et al, 1960). The effect of clay swelling in the presence of water is particularly important in connection with the determination of the permeability of some rock samples. Since, the degree of hydration of the clays is a function of the salinity of the water, it has been reported permeability changes of 50-fold or more between that determined with air and that determined with fresh water (Johnston and Beeson, 1945).

The other factor that can affect the liquid permeability measurement is the overburden pressure. Compaction of the core due to overburden pressure may cause as much as 60 per cent reduction in the permeability of various formations (Amyx et al, 1960). Some formations are much more compressible than others and therefore this factor must be taken into consideration.

Regarding permeability measurements using gas as a displacement fluid, the key factor to consider is the gas slippage effect. Discrepancies between liquid and air permeabilities have been reported by Muskat (1937), Fancher et al (1933) and Klinkenberg (1941). The authors found that, with highly permeable media, the differences between liquid and air permeabilities were small, whereas these differences were considerable for media of low permeability.

Klinkenberg (1941) showed that permeability determined with gases is dependent upon the nature of the gas, and is approximately a linear function of the reciprocal mean pressure. He argued that in capillaries with a diameter comparable to the mean free path of the gas (that is, the distance travelled by a gas molecule between successive molecular collisions) the interactions between the gas molecules and the capillary walls help move the gas molecules forward in the direction of flow. This gas slippage reduces "viscous" drag and increases permeability (McPhee and Arthur, 1991).

It has been proved by Kundt and Warburg in 1875 that, when a gas is flowing along a solid wall, the layer of gas next to the surface is in motion with respect to the solid surface. Therefore, if the wall is at zero velocity, then the velocity of the gas layer in the immediate vicinity of the wall is at that same velocity value. With that in mind, Klinkenberg (1941) idealized a laminar flow of fluids through a porous medium as one in which all the

capillaries in the material are of the same diameter and oriented at random through the solid material.

Consider a cube of this idealized material, as the one shown in Figure 2.2, and let there be n capillaries of radius r. The amount of liquid flowing through per unit time is found by applying Poiseuille's law:

$$\frac{Q}{A} = \frac{1}{3}\frac{n\pi r^4}{8\mu L}(P_1 - P_2) \tag{2.12}$$

combining Eqs. (2.6) and (2.11) gives:

$$k = \frac{1}{3}\frac{n\pi r^4}{8} \tag{2.13}$$

Klinkenberg found that the modified form of Poiseuille's law for a gas, if slipping of the gas in contact with the wall is taken into account is:

$$\frac{Q_b P_b}{A} = \frac{1}{3}\frac{n\pi r^4}{8\mu L}\frac{(P_1^2 - P_2^2)}{2}\left(1 + \frac{4c\lambda_m}{r}\right) \tag{2.14}$$

where, λ_m is the mean free path at the mean pressure $P_m = 1/2 * (P_1 + P_2)$ and c is a proportionality fact "slightly less than 1" (Klinkenberg, 1941). Combining Eqs. (2.13) and (2.12), gives:

$$\frac{Q_b P_b}{A} = \frac{k}{\mu L}\frac{(P_1^2 - P_2^2)}{2}\left(1 + \frac{4c\lambda_m}{r}\right) \tag{2.15}$$

or, combined with Eq. (2.8):

$$\frac{Q_b P_b}{A} = \frac{k}{\mu L}\frac{(P_1^2 - P_2^2)}{2}\left(1 + \frac{4c\lambda_m}{r}\right) \tag{2.16}$$

equations (2.8) and (2.15) lead to:

$$k_a = k\left(1 + \frac{4c\lambda_m}{r}\right) \tag{2.17}$$

as the mean free path is inversely proportional to pressure, it is possible to write that:

$$\frac{4c\lambda_m}{r} = \frac{b}{P_m} \tag{2.18}$$

where b is a constant, which is referred to as the gas slippage factor. Eq.(2.7) substituted in Eq. (2.16) gives:

$$k_a = k\left(1 + \frac{b}{P_m}\right) \tag{2.19}$$

Eq. (2.18) is a relation between the apparent and the true permeability of an idealized porous system to gas (Klinkenberg, 1941). From Eq. (2.17) it can be seen that at lower pressures, the mean free path increases, and the slippage effect, as well as gas permeability, is enhanced. At high mean pressures, the slippage effect is suppressed and permeability reduces until, at infinite mean pressure, the mean free path is reduced to zero, and the gas molecules are considered to behave as a liquid and therefore, $k_a = k$. Klinkenberg demonstrated that, by plotting gas permeability against the inverse mean pressure for a range of porous media samples, the data fell on a straight and the Y-intercept (that is, infinite mean pressure) is the true liquid permeability k as it can be seen in Figure 2.6. He also proved that b is smaller for higher permeability samples, as expected, since the slip factor is inversely proportional to the pore radius and directly proportional to mean free path.

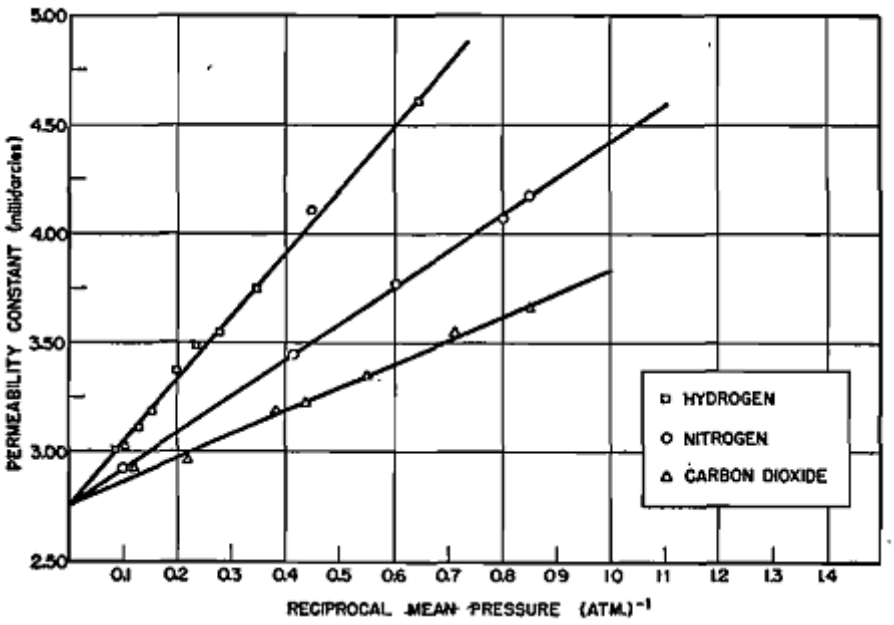

Figure 2.6. Permeability constant of core sample "L" to hydrogen, nitrogen and carbon dioxide at different pressures (permeability constant to isooctane, 2.55 mD) –(from Klinkenberg, 1941).

A more recent publication by McPhee and Arthur (1991) provided practical recommendations that can overcome or minimize experimental problems to obtain conventionally-derived Klinkenberg parameters. The authors point out the importance of selecting test flow procedures, optimizing process sensor accuracy and standardizing sleeve and net effective core pressures. It was also evidentiated that non-Darcy flow must be

recognized in any Klinkenberg measurement. Figure 2.7 shows an example of Klinkenberg plot taken from Noman and Kalam (1990). It can be seen that the points that follows the straight line are the ones in a laminar flow regime and therefore, can be used for the Klinkenberg analysis, and the ones that are not following the straight line are in a non-Darcy flow regime (turbulent flow regime) and may not be used in the aforementioned analysis. This plot can be used together with the one shown in Figure 2.5, to make sure that the points being analyzed are following Darcy's law.

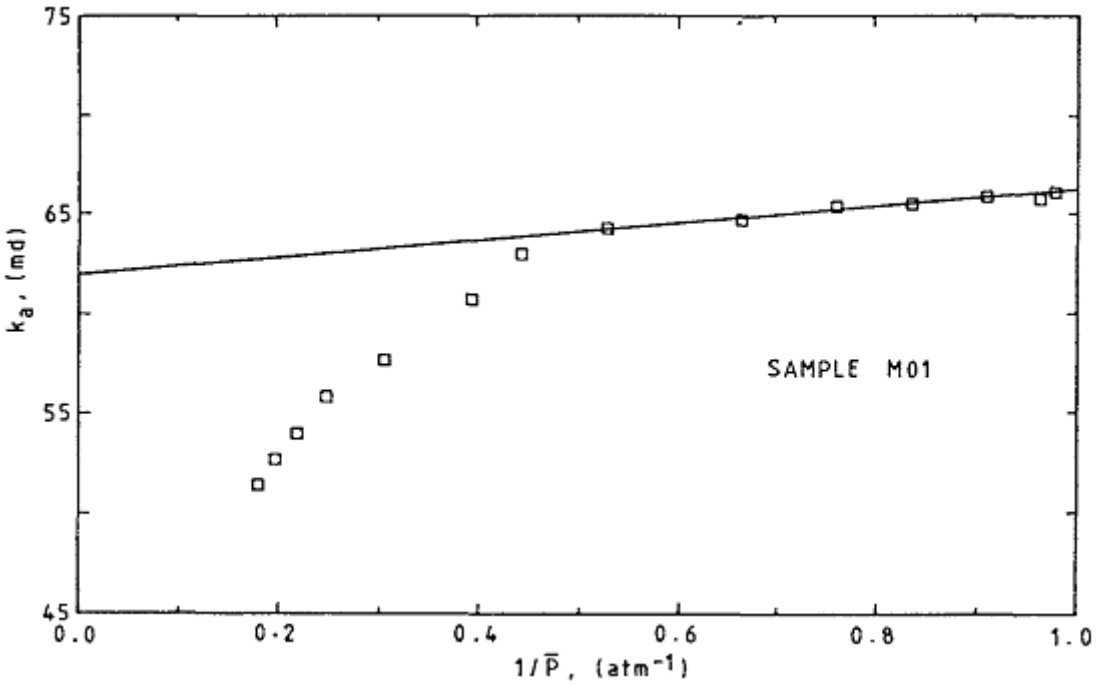

Figure 2.7. Example of Klinkenberg plot. (from Noman and Kalam, 1990).

Another important factor for measuring Klinkenberg permeability is, as pointed out by McPhee and Arthur (1991), to perform the measurements under backpressure. This, according to the authors, provides improved control of gas flow rate and core differential pressure, and assists in maintaining viscous flow at higher mean pressures. Rushing et al (2004) also noted the importance of using a finite backpressure in these measurements, because it improves the accuracy of steady-state flow measurements.

2.3.Dissolution of Carbonate Rocks

When CO_2 dissolves in water it forms carbonic acid (H_2CO_3) (Eq. 2.19) decreasing the pH level of water. This may, in turn, cause a reaction with the main

constituents of carbonate rocks, mainly calcite and dolomite. The equilibrium reaction governing the dissolution of calcite is shown in Eq. (2.21). According to Zhang et al (2007) the dissolution of dolomite takes place in two parts: the first one (Eq. 2.21) forming magnesium carbonate and a second slower reaction of the dissolution of the previously formed carbonate (Eq. 2.22).

$$CO_2 + H_2O \rightleftarrows H_2CO_3 \rightleftarrows H^+ + HCO_3^- \tag{2.20}$$

$$H^+ + HCO_3^- + CaCO_3 \rightleftarrows Ca^{2+} + 2HCO_3^- \tag{2.21}$$

$$H^+ + HCO_3^- + CaMg(CO_3)_2 \rightleftarrows MgCO_3 + Ca^{2+} + 2HCO_3^- \tag{2.22}$$

$$H^+ + HCO_3^- + MgCO_3 \rightleftarrows Mg^{2+} + 2HCO_3^- \tag{2.23}$$

The topic of dissolution of carbonate rocks has been studied by many authors using different laboratory techniques. Fredd and Floger (1998), Liu et al (2005) and Taylor et al (2006) used a rotating disk apparatus to evaluate the dissolution rate of carbonate. To evaluate changes in flow properties, like permeability and porosity, percolation experiments (core flooding experiments) were used by Bacci et al (2010); Grigg et al (2005); Izgec et al (2005); Luquot and Gouze (2009); Noiriel et al (2009) and Zekri et al (2009), to better mimic the natural reservoir conditions. Batch dissolution experiments were also used to study dissolution rates of carbonate rocks by Yadav et al (2008).

Fred and Floger (1998) studied the dissolution rate of calcite in various pHs and acetic acid concentration using a rotating disk. The rotating disk serves as a means of studying the complex interplay between transport and reaction for the dissolution under conditions in which the transport processes are well defined. The authors demonstrated that the rate of calcite dissolution in acetic acid solution is influenced by the rate of transport of reactants to the surface, the kinetics of the surface reaction, and the rate of transport of products away from the surface.

Liu et al (2005) used a rotating disk apparatus to investigate de dissolution rate of dolomite and limestone samples in CO_2 and water. They found that, under similar conditions not only were the initial dissolution rates of dolomite lower by a factor of 3-60 than those of limestone, but also there are different dissolution rate-determining mechanisms for limestone

versus dolomite. According to the authors, the stronger CO_2 conversion and mass trasport controlling mechanisms of limestone indicate that dissolution of limestone is mainly controlled by differential dissolution caused by flow rate for example. Dolomite dissolution is mainly homogeneous and determined by surface reaction.

Taylor et al (2006), also using a rotating disk, found that the dissolution rate of carbonate reservoir rocks in HCl acid will generally increase as the concentration of calcite increases. This trend is varied if significant amounts of clay are present in the rock. It is important to note that the authors observed that the anhydrite contained in the carbonate disks appears to have formed, after the experiments, fine needles that might cause formation damage in tight carbonate reservoirs. One of the samples in particular, named C2/T23, even though presented no Anhydrite in its XRD analysis (95.6 wt% Calcite, 3.4 wt% Dolomite and 1.0 wt% Quartz) have formed these needles, which can be seen in Figure 2.8.

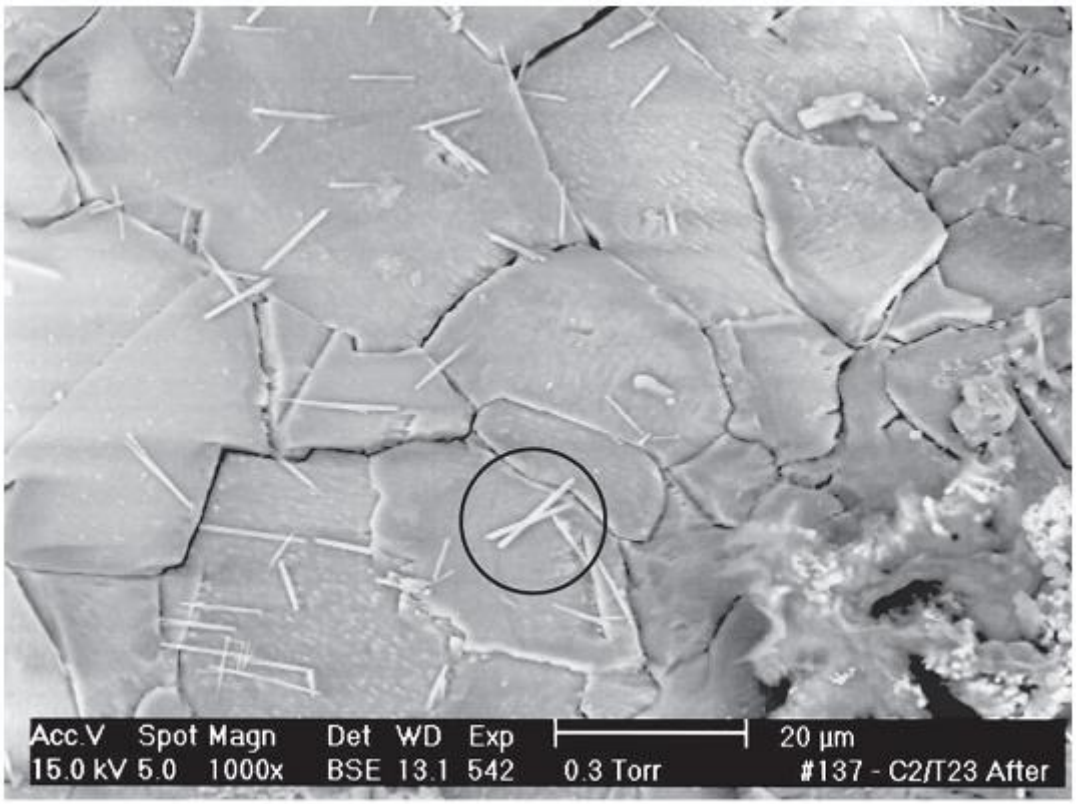

Figure 2.8. ESEM (environmental scanning electroscope) picture of Sample C2/T23 from Taylor et al (2006) after reaction in 1 M HCl at 85oC. Anhydrite needles are shown in circle.

The importance of formation damage due to the dissolution of carbonate rocks, together with any effects it may have during flow is difficult to evaluate using the rotating

disk apparatus. Bacci et al (2010) proposed a core flooding experiment to study the changes in injectivity due to the dissolution near wellbore and far field using an HCL solution to simulate the effect of CO_2 injection on carbonates. In their study they used two types of experimental set ups (Figure 2.9), the first one (Figure 2.9a) to study the effects of the pressure differences close to the injection point and in the reservoir bulk, and the second one (Figure 2.9b) to study the effects of the temperature differences also close to the injection point and in the reservoir bulk.

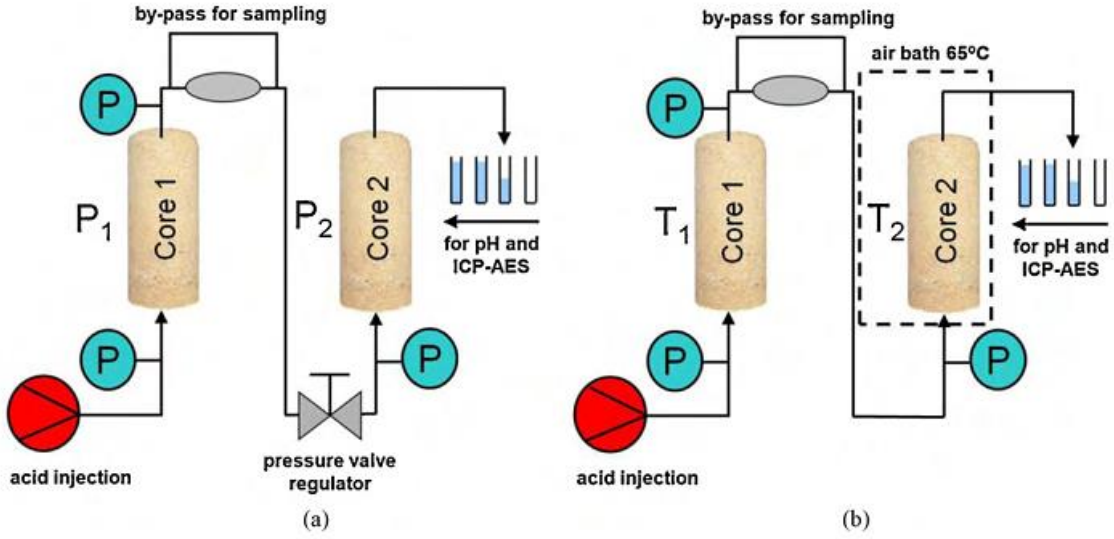

Figure 2.9. Experimental set ups used by Bacci et al (2010)

Bacci et al (2010) core flooding experimental results are summarized in Table 2.1. Their results indicated that the effect of pressure changes is small and it is not considered to be a major threat to CO_2 injectivity. It was also observed that the difference of temperature from the injection point to somewhere far in the field can lead to re-precipitation and permeability reduction. The authors also noted that, since they did not use CO_2 in their experiment, the results obtained are not directly applicable to real CO_2 injection cases, as the acidity of the solution used in the experiments was unrealistically high and the reactions observed may be different to those taking place in a real injection scenario. However, the results of their study can be a good indication of the changes in the petropysical properties of carbonate rocks due to variations in the thermodynamic conditions around an injection

wellbore regarding the change in pressure between the injection well and the reservoir as well as change in temperature.

Table 2.1. Petrophysical properties pre- and post- core flood (Bacci et al 2010)

Test	**Sample**	**Δϕ (%)**	**N_2 Permeability (m)**
Pressure difference (Figure 2.9a)	Core 1	+1.7	2.64 → 522.45
Pressure difference (Figure 2.9a)	Core 2	+0.30	2.71 → 2.97
Temperature Difference (Figure 2.9b)	Core 1	+1.39	2.91 → 7.90

Also according to Bacci et al (2010), the changes in the petrophysical properties of carbonate rocks due to variations in the thermodynamic conditions around an injection wellbore may lead to more injection impairments. In fact, an increase of temperature together with a decrease in fluid pressure in the far field would not only decrease the solubility of carbonates but also cause degassing of CO_2. Therefore, the concentration of carbonic acid in solution would also decrease resulting in an increase in pH. This would further increase the potential of carbonate deposition and therefore of an injectivity loss. The authors also pointed out that, in a real injection scenario the precipitation front would be progressively moving away from the wellbore, therefore, the impact on injectivity of the precipitation phenomena may be less than what may be observed in a linear geometry.

Grigg et al (2005) used core-flooding experiment to study the dissolution of carbonate rocks. They reported findings and comparisons of five large core flooding experiments performed on limestone and dolomite samples with co-injection or alternating injection of CO_2 and brine at reservoir conditions. They used only one core-holder in their experimental set up, therefore, to be able to evaluate change in porosity and permeability along the core, they divided the core into two segments. According to the authors, the dissolution of carbonates at reservoir conditions during co-injection of CO_2 and brine was confirmed by porosity and permeability increases, neutron CT, and brine compositional analysis performed on effluent brine samples obtained at reservoir conditions. When deposition occurred it was indicated by porosity and permeability reductions in the downstream core, back-scattered electron imaging (BSEI) identification, and modeling. It is also important to note that, in one of the core floodings, even though there was no evidence of

plugging in the entire core and its permeability was essentially the same, the second half of the core had a permeability reduction of about a half, which is an indication of deposition.

Izgec et al (2005) presented core flooding experiments with CO_2 monitored by computerized tomography to characterize the changes on carbonate core plugs. In their experiments, they first saturated the sample with the desired brine and then injected CO_2 into the sample, while measuring its porosity and permeability changes. They used core plugs with mainly calcite and 5% alteration. Figure 2.10 shows their results for the effects of temperature on the porosity and permeability changes in horizontally oriented core floodings. The tests performed in 18^{o}C and 50^{o}C showed an initial decrease of permeability to 40% and later, it started to decrease again. For the 35^{o}C experiment, the permeability did not follow a clear trend. The porosity did not follow the permeability trend.

The authors also studied the effects of salinity, on the same type of samples, in the permeability changes in vertically oriented core floodings. Figure 2.11 shows their results. They observed that salinity changes from 0 to 5% by weight of NaBr had no drastic effect on the changes in permeability. Also, when distilled water was used, the initial permeability increase was 40%, whereas for the saline cases, 20%. They also noted that as the salt content of the brine increased, permeability drop was more pronounced.

Luquot and Gouze (2009) studied a set of four flow-through experiments with CO_2 and brine in limestone samples using decreasing CO_2 partial pressures to mimic the increase in distance from the injection well. The brine composition was also changed as the distance from the injection well changed to mimic the ions transportation as the injection wave propagates. The three experiments that simulate the distances nearer to the injection indicated an increase in permeability and porosity, being this increase more pronounce as the distance to the injection point decreased. The one experiment that simulated a point in the far field presented a decrease in permeability and porosity. Using scanning electron micro-scope (SEM) they identified the cause of this decrease as an Mg-calcite precipitation as it can be seen in Figure 2.12.

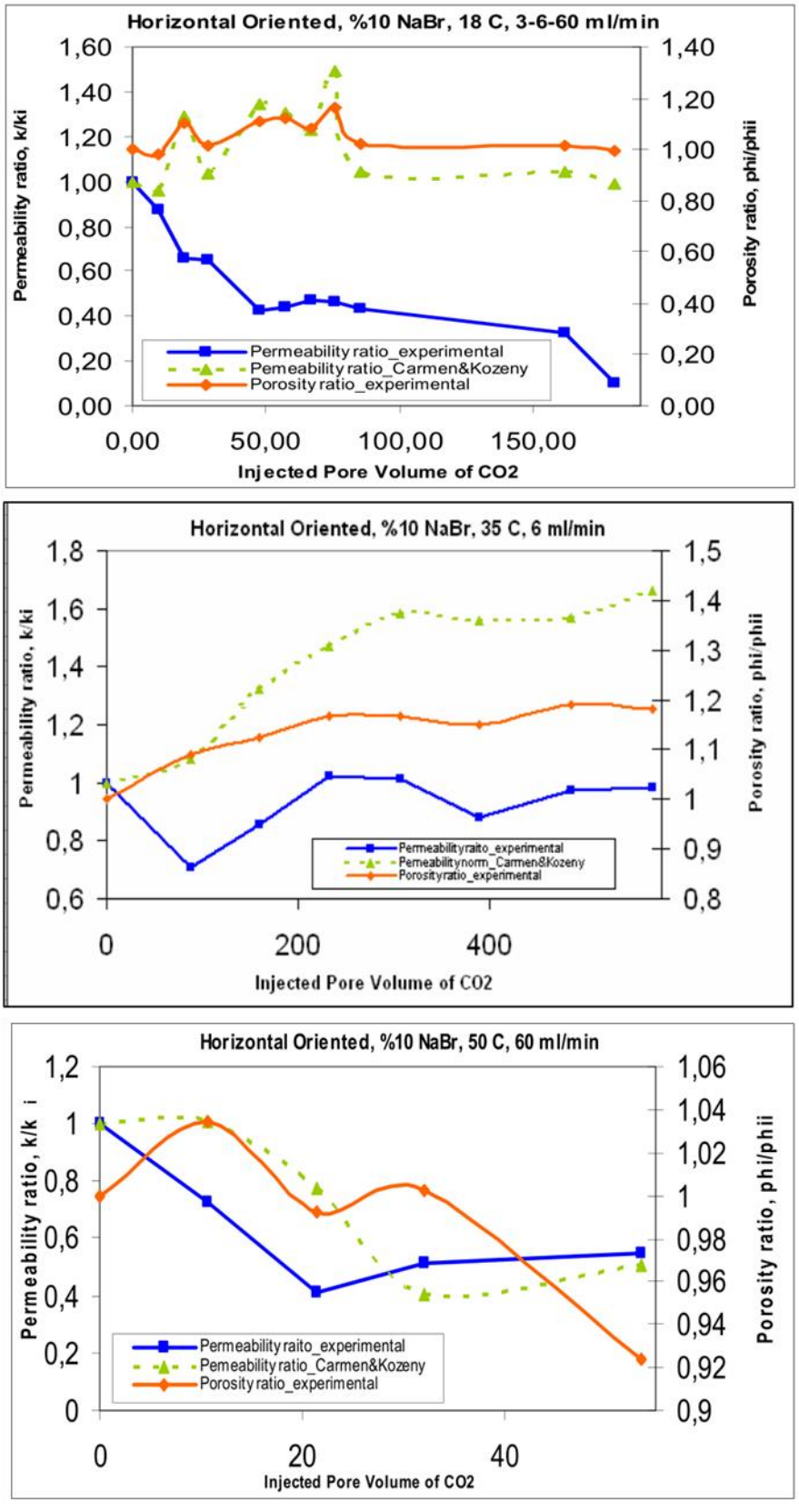

Figure 2.10. Effects of temperature on porosity and permeability change (from Izgec et al, 2005)

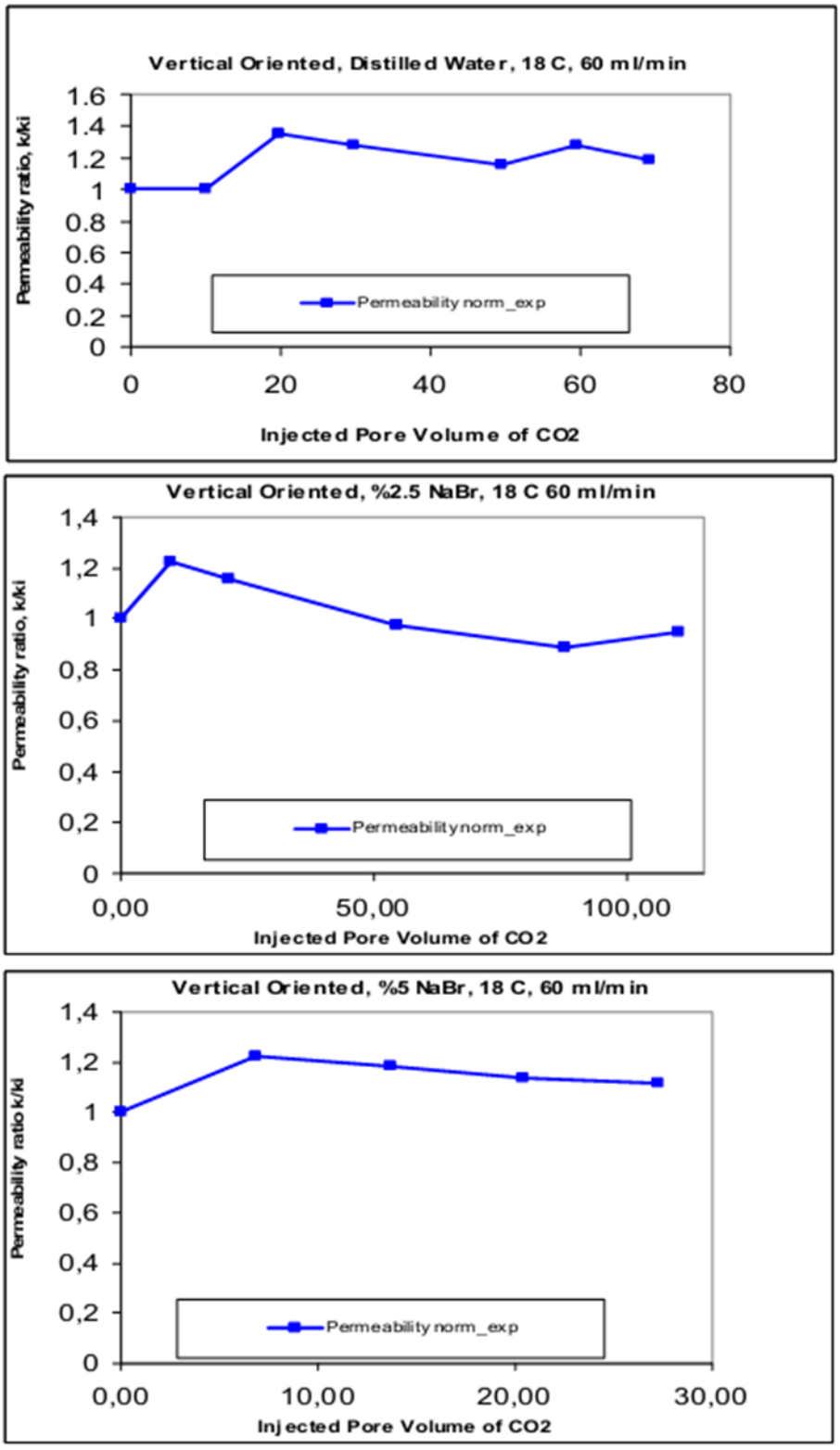

Figure 2.11. Effects of salinity on permeability change (from Izgec et al, 2005)

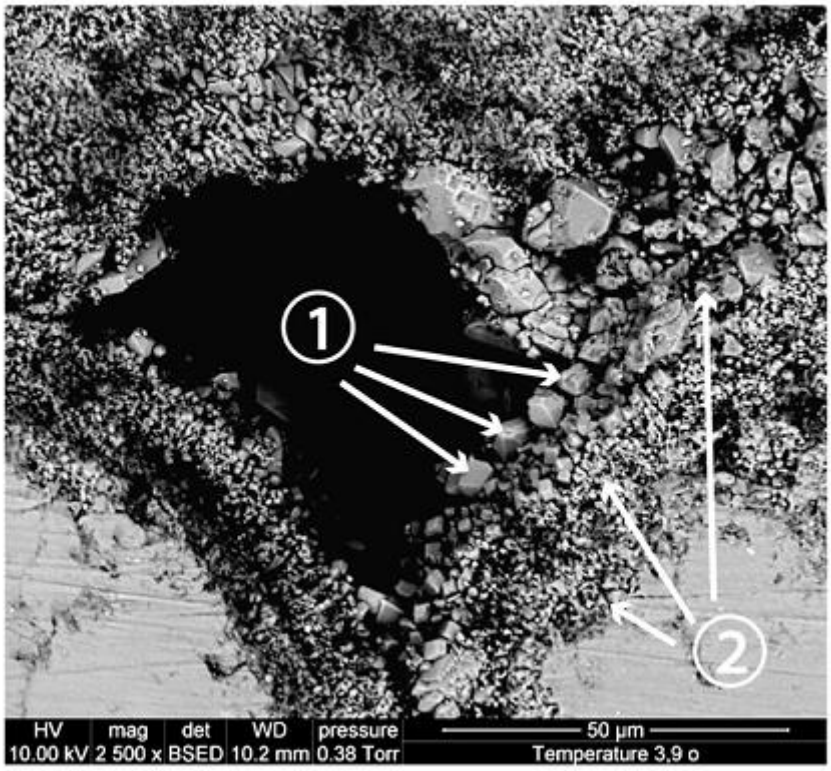

Figure 2.12. SEM micrograph in secondary electron mode showing Mg-calcite (1) precipitated and rock forming Mg-calcite (2). (from Luquot and Gouze, 2009).

Noiriel et al (2009) investigated the change in the reactive surface area of a limestone sample during a flow-through experiment using CO_2 rich water with the aid of X-ray microtomography. The authors indicated that dissolution occurs in areas where the pore connectivity is the highest. They also noted that the porosity changes were not evenly distributed, and that the porosity increase was slightly higher near the sample inlet.

Zekri et al (2009) studied coreflooding experiments with limestone samples to evaluate interactions between CO_2-water-carbonate rock, and CO_2-oil-carbonate rock. Their analysis of experimental data showed that dissolution and precipitation can occur in the core during a given experiment.

Yadav et al (2008) conducted static experiments using buffer solutions with various pHs to study the dissolution kinetics of calcite, dolomite, leucogranite and gneiss. The authors used SEM microtomography to characterize the samples. It was found that although the samples were ultrasonically cleaned prior to experiment, the calcite grains seem to be attached with very few ultrafine particles, while the dolomite grains presented many ultrafine

particles adhering to them. The authors suggested that the decrease in the specific surface areas of dolomite is most likely due to rapid preferential dissolution of fine particles and other highly soluble phases during the short experimentation period.

Surface adsorption and desorption may also play a role in the rock fluid equilibrium. Studies of the impact of different salinity water in the oil recovery in carbonates has shown how the ions Mg^{2+}, Mg^{2+} and SO_4^{2-}, may alter the wettability of carbonates (Zhan et al, 2007). The authors explained this effect by the adsorption and desorption of the aforementioned ions. Throughout this work, this effect was considered in conjunction with the overall dissolution and precipitation mechanisms of carbonate rocks in carbonated water.

To summarize, when CO_2 dissolves in water, it forms carbonic acid, which causes a decrease in pH of the water. The acid will react mainly with the calcite and dolomite present in carbonate rocks. The dissolution rate of dolomite is lower than that of limestone. As CO_2 is injected in a carbonate rock filled with brine, the dissolution reaction will be predominant close to the injection point, and as the flow front moves away from the injection point, precipitation can occur. The dissolution is usually characterized by an increase in permeability and porosity, and precipitation is usually characterized by a decrease in both properties. This behavior will change with changes in temperature, brine composition, pressure and rock composition.

2.4. Carbonate Rocks

According to the U.S. Bureau of Mines Staff (1996), a “carbonate rock is a sedimentary rock composed of more than 50% by weight of carbonate minerals, e.g. limestone, dolomite or carbonatite”. These carbonate minerals are formed by the combination of the radical $(CO_3)^{-2}$ with cations. In the laboratory studies performed for this dissertation coquina and dolomite samples were used as they are considered analogues to the pre-salt reservoirs.

The U. S. Bureau of Mines Staff (1996) defines coquina as “a detrital limestone composed wholly or chiefly of mechanically sorted fossil debris that experienced abrasion and transport before reaching the depositional site and that is weakly to moderately cemented, but not completely indurated”. The coquina sample used in all experiments reported here is from Morro do Chaves outcrop in Alagoas-SE sedimentary basin. According to Nogueira et al (2003), “The sedimentary sequence of Eocretaceous of Morro do Chaves Member in the Alagoas Basin represents the deposition of "coquinas" beds, interbedded with calcilutites and

shales that show porosity variations on vertical section". They also pointed out that the importance of this formation is the fact that the Lagoa Feia Formation in Brazil and Toca Formation in Africa are important oil bearing carbonate rocks formation comprised by coquinas.

A scanning electron microscope with energy-dispersive x-ray (SEM-EDX), model Zeiss Ultra 55, was used by a team member of the Laboratory of Miscible Recovery Methods (LMMR), in CEPETRO – Unicamp, to analyze the chemical composition of one small sample of the coquina samples (Munõz, 2015). Table 2.2. Chemical composition of coquina samples shows the results obtained by his analysis. It can be seen that the only elements detected by the equipment were Carbon, Oxygen and Calcium. This is an indication of the purity of these samples. However, when the percentage of calcite ($CaCO_3$) is calculated using the numbers of Table 2.2, by assuming that all the Calcium is in the form of calcite, it was obtained 96.7% of this mineral, which means that this rock is composed mainly by calcite.

Table 2.2. Chemical composition of coquina samples

Element	Wt%
C	13.86
O	47.38
Ca	38.75

The experimental results presented in this dissertation also refer to dolomites from Silurian Formation (US). The definition of dolomite by the U. S. Bureau of Mines Staff (1996) leaves room for variation: "a carbonate sedimentary rock consisting of more than 50% to 90% mineral dolomite, depending upon classifier, or having a Ca:Mg ratio in the range 1.5 to 1.7, or having an MgO equivalent of 19.5% to 21.6%, or having a magnesium-carbonate equivalent of 41.0% to 45.4%". The mineral dolomite has the formula $CaMg(CO_3)_2$. With that in mind, the same experiment mentioned above was performed by the same team member, with a sample of this dolomite. Table 2.3. Chemical composition of dolomite samples shows the chemical composition obtained for these samples. It can be seen that there is very little Calcium in these samples and besides Magnesium there is also traces of Iron, in comparison with the coquina samples.

It was also calculated the maximum amount of the dolomite mineral that may be present in these rocks, by assuming that all the calcium is in the form of dolomite ($CaMg(CO_3)_2$). The value obtained was 32.1%.

Table 2.3. Chemical composition of dolomite samples

Element	**Wt%**
C	20.28
O	25.84
Mg	45.74
Ca	7.46
Fe	0.68

In summary, the carbonate rocks that were used in the laboratory studies, were coquinas and dolomites, coquinas composed mostly by calcite minerals and the dolomites formed by multi-minerals with predominance of the ones composed with magnesium.

3. COMPARISONS OF GAS AND LIQUID PERMEABILITY

The Comparisons of Gas and Liquid Permeability was performed to address the secondary objective of this work, which is to delineate the best practices for measuring porosity and permeability in laboratory conditions. This chapter reports the experimental work performed to investigate the issue of converting gas permeability measurements to liquid permeability measurements.

3.1.Materials and Methods

The samples used in this experimental series were five dolomite samples, from Silurian Formation - USA, and five coquina samples, from Morro do Chaves Outcrop – Brazil, shown in Figure 3.1. To make sure there were no organic substances left in these rocks, they were cleaned prior to commencing the experiment. First, they were stacked together with a paper filter between them (to ensure capillarity continuity), then toluene was injected in the rocks until it was clear in the outlet. After this, the samples were dried in a heater at 80^{o}C for at least 48 hours.

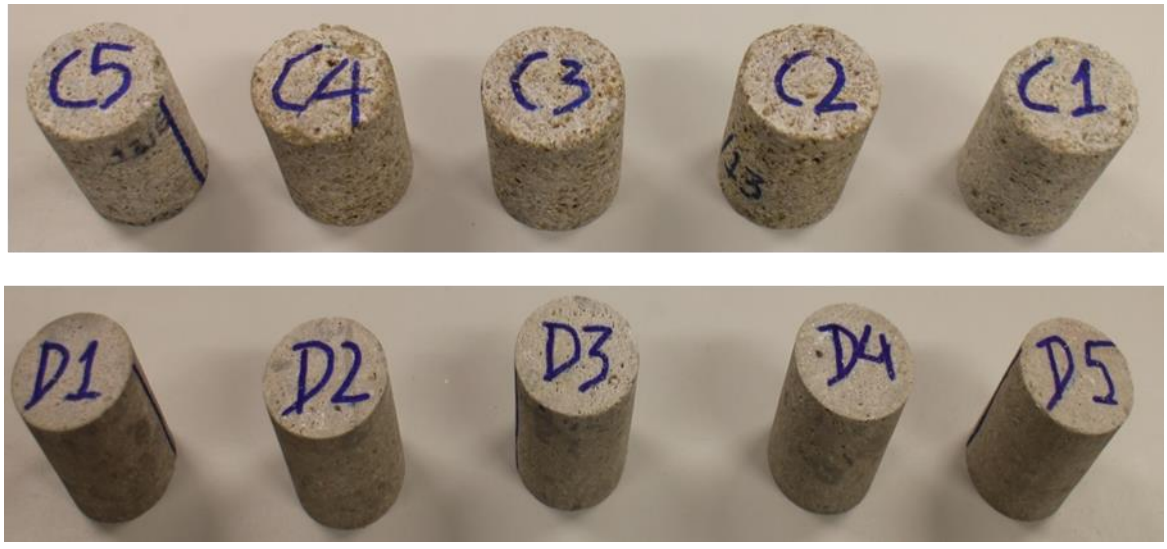

Figure 3.1. Rock Samples used for the air-to-liquid permeability study (C is for coquina and D for dolomite)

After cleaning, the rock characterization was performed. First, a paquimeter was used to measure the diameter and length of the samples. Next, the air permeability was

measured using an Ultra-Perm 500 permeabilimeter (Figure 3.2) and finally the porosity of the samples was measured using an Ultra-Pore 300 (Figure 3.3).

The air permeability measurements were done for each sample varying the flow rate so that the entire range of flow rate from the equipment was used. The error of the gas permeability measurement was calculated as explained in APENDIX B. The porosity measurement of each sample was repeated five times so that a standard deviation could be calculated.

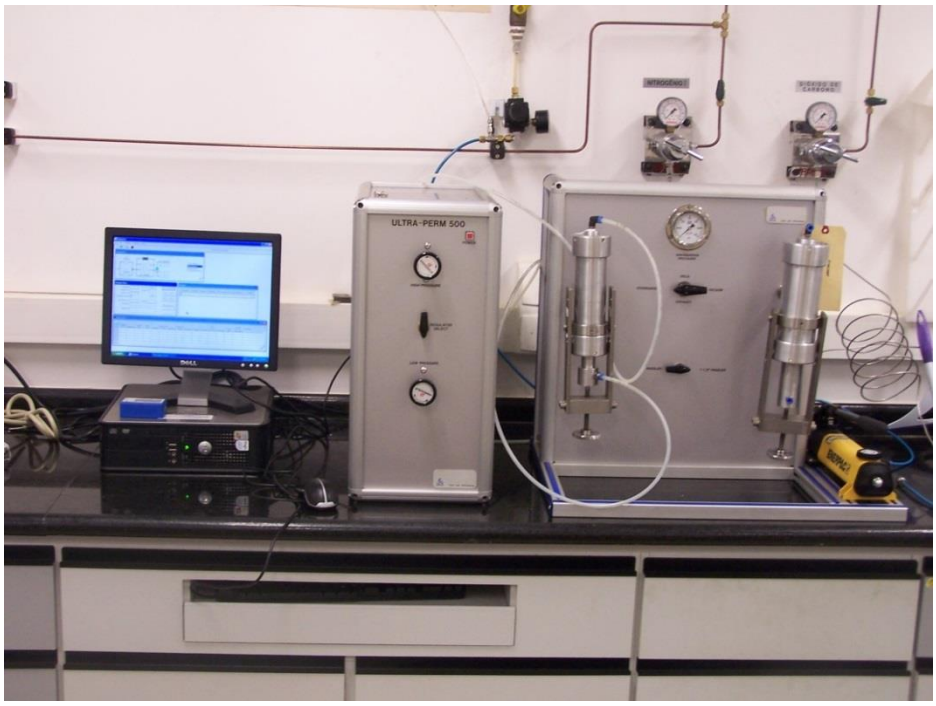

Figure 3.2. Permeabilimeter Ultra-Perm 500

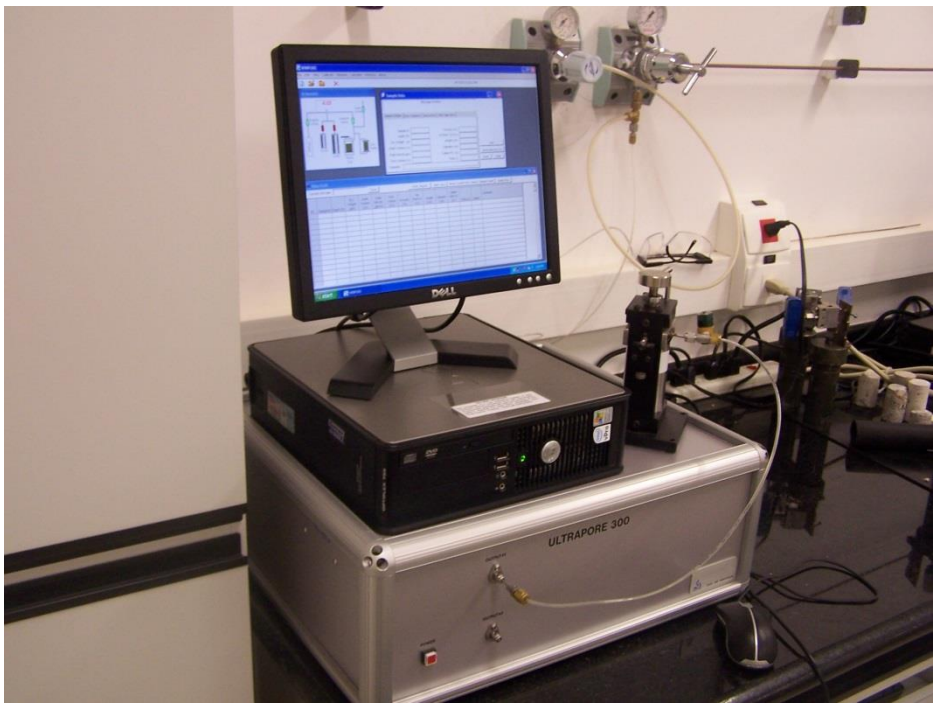

Figure 3.3. Porosimeter Ultra-Pore 300

Now, to determine the liquid permeability of these rocks, first a chemically inert liquid to carbonate rocks was chosen. The mineral oil EMCA was selected over water, because carbonates may be reactive with the latter. The EMCA oil was filtered and deaerated before use. The viscosity of this oil was then measured in the pressure and temperature of the experiment.

To begin the viscosity measurement, some of EMCA oil was inserted in a high pressure container, connected at one end to the high pressure pump and at the other end to the high pressure viscometer (Figure 3.4). The viscosity measurement was then performed with pressures from zero to 2,400 psi in steps of 400 psi. The temperature varied in each step from 19.5^{o}C to 23.0^{o}C.

Figure 3.4. In the left is the high pressure pump, and to the right the high pressure viscometer

Following sample cleaning and characterization, a core-flooding was performed to measure the liquid permeability of each sample. First, the sample was loaded in a core-holder with a confining pressure of 2,500 psi. The core-holder was then connected to a vacuum pump (Figure 3.5) and the pressure was decreased to below 10^{-1} bar.

After that, the core-holder was connected to the experimental apparatus, seen in Figure 3.6 in a schematic diagram and in Figure 3.7 as disposed in the laboratory. The core holder was connected at the inlet to the high pressure pump, and in the outlet to a back pressure valve, adjusted to maintain pressure of 1,000 psi. The outlet of the back pressure valve was collected in a glass beaker. The high pressure pump was connected in the inlet to a big filtering flask filled with EMCA oil. A differential pressure transducer was connected to both ends of the core holder. The pressure transducer and the high pressure pump were connected to a computer, where all the data were recorded.

Figure 3.5. Vacuum experimental set up

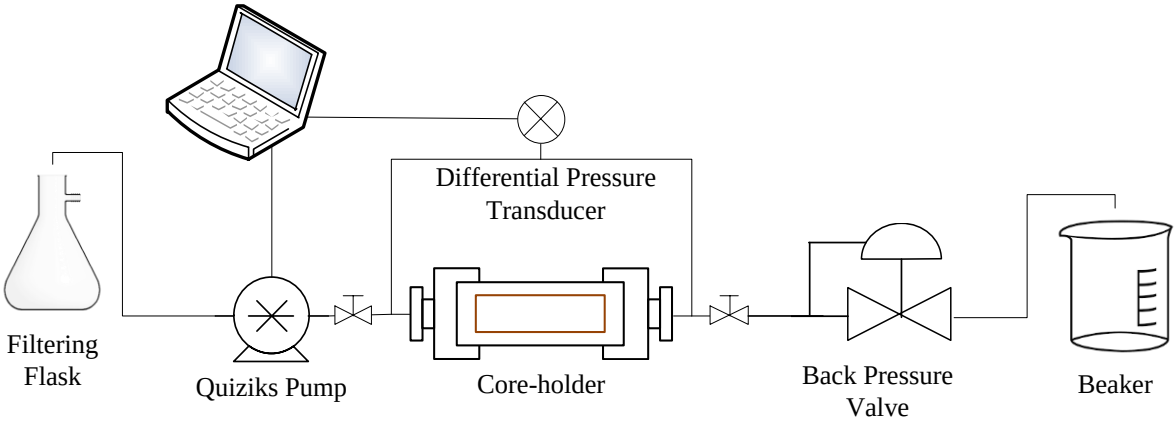

Figure 3.6. Schematics of the experimental apparatus

In the beginning of core-flooding, the EMCA oil was injected at a very slow rate (0.1 cc/min), for at least two pore volumes, to guarantee that the sample was completely saturated. After that, the experiment took place with increasingly higher flow rates, depending on the sample permeability and the liquid permeability of each sample was determined. The procedure used to calculate the error of this measurement is shown in detail in APENDIX B.

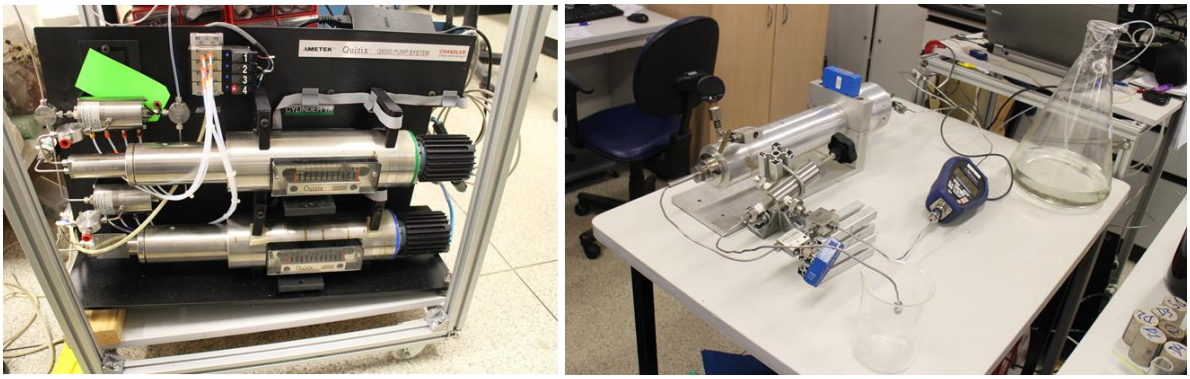

Figure 3.7. In the left is the high pressure pump, and to right the rest of the experimental apparatus.

3.2.Results

The initial properties of the coquina and dolomite samples used in this chapter are shown in Table 3.1. The dolomite samples are 38.1 mm in diameter by 50 mm in length. Their porosity varied from 14.4 % to 17.5 % and their average air permeability varied from 90.0 mD to 318 mD. The coquina samples, on the other hand, are 37.8 mm in diameter by 50 mm in length, with porosities varying from 14.9% to 17.0 % and average air permeability from 58.3 mD to 131 mD.

It is important to note for future reference that, the air permeability measurements were obtained by varying the flow rate seeking to cover the entire equipment range and the computed air permeability is the average of all the values obtained for each sample.

Figure 3.8 displays the results of the viscosity measurements of the EMCA oil. As expected, the viscosity is directly proportional to pressure and temperature in the covered ranges. There is an increase of more than 10 cP in the EMCA oil viscosity from 0 to 2.400 psi and 4 cP when the temperature raised form 19.5^{o}C to 23^{o}C.

Table 3.1. Main properties of the samples

Sample	m (g)	l (mm)	D (mm)	Ø (%)	K_{air_ave} (mD)
D1	137.1631	50.1	38.1	14.4	90.0 ± 1.9
D2	131.4184	49.9	38.1	17.5	300 ± 5.4
D3	134.1650	50.5	38.1	17.0	318 ± 6.4
D4	134.5696	50.4	38.1	16.5	185 ± 3.8

D5	134.6895	50.0	38.1	15.9	195 ± 3.9
C1	127.3597	50.4	37.8	16.7	58.3 ± 1.3
C2	130.3604	50.6	37.8	15.3	131 ± 2.6
C3	130.7775	50.5	37.8	14.9	129 ± 2.6
C4	130.2795	50.8	37.8	15.6	105 ± 2.1
C5	127.5713	50.7	37.8	17.0	130 ± 2.5

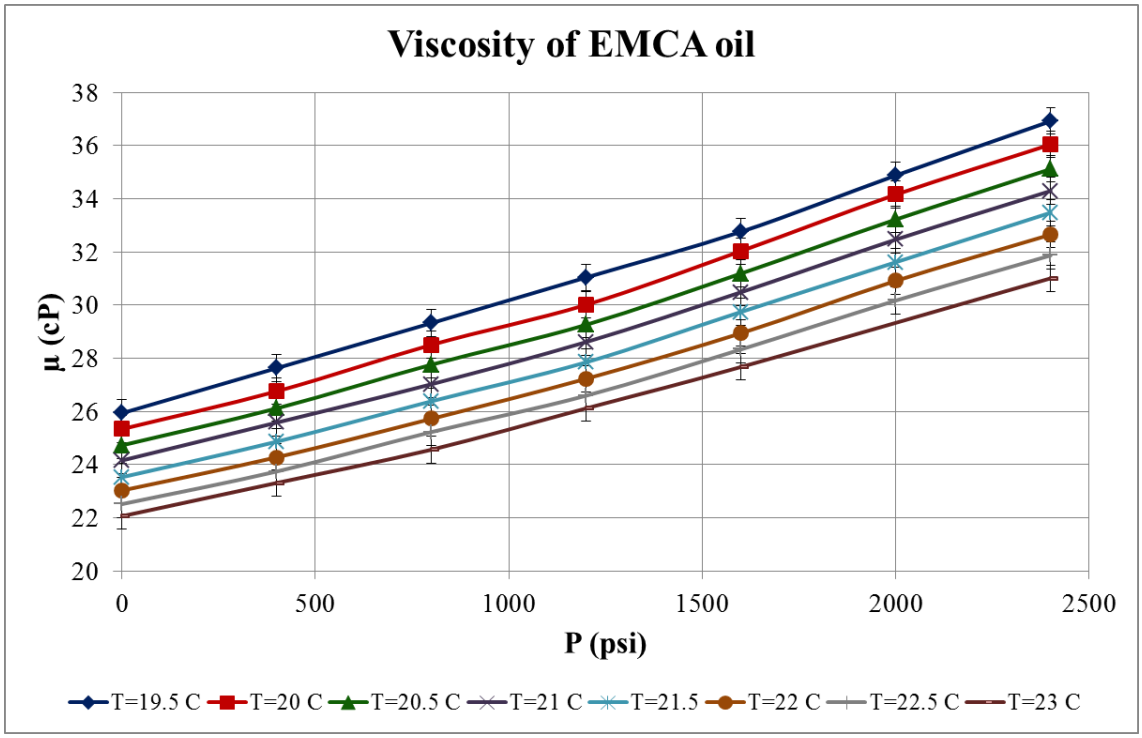

Figure 3.8. Viscosity results of EMCA oil

At least four different flow rates were used for each sample considering the high pressure pump flow rate limitations and the permeability of the rocks. For the same sample, the flow rate was only changed after the mean pressure and the differential pressure from the inlet and outlet of the core holder reached stabilization.

Figure 3.9 charts the average pressure (Pmean) and differential pressure (dP) between the inlet and outlet of the core-holder for sample D1. The plot shows that with each increase in flow rate, there was an increase in dP, as expected. Liquid permeability was calculated using Darcy's Law, after an average in the region where Pmean and dP stop varying. Similar results are shown in Figure A1 – Figure A7 (Appendix A) for the samples

C2, D3, C3, D4, C4, D5 and C5, respectively. It can be seen that for all the samples it was possible to obtain a value of liquid permeability at each flow rate, the only exception being sample D3. For the slowest flow rate, the pressure difference kept too close to the pressure gauge resolution, therefore the results were discarded. At q = 1 cc/min the pressure difference measured did not reach a stabilized value, therefore it was not possible to define a permeability value for this rate. It was not possible to carry out the liquid permeability evaluation for the samples C1 and D2 because of operational issues.

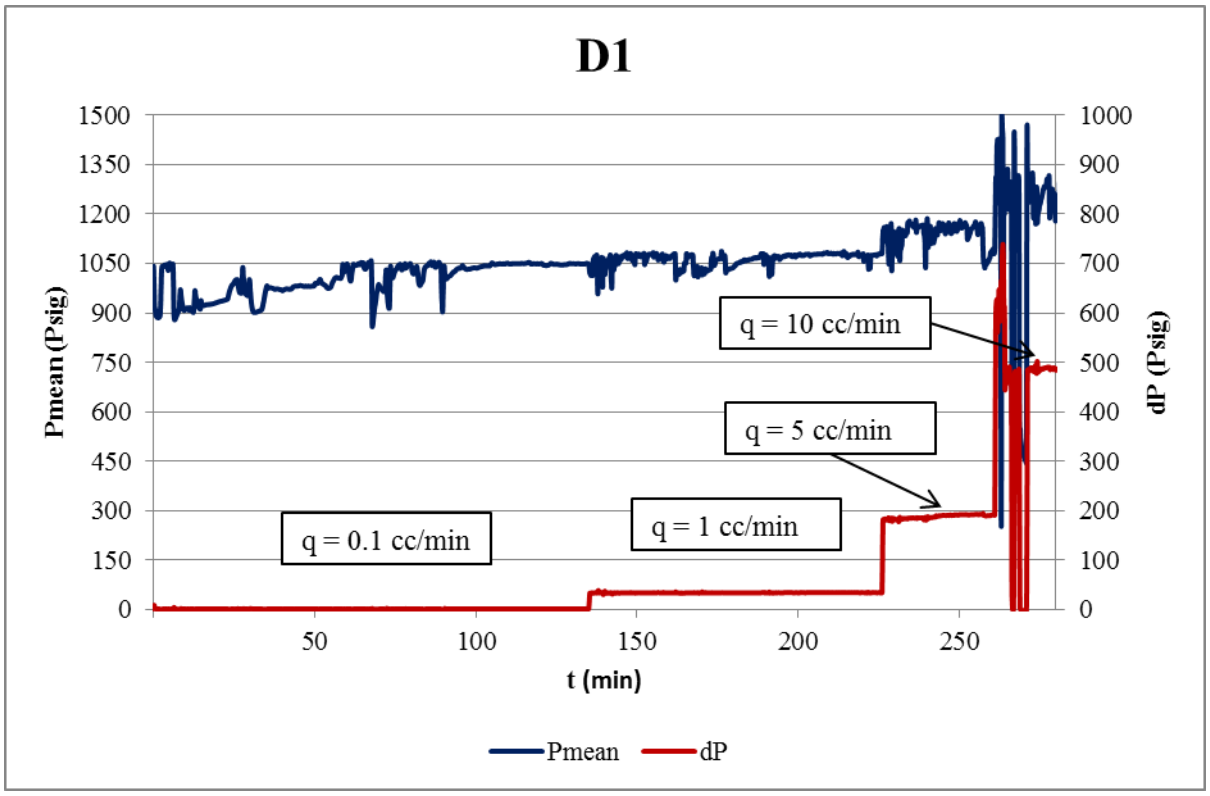

Figure 3.9. Pressure results for sample D1

The calculated values of liquid permeability are shown in Figure 3.10 and in Figure 3.11 as a function of the flow rate, for the dolomite and coquina samples, respectively. It can be seen that as the flow rate increases the permeability error decreases. Because of that behavior, the liquid permeability value for each sample was defined as the one with the lowest error.

In Table 3.2 it is shown, for comparison, the values of the average air permeability of all samples, and the calculated liquid permeability of them. In a first glance, it can be said that the simple average of the gas permeability yields permeability values closer to the liquid

permeability for the dolomite sample, but the same is not true for the coquina samples. The gas average permeability will vary depending on the pressure difference points chosen.

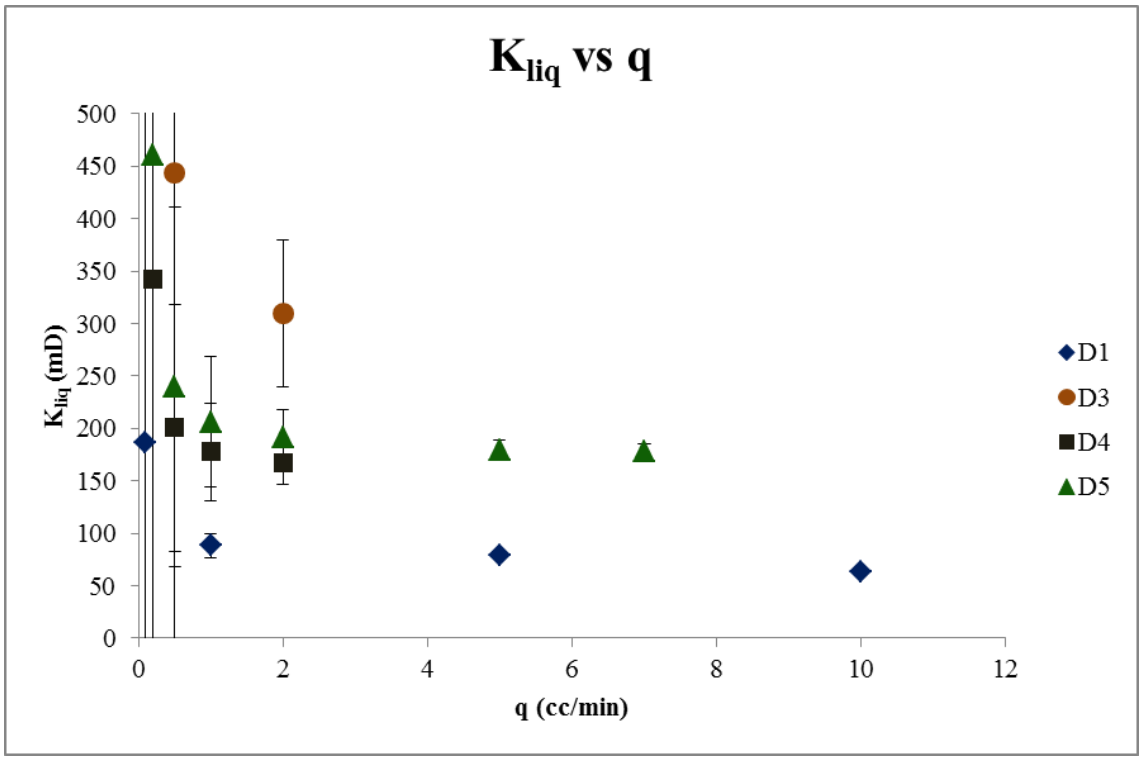

Figure 3.10. Liquid permeability versus flow rate calculated for dolomite samples

Liquid permeability may be correlated to gas permeability. As explained in Section 2.2.2, Klinkenberg (1941) provided a procedure to calculate liquid permeability of a sample using the gas permeability of the same sample, measured at more than one mean pressure. First, it is necessary to make sure that viscous flow is hold during the measurement. To do that, a plot such as the one shown in Figure 2.5 was made for each measurement, omitted here for cleanness. It confirmed that all permeability measurements, not only in this section, but of this entire dissertation, were performed in the viscous flow regime.

Second, Klinkenberg's procedure consists in plotting the measured gas permeability against the inverse of the mean pressure and fitting a line straight line to the data points. The Y-intercept of the line should be the liquid permeability. All values calculated using the procedure in the work were either too low or negative. Rushing et al (2004) mentioned in their paper that non-Darcy effects can be identified as deviations from the straight line in the Klinkenberg's plot at high mean pressure, as it can be seen in Figure 3.12.

The same behavior is seen in the permeability measurements reported here, and it will be further analyzed in the next paragraphs.

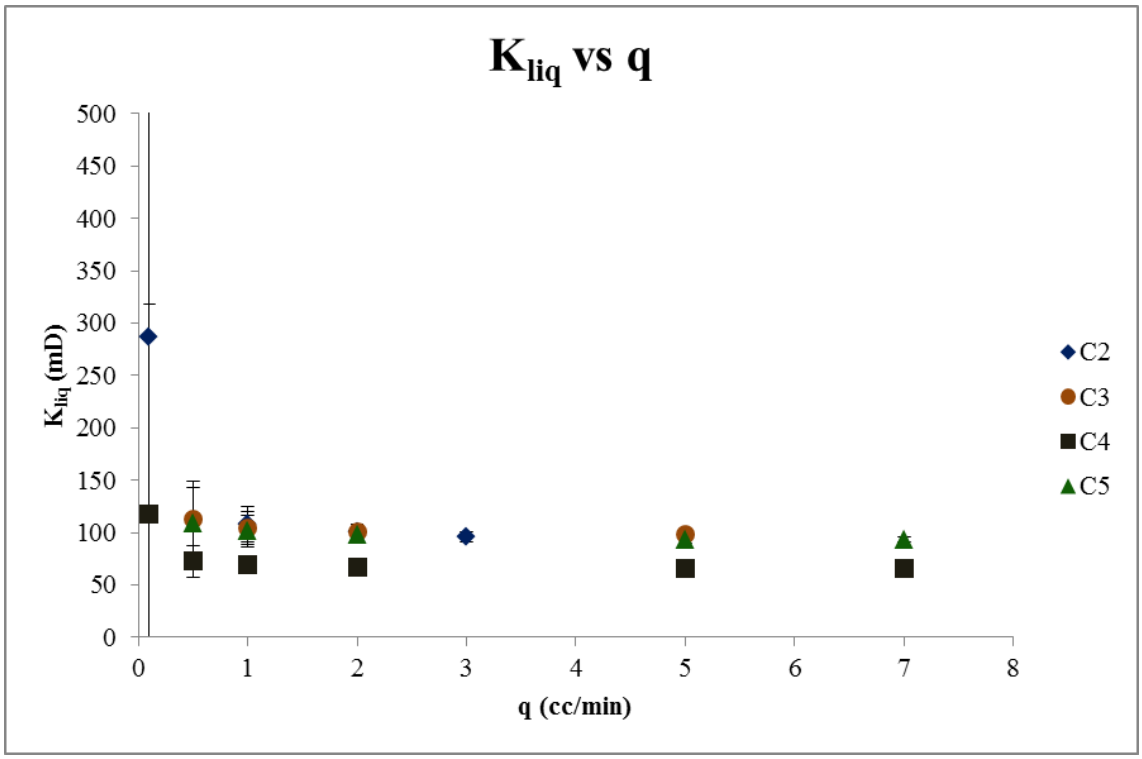

Figure 3.11. Liquid permeability versus flow rate calculated for coquina samples.

Table 3.2. Liquid and air permeability for the samples

Sample	K_{air_ave} (mD)	K_{liq} (mD)
D1	90.0 ± 1.9	79.3 ± 2.3
D2	300 ± 5.4	-
D3	318 ± 6.4	309 ± 70
D4	185 ± 3.8	168 ± 21
D5	195 ± 3.9	178 ± 7.3
C1	58.3 ± 1.1	-
C2	131 ± 2.6	95.5 ± 4.6
C3	129 ± 2.6	97.7 ± 3.2
C4	105 ± 2.1	66.1 ± 1.5
C5	130 ± 2.5	93.2 ± 2.4

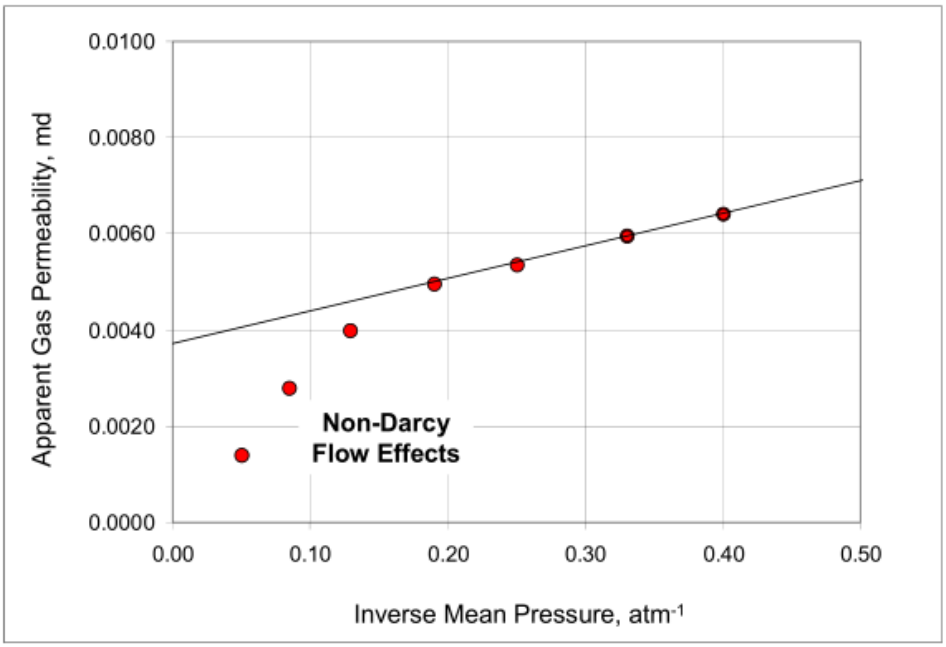

Figure 3.12. Hypothetical Klinkenberg plot showing non-Darcy flow behavior identified as deviations from line at high mean pressure (Rushing et al 2004)

The Klinkenberg plots for the samples C2 and C3 are shown in Figures 3.13 and 3.14. For samples C2 and C3, the first point measured with the lowest mean pressure was left out of analysis because it had a higher permeability error when compared with the other data points. A first linear trend line was fit, in red, with the remaining points. As it can be seen, the line fit is good, but the Y-intercept value is negative for C2. Similar results were obtained for sample C3, with the Y-intercept much lower than the measured liquid permeability . An attempt was made to fit a line with the Y-intercept fixed as the liquid permeability measured, and by eliminating from the analysis the permeability values with the highest P_{mean}. This line is shown in black. It was not possible to obtain an adequate fit. Therefore, it is probable that all the measurements of these samples were done in non-Darcy flow regime, and a correlation between gas permeability and liquid permeability cannot be obtained.

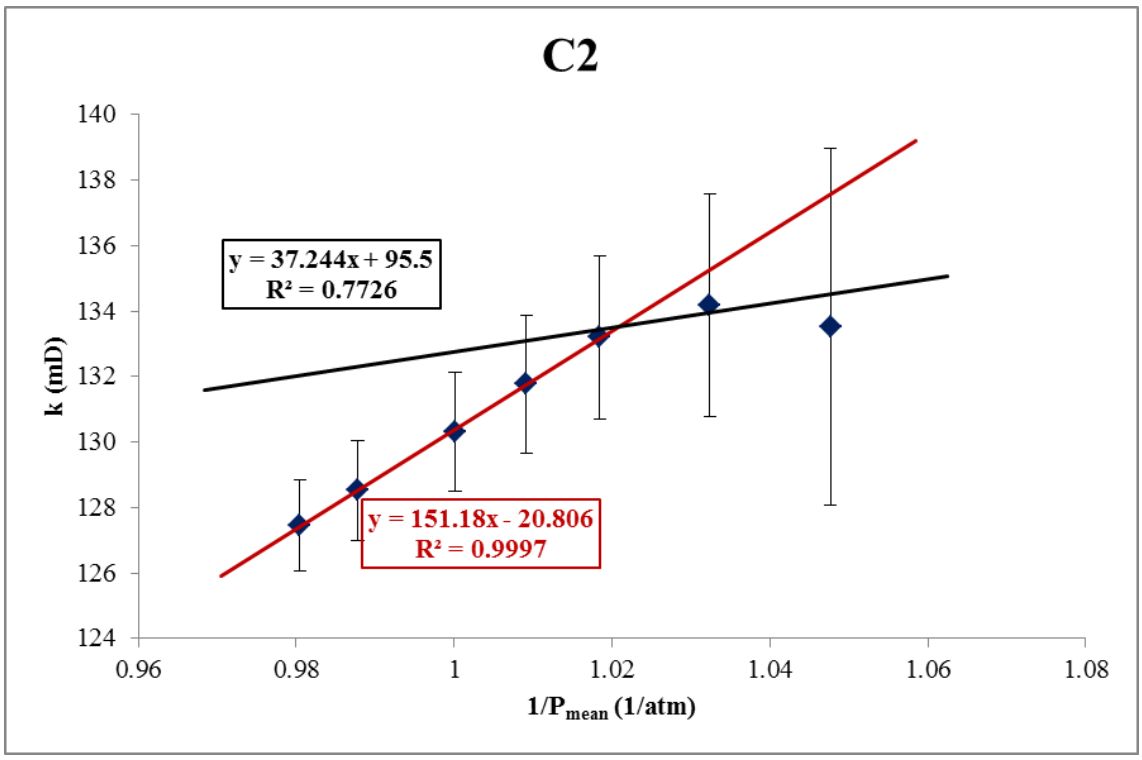

Figure 3.13. Klinkenberg plot for sample C2

The Klinkenberg plot for the sample C4 is shown in Figure 3.15. Here again the point obtained with the lowest mean pressure was not used in the analysis for the same reason as before. The same procedure was applied: the red line indicates the linear fit performed for the remaining points, rendering a very small liquid permeability value (compared with the one measured). After that, a line with the Y-intercept fixed as the liquid permeability measured was fitted using the two points with the smallest P_{mean}, after the eliminated point. The line is shown in black in the graph. This time, an adequate match was obtained. It can be seen that these two points were measured in a Darcy flow regime, while the other points clearly fall below the line, indicating that they were probably measured in a non-Darcy flow regime. Figure 3.16 shows the results of the same procedure applied for sample C5. Here no point was eliminated in the analysis. Again, the red fitted line showed a negative permeability value. The black line, with the Y-intercept fixed as the liquid permeability measured, was fit using the three points with the lowest mean pressure used in the measurement. A good match was also obtained, indicating that the points used in the matching were measured in the Darcy flow regime, and the points that do not follow this trend were measured probably in a non-Darcy flow regime.

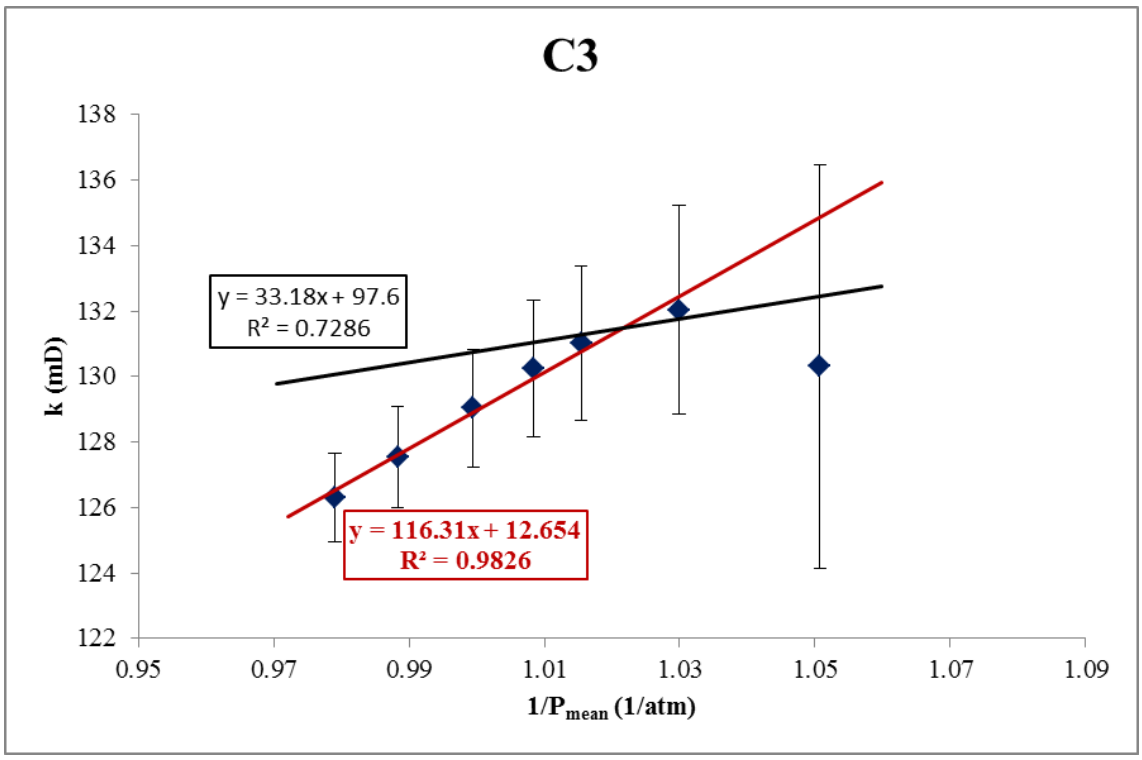

Figure 3.14. Klinkenberg plot for sample C3.

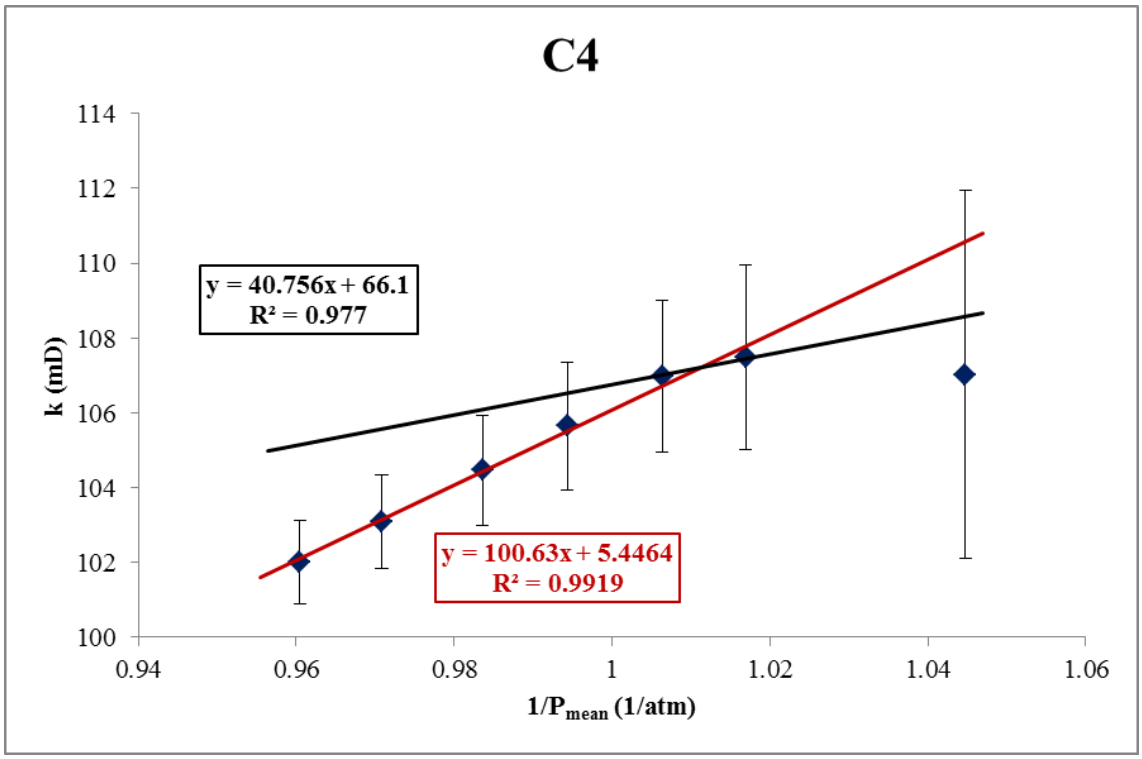

Figure 3.15. Klinkenberg plot for sample C4

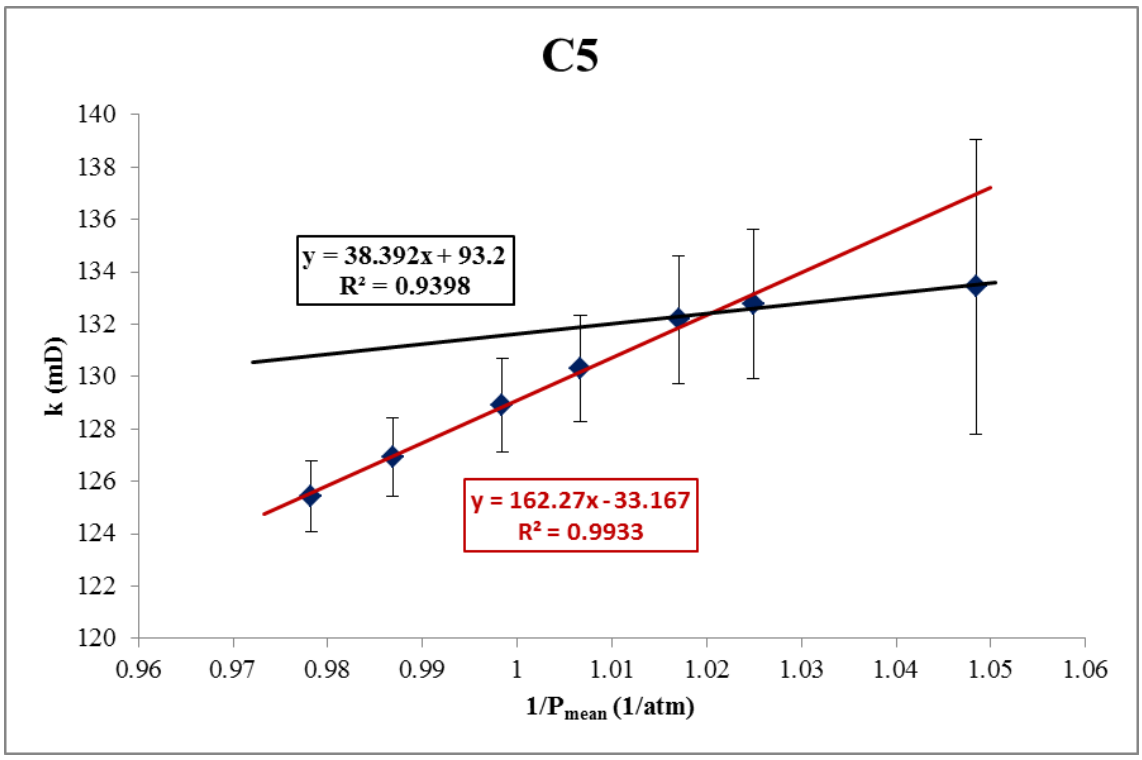

Figure 3.16. Klinkenberg plot for sample C5

Figure 3.17, Figure 3.18, Figure 3.19 and Figure 3.20 show the results of the same procedure applied for the samples D1, D3, D4 and D5, respectively. For all these samples, the two points with the smaller P_{mean} used, had to be eliminated from the curve fits, due to the high calculated errors. Again, all red fitted lines obtained a liquid permeability value either negative or significantly smaller than the liquid permeability measured. The black line, obtained by fixing the Y-intercept as the liquid permeability measured, and by eliminating from the analysis the permeability values with the highest P_{mean}. Again, it was not possible to obtain good fits for the black lines, using the procedure. This indicates that probably all the measurements, for all dolomite samples, were done in non-Darcy flow regimes, and therefore, a correlation between liquid and gas permeabilities was not obtained.

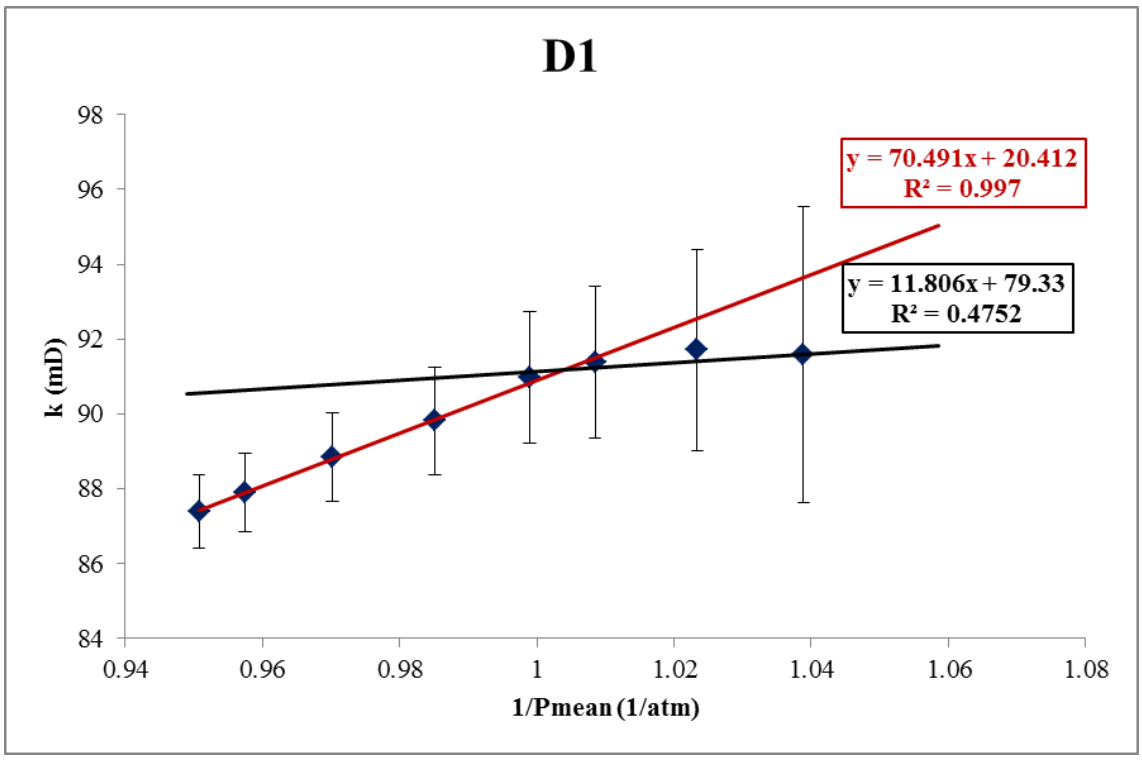

Figure 3.17. Klinkenberg plot for sample D1

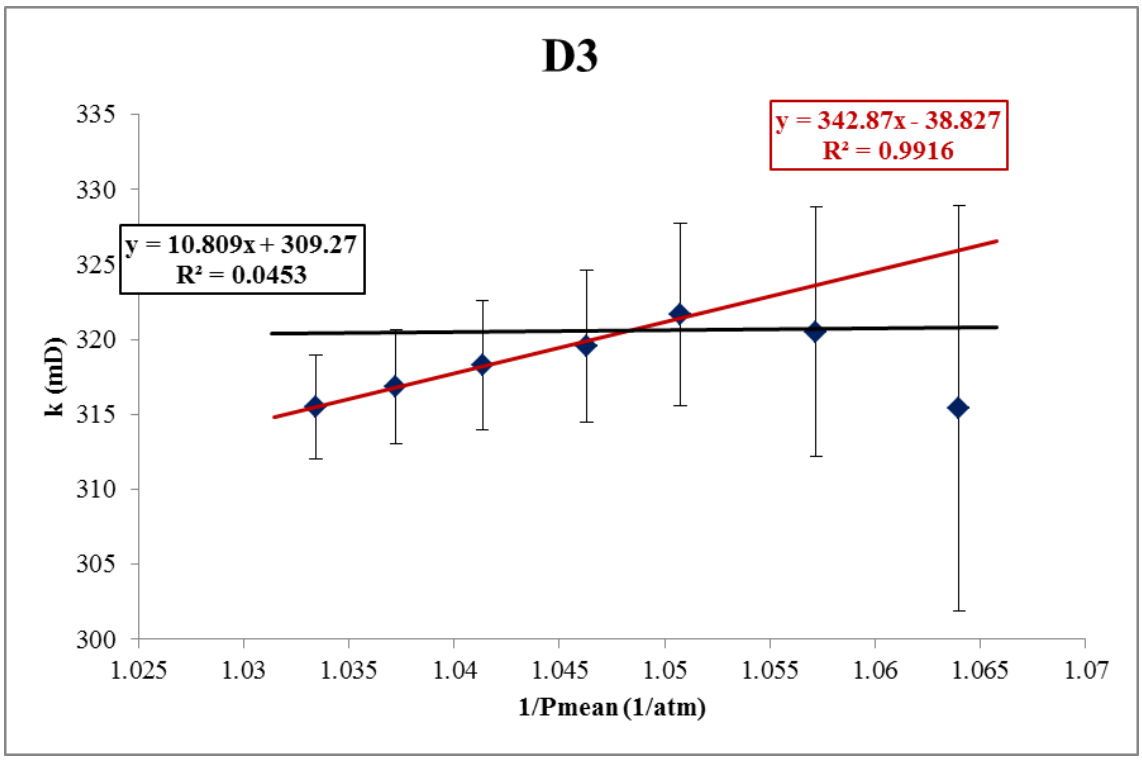

Figure 3.18. Klinkenberg plot for sample D3

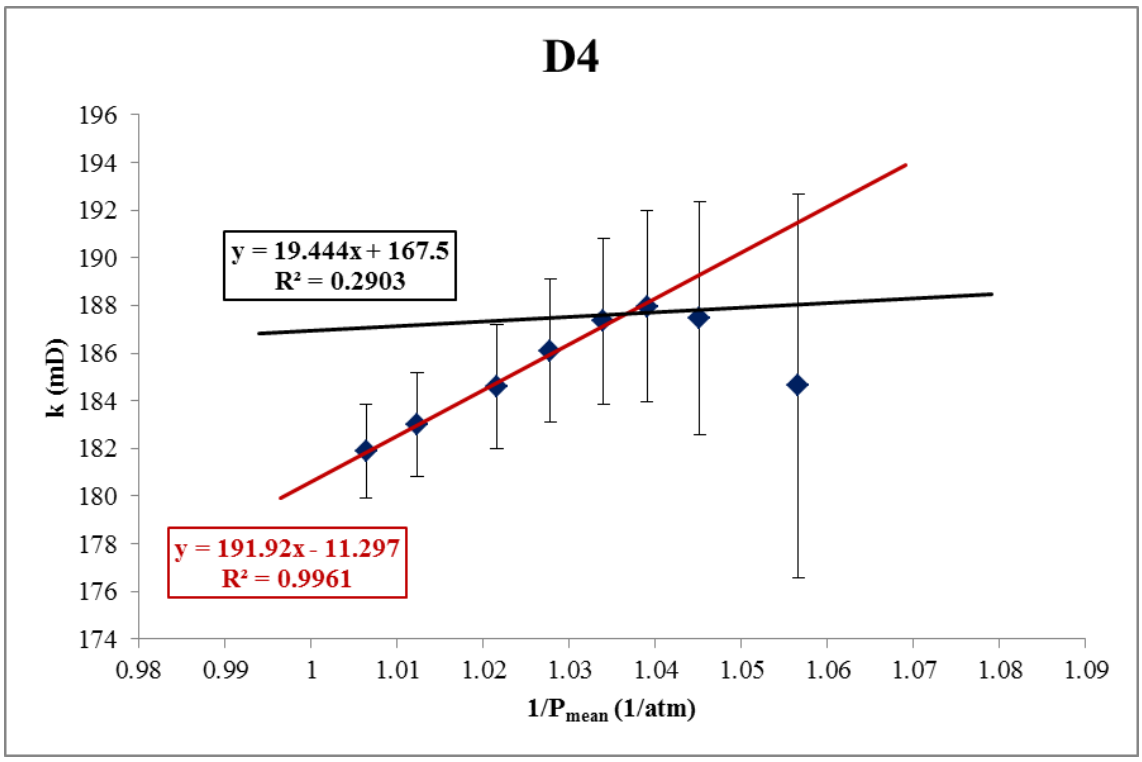

Figure 3.19. Klinkenberg plot for sample D4

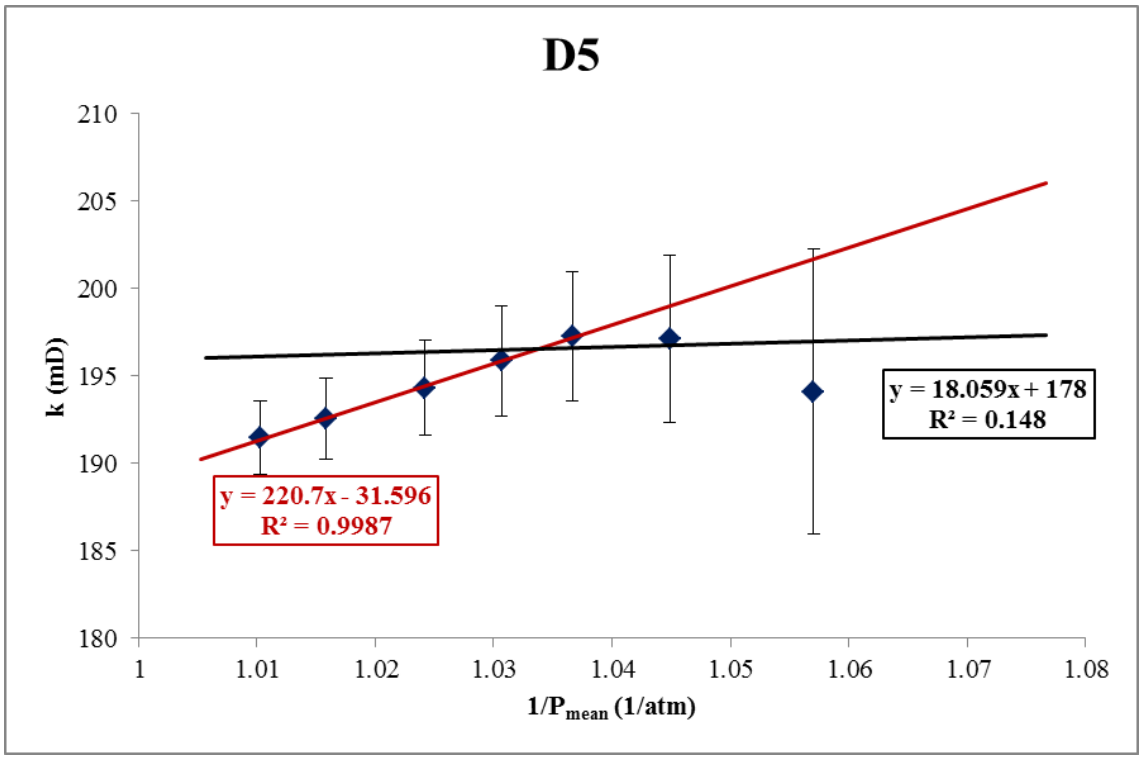

Figure 3.20. Klinkenberg plot for sample D5

3.3. Discussions

The correlation between the gas permeability and the liquid permeability was first proposed by Klinkenberg, using a plot of the gas permeability versus the inverse of the mean pressure. The experiment presented in the section showed that gas permeability values cannot be used to calculate the liquid permeability values in a simple manner. Non-Darcy flow regimes can be present in higher mean pressures measurements and for lower mean pressures the error of the permeability value is significant. The behavior was found in every sample used in this dissertation and identified as explained above.

For all the samples used, with the exception of sample C5, it was not possible to obtain reliable gas permeability values for very small mean pressure measurements. One data point had to be eliminated in the analysis of the coquina samples and two data points in the dolomite cases. The analyses point that measurements were in the Darcy flow regime only for the samples C4 and C5 , while as for the samples C2, C3, D1, D3, D4 and D5, the measurements were done in non-Darcy flow regimes at the lowest mean pressures.

The author recommends that a different experimental set up be tested in order to calculate the liquid permeability of rock samples using gas permeability data. The set up should include a back pressure regulator, because it provides improved control of gas flow rate and core differential pressure, as well as it may assist in maintaining viscous flow in higher mean pressures, as it is recommended by McPhee and Arthur (1991).

In conclusion, it was not possible to calculate the corresponding liquid permeability using only gas permeability data from the experimental set up used. As the pressure difference used in the gas permeability measurement increased, the permeability decreased more than it was expected by Klinkenberg's analysis. Therefore, the experimental study in REPEATABILITY ASSESSMENT OF GAS PERMEABILITY AND POROSITY MEASUREMENT was performed in order to evaluate if this variation in permeability is permanent and what is the best procedure for this measurement.

4. REPEATABILITY ASSESSMENT OF GAS PERMEABILITY AND POROSITY MEASUREMENT

In the previous chapter it was shown that it was not possible to obtain a general correlation between liquid permeability and gas permeability. The decrease in gas permeability with the increase in the pressure differential was higher than expected in the Klinkenberg's analysis. Therefore the current chapter will present the experimental study performed in order to evaluate if this variation in permeability is permanent and what is the best procedure for gas permeability and porosity measurement.

4.1.Materials and Methods

Industry standard gas permeabilimeter and porosimeter Ultra-Perm 500 (Figure 3.2) and Ultra-Pore 300 (Figure 3.3) are the object of the study. They were used connected to a pure N_2 source. The rock samples were two dolomites (from Silurian Formation, USA), two coquinas (from Morro do Chaves Outcrop, Brazil) and two sandstone (from Botucatu Formation, Brazil) all measuring 1" in diameter by 1" in length. For the permeabilimeter study,a metallic standard was also used.

The study of the gas permeabilimeter was designed to cover a range of pressure differences as wide as possible, exploring the equipment range. The equipment is limited in the experiment by its flow transducer, which did not allow the pressure difference to go high., Four levels of pressure difference were considered for every sample.

The study procedure was to load the sample into a core-holder, submit it to a confining pressure of 600 psi and measure permeability in four pressure differences, pre-defined in an increasing pressure order. The sequence is called here a cycle of permeability measurements. For each sample, the flow direction of the permeability measurement was also noted, either as the upward or downward flow. The first test consisted of 10 cycles of permeability measurements in alternating flow directions, followed by a 5 min injection of N2 at 290 psi in the upward direction. The procedure was repeated one more time and the experiment finished with 6 cycles of permeability measurements in alternating flow directions. The permeability error was calculated as explained in APENDIX B.

For the study of gas porosity measurement, one cycle was determined to be the procedure of injecting the sample with N2 and measuring its porosity. The cycle was then

repeated 7 times. The injection of N2 was made in the same flow direction at 290 psi and during 5 min. Each porosity measurement, for every cycle, was performed 5 times, so that a standard deviation could be calculated.

4.2. Results

Figure 4.1 shows the results of the permeability measurement study for the metallic standard. This metallic standard is made of an outer metallic shell filled with consolidated grains with a determined permeability. Note that between cycles 10 and 11, as well as, between 20 and 21, it was when the N_2 burst at 290 psi for 5 min took place. It can be seen that, the average permeability at each cycle changed very little (less than 1% difference) and within the calculated error, even after the N_2 burst. In the same cycle, the permeability varied less than 2%, and it is also within the calculated error.

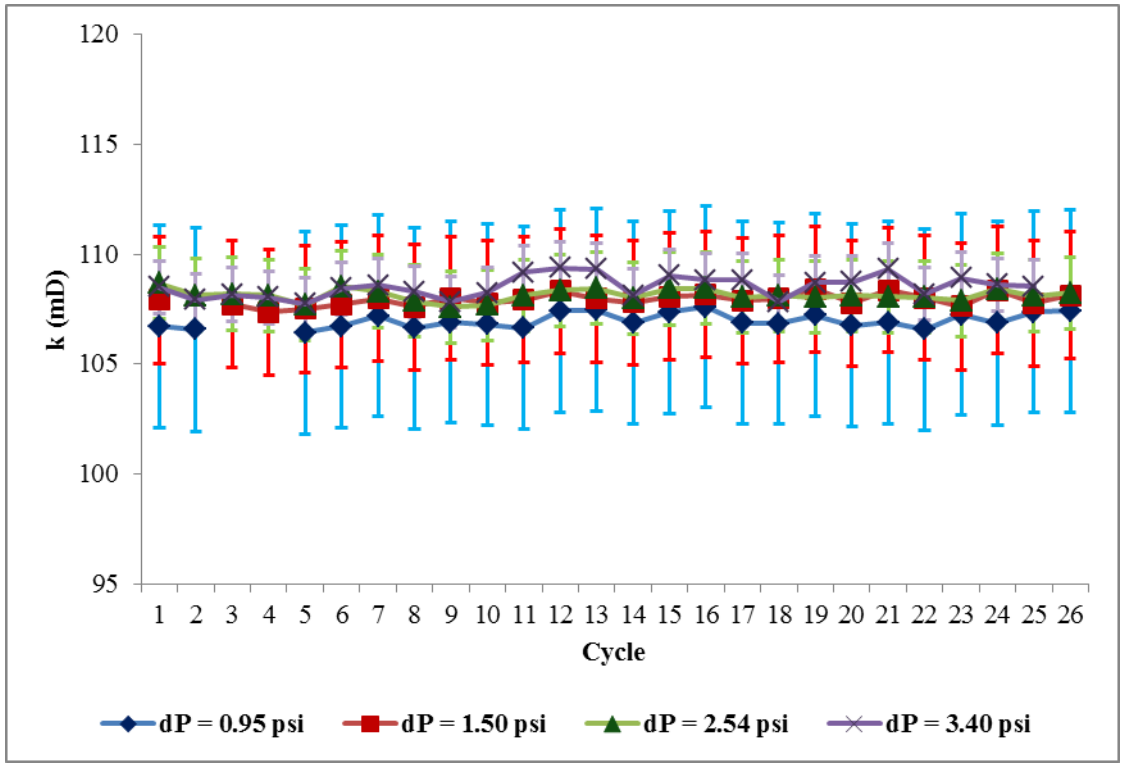

Figure 4.1. Gas permeability measurement results for the metallic standard

Figure 4.2 depicts the results of the permeability measurement study for the sandstone sample. The sample is fairly homogeneous and well sorted. It can be seen that before the first N_2 burst, the permeability varied 2% between measurement cycles. This

variation is within the measurement error. After the first N_2 burst, there was a 5% decrease in the permeability from cycles 10 to 11, and this value was maintained in the following measurement cycles. This can mean that this sample was not very well consolidated, since the injection of the N_2 at 290 psi was enough to decrease its permeability. Within the same cycle, the permeability varied 2%, which is within the calculated measurement error.

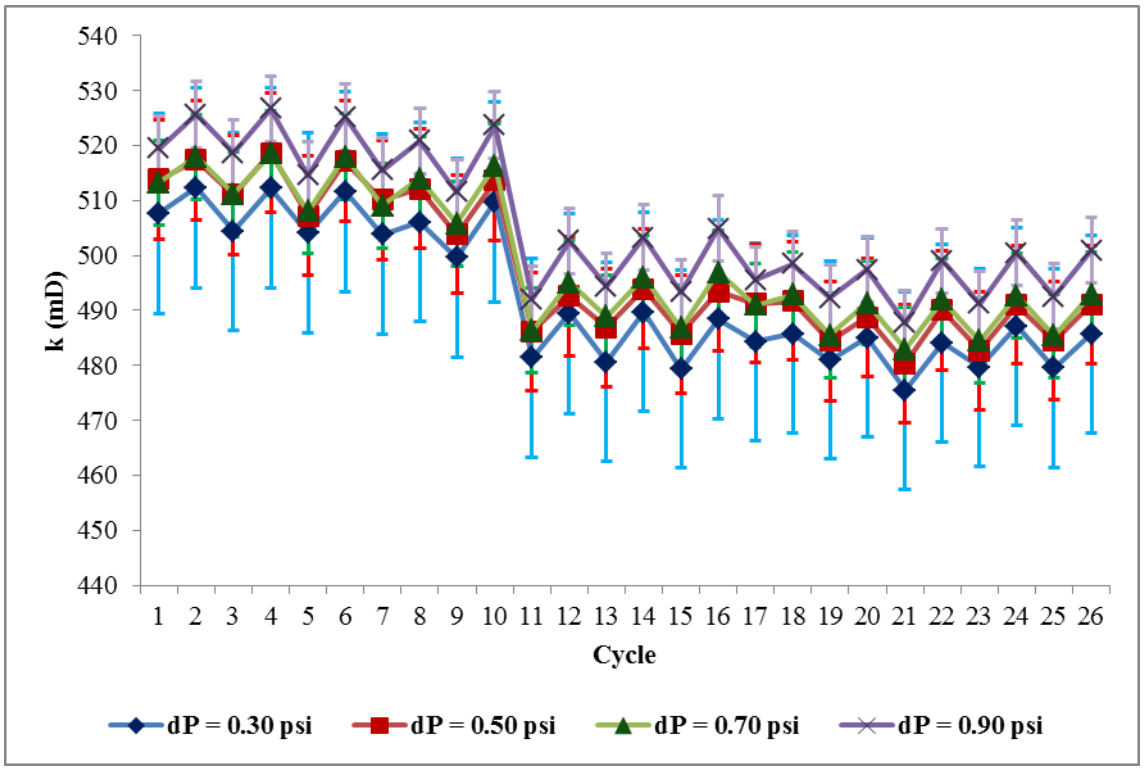

Figure 4.2. Gas permeability measurement results for the sandstone sample

The next set of results can be seen in Figure 4.3 for the permeability measurements of the coquina sample. It can be seen that the average permeability varied less than one 1% before and after cycle 6 where a 15% increase in permeability happened. This is maybe due to the poorly-consolidated nature of this sample, which could cause movement of particles from one pore throat to the other and this permeability increase may have been caused by the unblocking of a pore throat with one such particle. In the same cycle a difference between the lowest and highest pressure difference of around 5% is seen, and as the pressure increases there is a decrease in permeability. This is the behavior expected when the slippage effect takes place, but as it was discussed in the previous chapter, due to non-Darcy flow effects it was not possible here as well to perform a Klinkenberg analysis and calculate the liquid permeability of the sample.

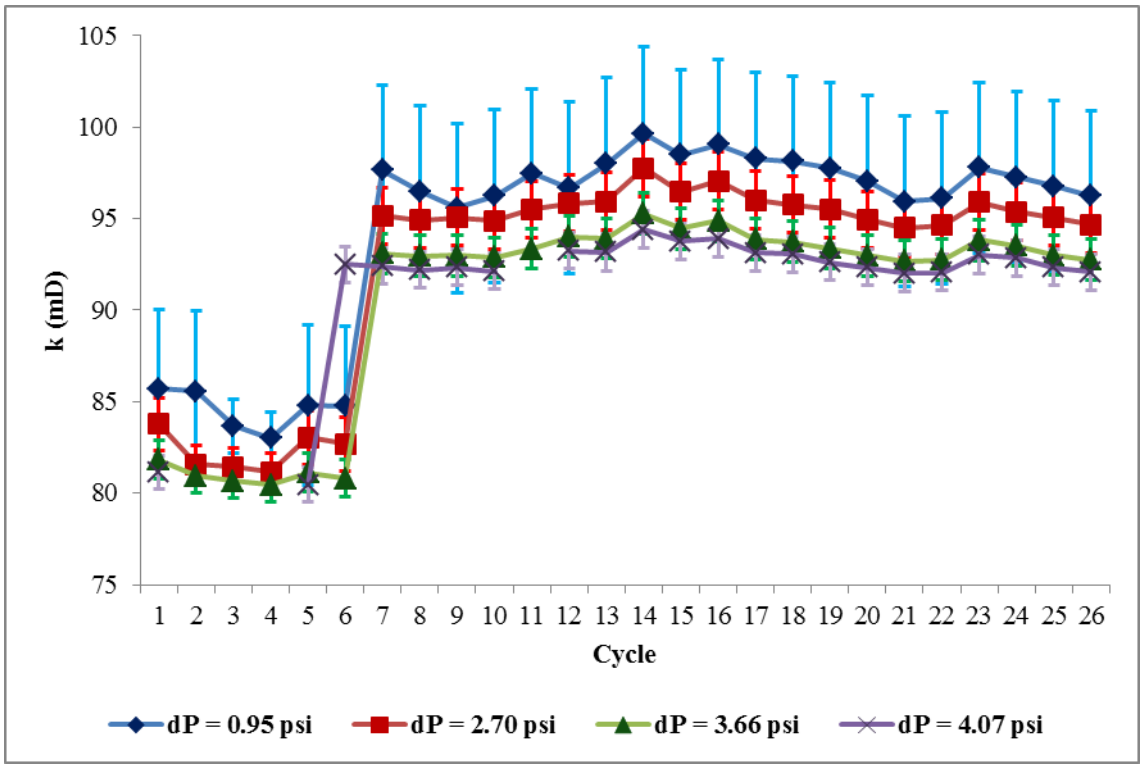

Figure 4.3 Gas permeability measurement results for the coquina sample

The final set of experiments for the permeability measurement study is shown in Figure 4.4, where it is found the permeability results for the dolomite sample. These results showed less than 1% variation on the average permeability except for the first N2 burst which caused a 2.5% permeability decrease and the second, which caused a 1.5% increase. These changes of average permeability before and after the N_2 burst is probably an indication of the unconsolidated nature of outcrop samples that as it was explained for the coquina sample, may have very small particles that can move from one pore throat to another causing blockage and opening of the path for fluid flow. It can also be seen that in the same time-step the difference between the highest and lowest permeability are around 10% and as the pressure increases, the permeability decreases, as expected due to the gas slippage effect takes place. For the dolomite sample, this permeability difference in the same time-step was twice as higher than for the coquina samples. This effect was also seen in COMPARISONS OF GAS AND LIQUID PERMEABILITY.

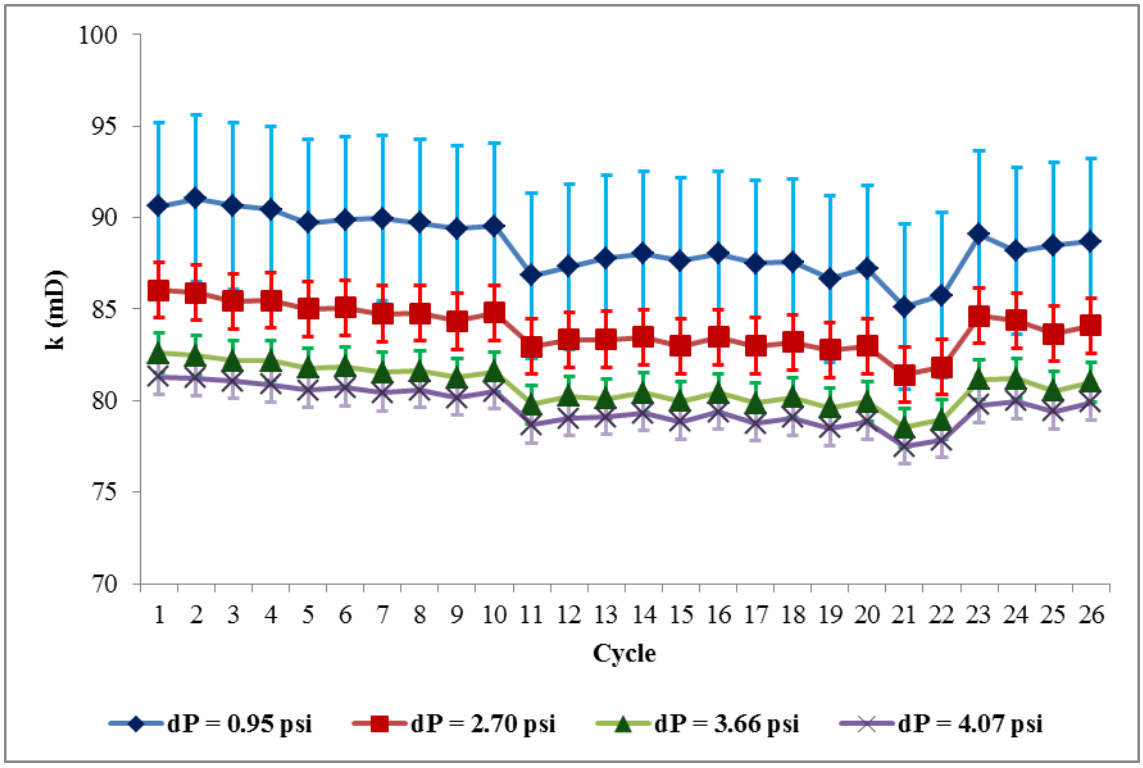

Figure 4.4. Gas permeability measurement results for the dolomite sample

The results for the last 3 samples are shown in Figure 4.5. In the graph the permeability of each sample was normalized with its initial permeability for easier comparison. It can be seen that if the effects of the permeability changes due to the presence of unconsolidated grains in the samples (like the sudden change in permeability in the coquina sample) are not taken into consideration, the average value of consecutive permeability measurements, done within the same pressure difference range, can be compared within the measurement error. This means that the gas permeability measured in the Ultra-Perm 500 can be used to evaluate permeability changes in samples if the measurements are made using always the same flow conditions (flow rate or pressure difference).

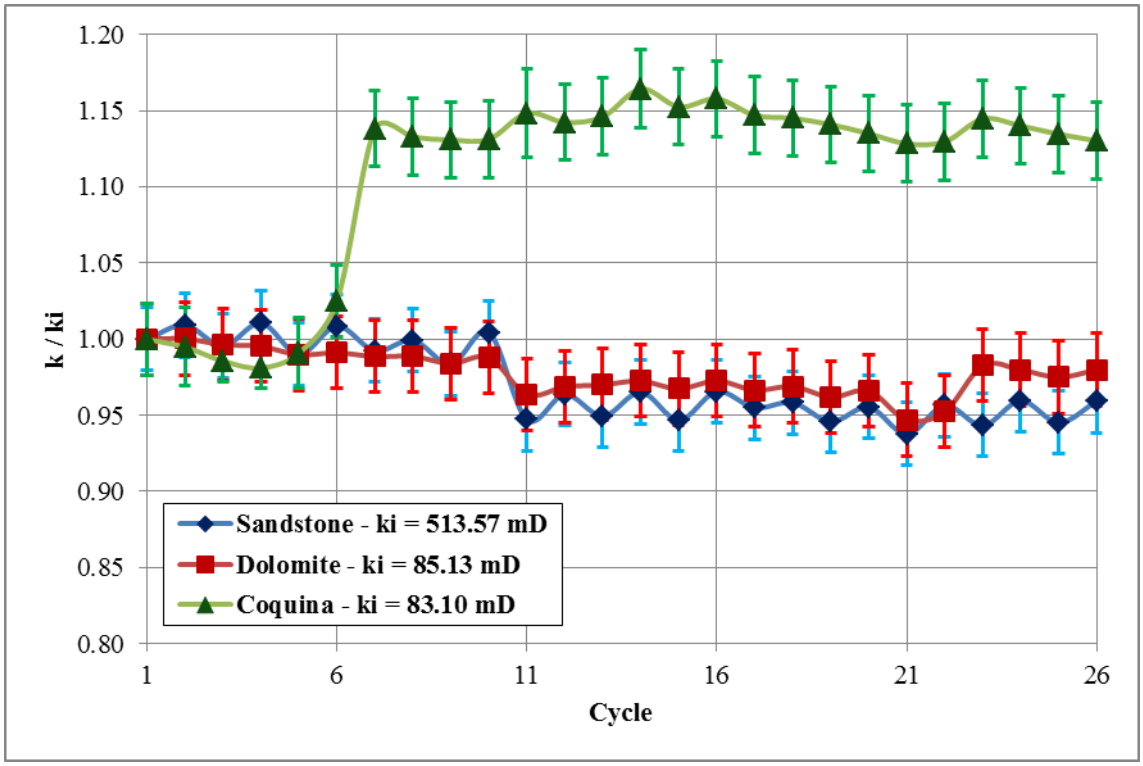

Figure 4.5. Normalized results for the permeability measurement experiment for sandstone, dolomite and coquina samples

Besides the permeability measurement study, a porosity study was also carried out, to evaluate the Ultra-Pore 300 precision and the conditions that the measurements can be best done. It was not necessary to use a standard plug, because the measurement of porosity is performed by calibrating the equipment using closed metallic cylinders. Therefore, before using the equipment, a calibration is performed for a set of metallic cylinders with defined grain volumes. The calibration is then used to calculate the grain volume of each sample.

During this experiment, it was found that the calibration does not last for more than 5-10 measurements. It is speculated that the changes in the temperature of the cylinder of N_2, located outside of the laboratory, can change significantly (especially in the middle of the day) causing the calibration to expire. That is why, in this experiment, the calibration was performed for every new 5 porosity measurements.

The results of the study are shown in Figure 4.6. It can be seen that the N_2 burst did not only increase porosity but also decreased it. This decrease in porosity is only possible because the gas porosimeter measures the effective porosity. Therefore, due to the poorly-consolidated nature of the samples and possibly the presence of fine particles, the N2 burst caused the isolation of pores (by blockage of pore throats) or the addition of pores (by unblocking of pore throats).

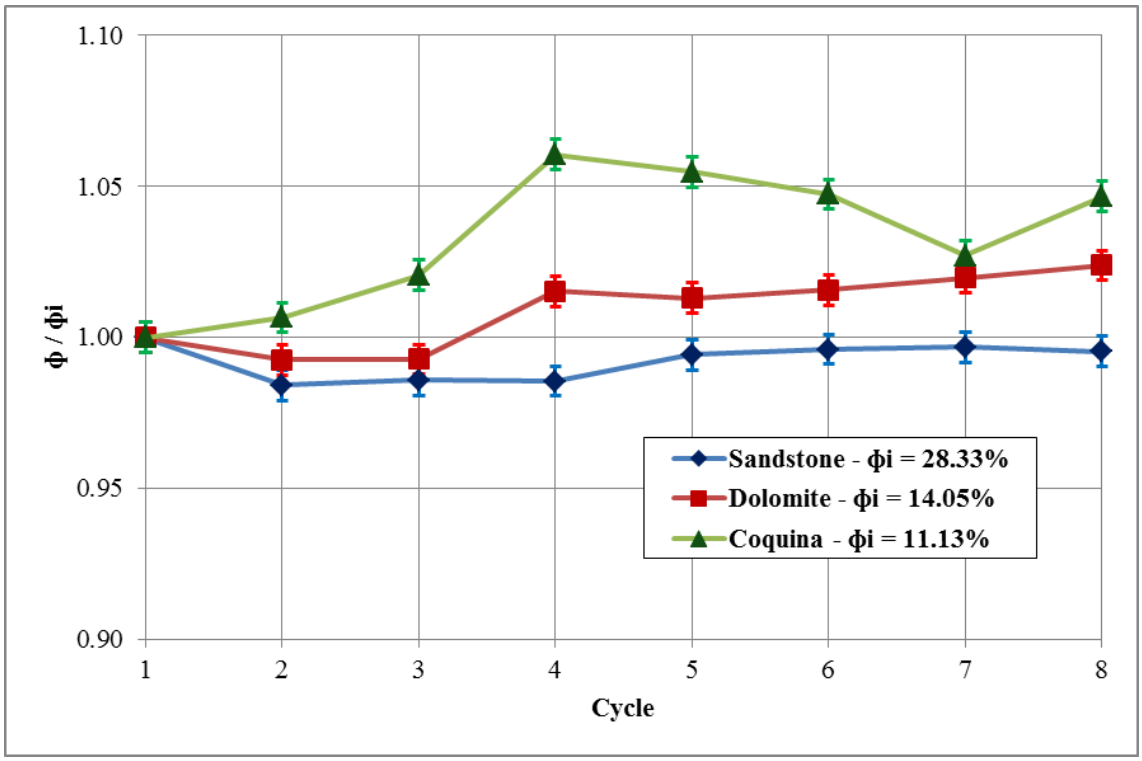

Figure 4.6. Normalized results for the porosity measurement experiment for sandstone, dolomite and coquina samples

4.3. Discussions

The main objective of this dissertation is to evaluate how permeability and porosity of carbonate rocks changes due to exposure of CO_2 and water at conditions close to that of the pre-salt reservoirs the effects. Therefore, permeability and porosity are key properties that need to be properly measured and compared in laboratory conditions. In COMPARISONS OF GAS AND LIQUID PERMEABILITY it was shown that it was not possible to obtain a general correlation between the gas permeability and liquid permeability. Generally, the decrease in gas permeability with the increase in the pressure differential was higher than expected in the Klinkenberg's analysis.

In the current Chapter it was presented an experimental study evaluate if this variation in permeability is permanent and what is the best procedure for gas permeability and porosity measurement. It was seen that this change in permeability with increase in measurement pressure is not permanent for any of the samples. It was also shown that the average permeability for the same sample, measured in similar conditions (same pressure

difference or gas rate), can be used to evaluate changes in a sample's permeability within measurement error. The gas porosity measurement can also be used, with the condition that a calibration is performed after every 5 consecutive porosity measurements.

The samples of sandstone, coquina and dolomite used in this study are not so well consolidated, since considerable changes in permeability and porosity took place due to the N_2 burst and sometimes even before (as it was seen for the coquina sample). It is reasoned that these changes are due to movements of fine particles in the pore system, blocking or releasing the flow path. Another conclusion that can be made from this study is that for homogeneous and grained samples, such as the metallic standard and the sandstone samples, it was not possible to detect the typical changes of permeability due to the slippage effect.

5. DISSOLUTION OF CARBONATE ROCKS: EFFECTS OF PRESSURE

Chapters 3 and 4 of this dissertation addressed the secondary objective of this work, which is to delineate the best practices for measuring porosity and permeability in laboratory conditions. study the current methods of measuring the permeability and porosity of carbonate core samples and determine the best procedure to do so. It was shown that the average permeability for the same sample, measured in similar conditions (same pressure difference or gas rate), can be used to evaluate changes in a sample's permeability within measurement error. This conclusion was taken into consideration in the following chapters whenever the permeability and porosity of the samples were measured.

This chapter addresses the main objective of this work, which is to evaluate how permeability and porosity of carbonate rocks changes due to the exposure of CO_2 and water at conditions close to that of the pre-salt reservoirs (9,000 psi and 64^oC). The experimental study presented here was designed to evaluate how the permeability and porosity of coquina and dolomite outcrop rocks varies in fresh water/CO_2 systems, with increasing pressure (up to 9,000 psi) at constant temperature (64^oC).

5.1.Materials and Methods

In the study, 5 core samples of coquina (from Morro do Chaves outcrop, Brazil) and 5 of dolomite (Silurian Formation, USA), measuring 1" in diameter and 1" in height were used. All the experiments were performed at 64^oC and each of 5 dolomite samples and 5 coquina samples were tested at pressures of 500 psi, 2,000 psi, 4,500 psi, 6,500 psi and 9,000 psi. Table 5.1 shows a list of the samples with their assigned pressure.

Table 5.1. Samples names and assigned pressures

Sample	P (psi)
D11	500
D13	2,000
D14	4,500
D15	6,500
D16	9,000

C12	500
C13	2,000
C14	4,500
C16	6,500
C18	9,000

The rock characterization procedure performed on these samples consisted of the sequence: mass measurement using a semi-analytical scale, permeability measurement with the Ultra-Perm 500 (Figure 3.2) connected with a filtered air source and the porosity measurement with the Ultra-Pore 300 (Figure 3.3) connected with a pure N_2 source. Permeability measurements in each sample were done at five different pressure differences, which did not changed in the entire experiment. The permeability error was calculated as explained in APENDIX B. The porosity measurement was done five times for each sample, so that a standard deviation could be calculated.

To begin the experiments, all the samples were characterized, using the aforementioned procedure. After that, each rock was loaded in a high pressure vessel (Figure 5.1) with 20 ml of fresh water. Then, a high pressure transfer cylinder (Figure 5.2) was filled with CO_2. They were both left in an air bath heater (Figure 5.3) until they reached the desired temperature of 64^{o}C. The high pressure transfer cylinder was then connected by the hydraulic fluid end to the high pressure pump (Figure 5.4) and to the high pressure vessel in the CO_2 end. The experimental set up can be seen in Figure 5.5. Next, CO_2 was injected in the vessel until it reached the assigned pressure and was left pressurized for 48h in the heater. In the end, the vessel was depressurized, the remaining water was collected and the sample was dried at 80^{o}C for 16 hours in the heater and the rock characterization repeated. The entire procedure, starting from the characterization of the rocks, was repeated 5 times for each sample, resulting in a total of 240 hours of experiment. The remaining water from samples D11, D14, C12 and C14 were taken to an analytical laboratory to determine the Mg^{2+} Ca^{2+} concentrations at time-step t=48, 144 and 240 hours, while the water from samples D16, C18 were taken for the same analysis at every time-step.

Figure 5.1. High pressure vessels

Figure 5.2. High transfer cylinder

Figure 5.3. Air bath heater

Figure 5.4. High pressure positive displacement pump

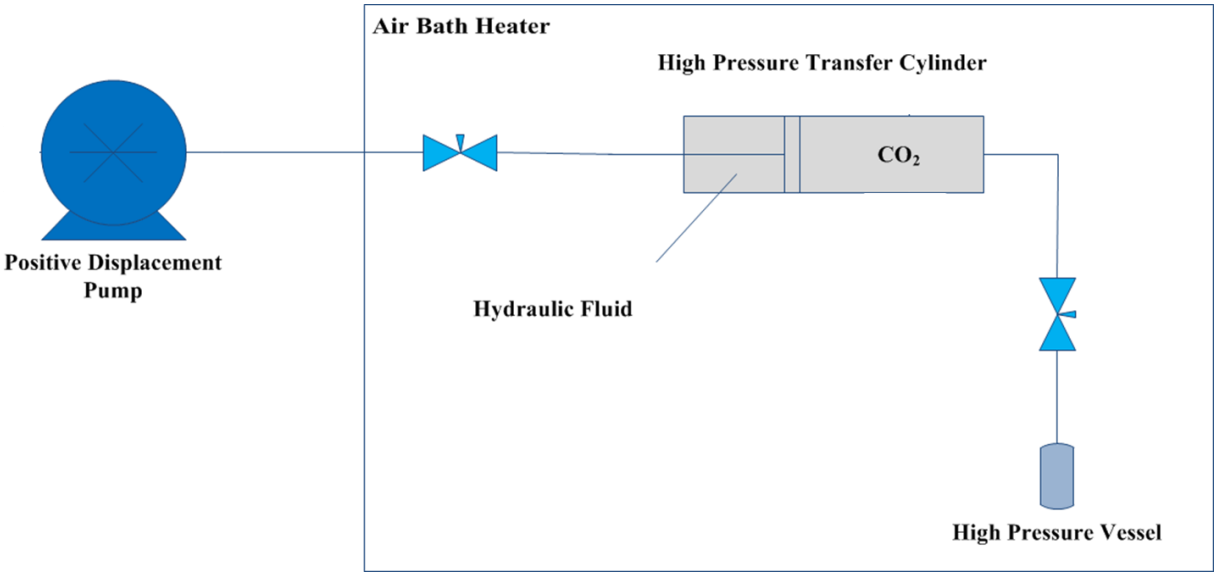

Figure 5.5. Experimental set up

5.2. Results

The results of the initial rock characterization are shown in Table 5.2. Figure 5.6 shows the mass variation results for the dolomite samples. These results are presented in a normalized form, so that the comparison between samples can be better visualized. It is important to note that sample D14 broke in the fourth time step and was reconstituted to continue the experiment. The mass, permeability and porosity variations from the breakage was measured but not considered in the analysis.

Table 5.2. Initial rock characterization of the samples

Sample	m_i (g)	ϕ_i (%)	K_i (mD)
D11	28.99	16.12±0.08	42.1±0.8
D13	31.42	13.45±0.07	5.27±0.3
D14	28.78	17.30±0.09	135±2
D15	28.75	18.60±0.09	242±5
D16	30.87	15.36±0.08	43.7±0.8
C12	28.03	14.12±0.07	14.4±0.2
C13	29.42	12.13±0.06	2.41±0.2
C14	28.87	9.32±0.05	2.47±0.2
C16	29.08	11.28±0.06	9.42±0.2
C18	25.25	13.39±0.07	5.42±0.2

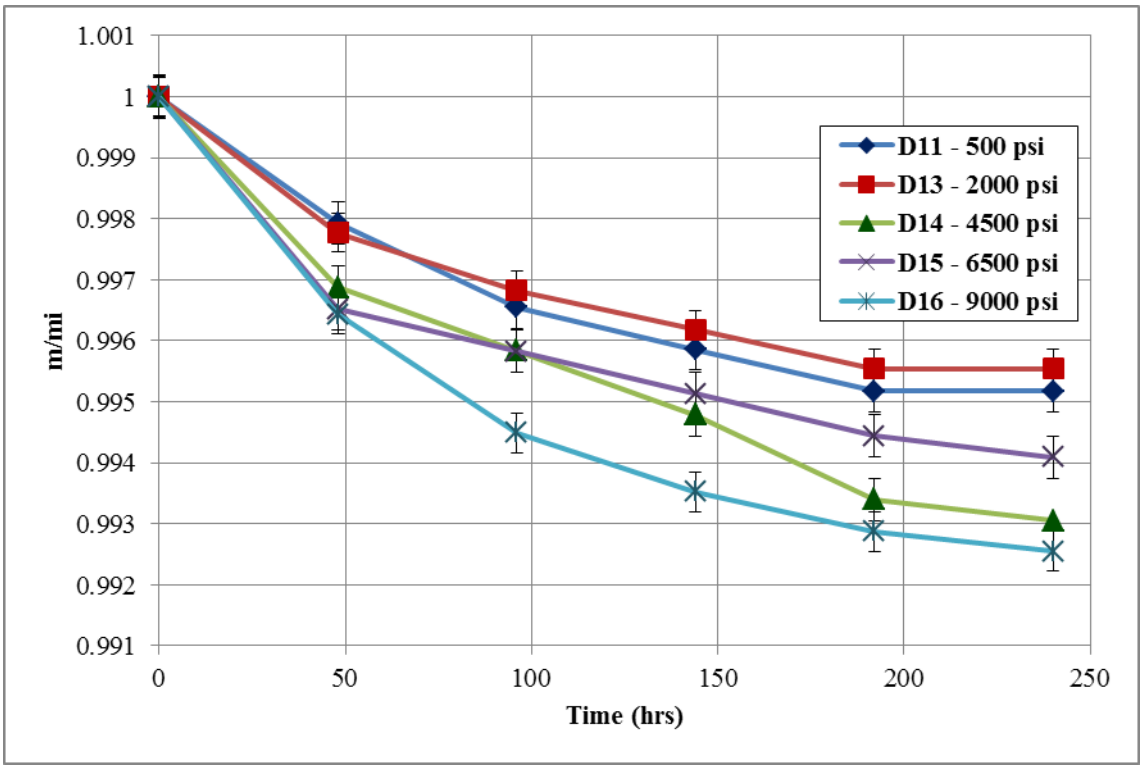

Figure 5.6. Dolomite mass variation vs time with varying pressure

In the batch reactor dissolution experiments, the whole system is static in constant pressure and temperature conditions, with an excess of CO_2. Therefore, it is expected that dissolution takes place during the entire experiment. The total mass of the samples is inversely proportional with dissolution rate, consequently all the samples showed a negative mass variation. There was an overall tendency of decrease in mass variation with time.

Equations (2.20) - (2.23) show the dissolution reaction of dolomite and limestone. The reactants in the reactions are carbonic acid (formed by the reaction of CO_2 and water) and the minerals of dolomite or limestone. As the pressure of the experiment increases, the amount of CO_2 dissolved in water increases, and the amount of carbonic acid is also higher. Also, the amount of dolomite and limestone available for the reaction is directly proportional to porosity Therefore, it is expected that as the dissolution rate is directly proportional to the pressure of the system and the porosity of the sample.

Sample D16, submitted to the highest pressure, showed the highest dissolution rate as expected. In the lower pressure spectrum, sample D13 that was assigned to the pressure of 2,000 psi, presented a lower mass loss (lower dissolution rate) than sample D11,

assigned to the pressure of 500 psi. This happened because the porosity of sample D11 is considerably higher than that of sample D13. Looking at the results of the last two samples left, D14 and D15, it can be seen that in time-step 1, sample D15 with the highest working pressure (6,500 psi) showed a higher dissolution rate than sample D14 (working pressure of 4,500 psi). After that, the mass loss of sample D14 increased a lot, especially after breakage. It is possible that this last sample was more fragile than the others and the mass loss cannot be attributed only to the dissolution reaction.

Figure 5.7 shows the permeability results for the dolomite samples. As discussed in Section 2.3, dissolution is related with increases in permeability, while deposition with decreases in permeability. In the considered static regime, it is expected that only dissolution occurs, with increases in permeability. As it can be seen in the aforementioned plot, decreases in permeability also took place. By analyzing the experimental methodology further, it can be concluded that since the permeability measurement is made after the depressurization of the system, which may cause deposition to occur.

Therefore, the decreases in permeability seen in the graph of Fig 5.7 may not be due to the intended experiment, but an artifact brought in by the depressurization after the experiment. Comparing the permeability results with the mass variation results, for each sample, it can be seen that the sample that presented the highest dissolution rate, presented also the lowest change in permeability. Sample D14 showed the higher permeability variation, with an increase in the permeability after the fourth time-step, even after the increase in permeability due to the breakage was removed from the analysis.

The porosity results for the dolomite samples are shown in Figure 5.8. Overall, there were very small changes in porosity to the negative and to the positive side. The changes in porosity to the negative side can be explained in the same way as it was for permeability, since the equipment used measures effective porosity. The two samples that sustained the highest change in porosity were D16 and D11. The D16 sample (working pressure of 9,000 psi) was the one with the highest dissolution rate, therefore its porosity increased. The D11 sample (working pressure of 500 psi) presented the second lowest dissolution rate, but since its permeability changed markedly to the negative side, this may have an effect in the effective porosity as well.

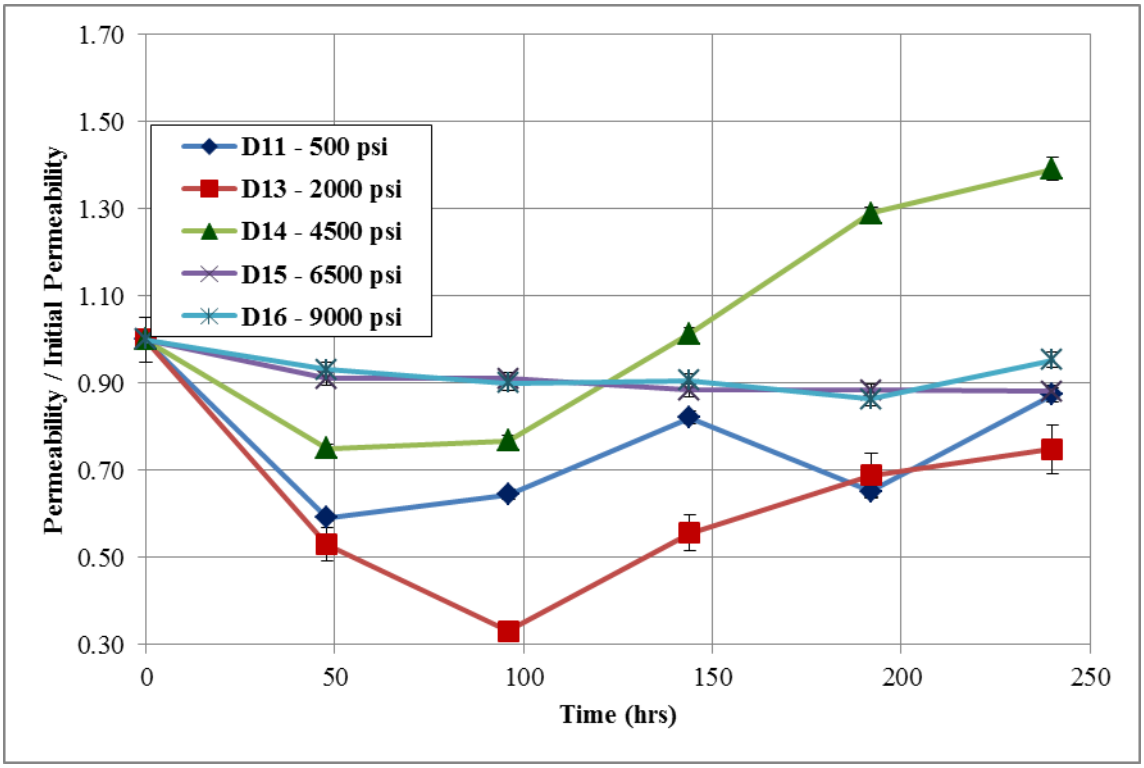

Figure 5.7. Dolomite permeability variation vs time.

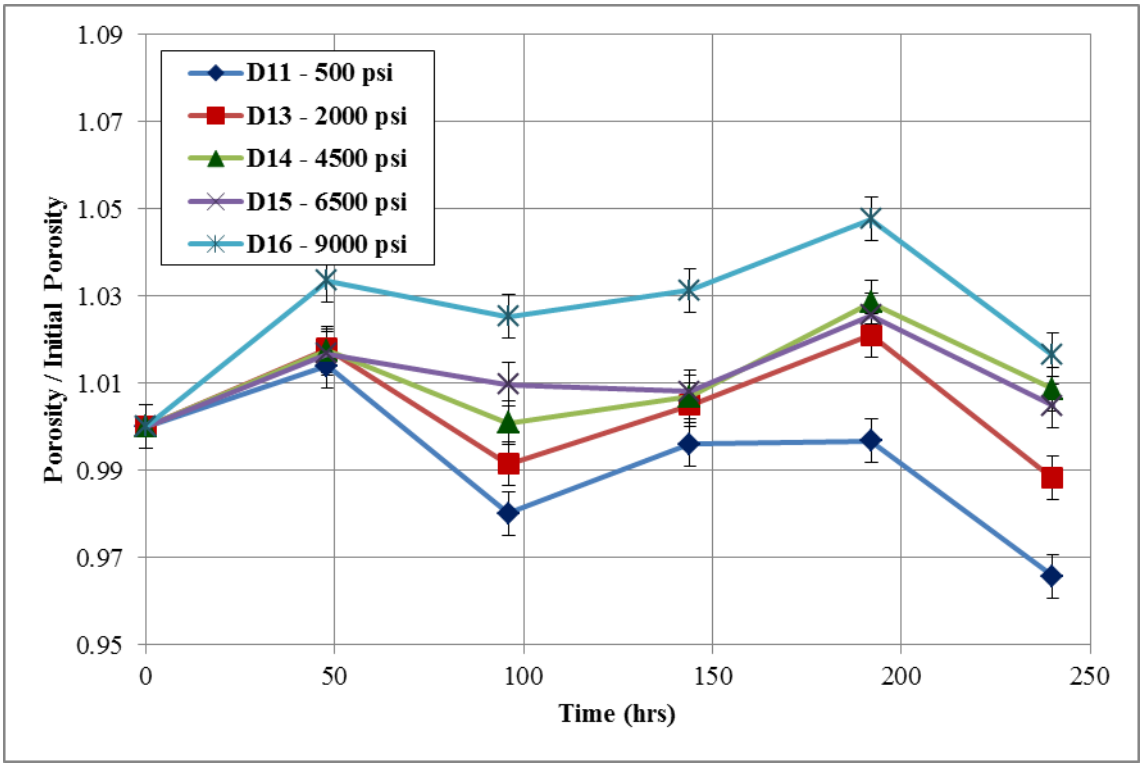

Figure 5.8. Dolomite porosity variation vs time.

Mass variation of the coquina samples is shown in Figure 5.9. It is important to note that sample C18 broke in the last time-step and was reconstituted to continue the experiment. The mass, permeability and porosity variations due to the breakage was measured and not considered in the analysis. The same behavior expected for the dolomite samples is expected for the coquinas samples, in a higher degree, as indicated in Section 2.3. Therefore, the mass of the samples are inversely proportional to the dissolution rate, which in turn, is directly proportional to the pressure and to the porosity of the sample.

The sample submitted to the highest working pressure (C18) was also the one that presented the highest mass variation. Sample C12 had the lowest working pressure and its dissolution rate was lower only than that of sample C18. This is because the latter is also the one with the highest porosity out of the coquina samples. Sample C13 presented the lowest mass variation, since it was tested at the lowest working pressure. The dissolution rate of samples C14 and C16 were very similar, although it was expected that sample C16 should stand a higher dissolution rate, because it was under a higher working pressure and had a higher initial porosity.

Figure 5.10 and

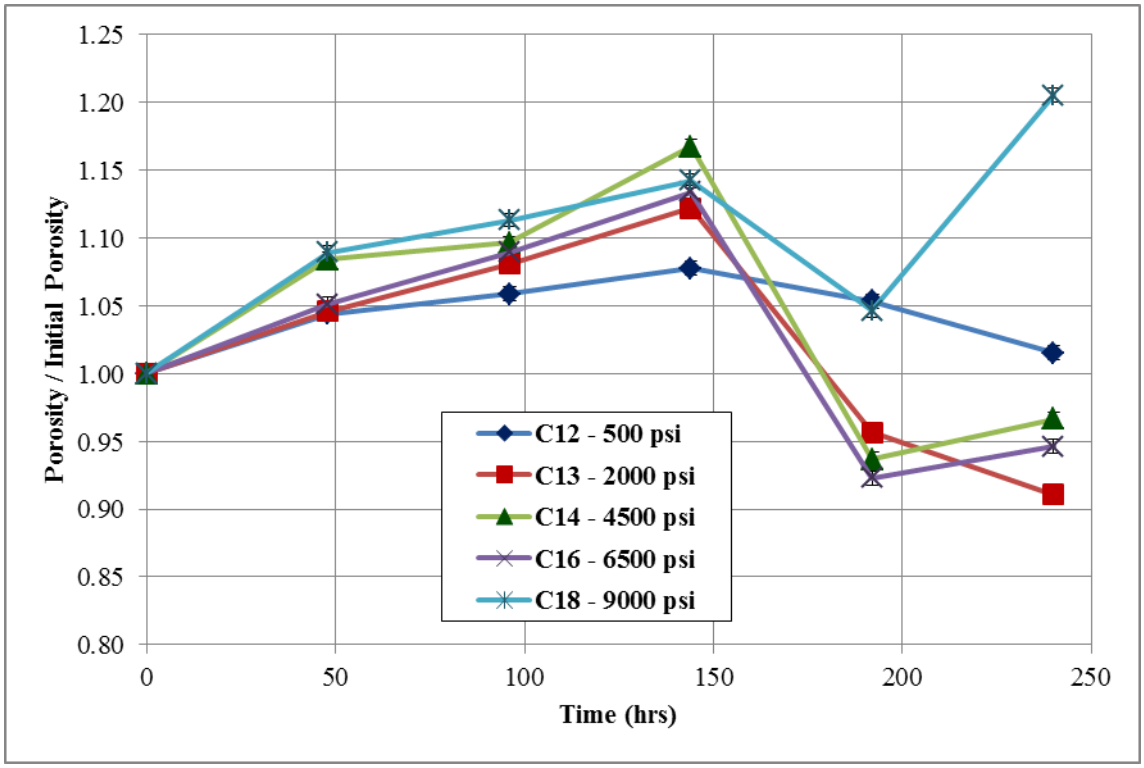

Figure 5.11 show the permeability and porosity variations results, respectively. Here again, any decrease in porosity and permeability of the samples are related to the deposition reaction caused by the depressurization of the system after the experiments. It can be seen that the

coquina samples presented an overall increase in permeability and porosity, although from t = 144 h t = 196 all samples porosity decreased.

Comparing the results for the coquina samples with those for the dolomite samples, it can be seen that the dissolution rate of the latter is much lower than of the former. It can also be seen that the dolomite samples had an overall permeability variation to the negative side, while the coquina samples presented an overall permeability variation to the positive side. Also, the overall variation of permeability for the dolomite samples was higher than for the coquina samples. The variation of porosity was low for the dolomite samples, while for the coquina samples there was a variation to the positive side up until t = 144 h and after that the variation was to the negative side.

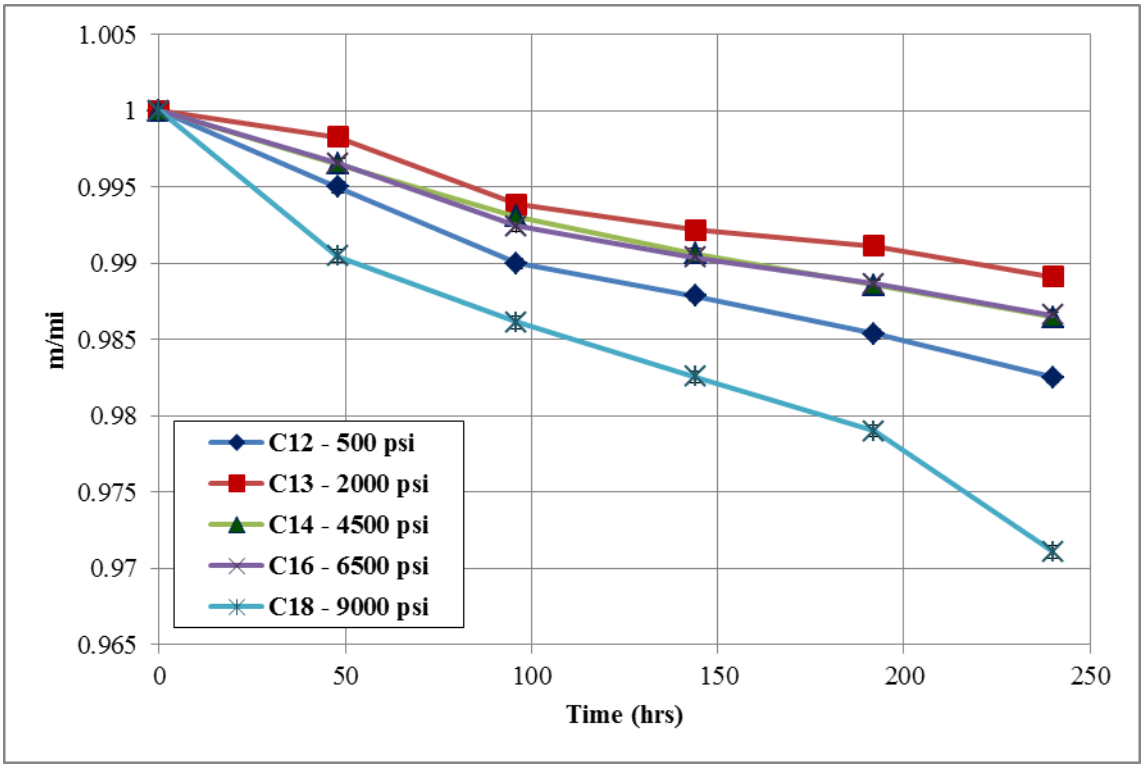

Figure 5.9. Coquina mass variation vs time.

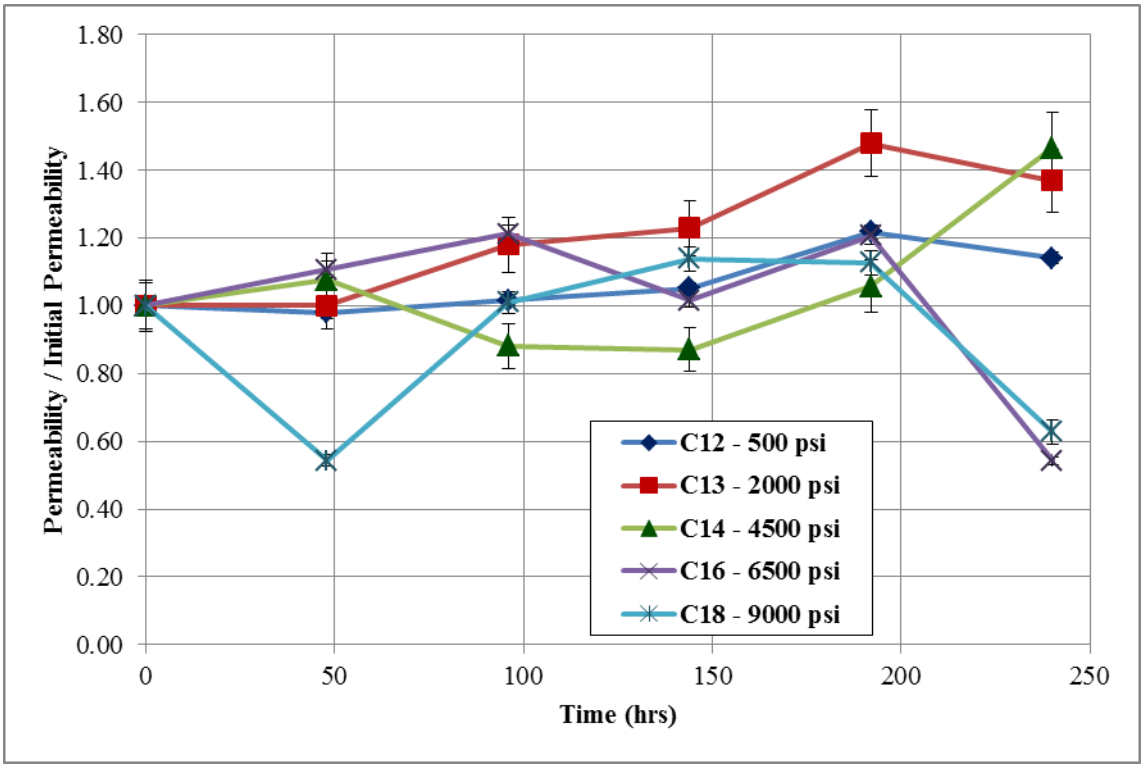

Figure 5.10. Coquina permeability variation vs time.

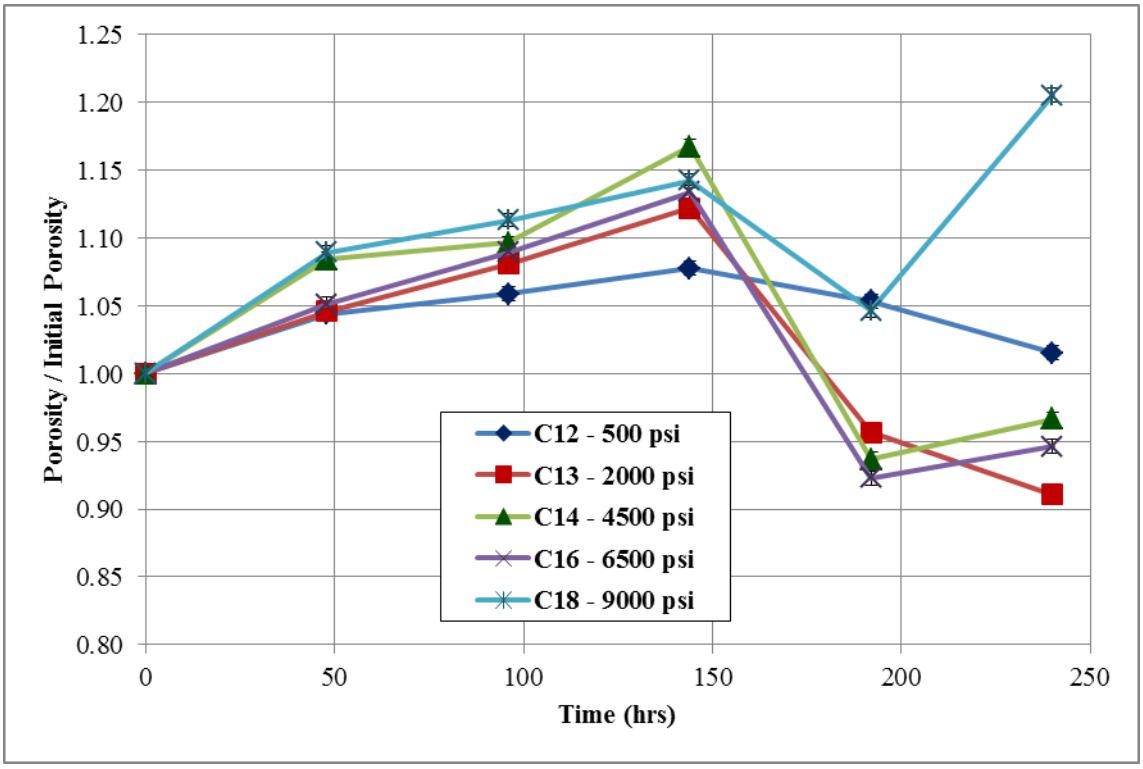

Figure 5.11. Coquina porosity variation vs time.

Results of the water analysis for the dolomite samples are shown in Figure 5.12 and Figure 5.13 in terms of **[**Ca^{2+}] and **[**Mg^{2+}], respectively. The same results are shown in

Figure 5.14 and Figure 5.15 for the coquina samples. From the dolomite results it can be seen that these samples released very little **[**Ca^{2+}] in the water and a lot of **[**Mg^{2+}]. It can also be seen that the concentrations of these ions did not show any tendency of increase or decrease, meaning that the dissolution reaction of the dolomite samples take longer to occur. The coquina water results shows that the coquina samples may have impurities in them, since it was seen a detectable amount of in the water. And, as expected, the **[**Ca^{2+}] concentration in water is much higher than that of **[**Mg^{2+}]. It can also be seen that the dissolution is very fast up until t = 144 h (as it was seen before) and after that it slows down (as it can be seen in both **[**Ca^{2+}] and **[**Mg^{2+}]).

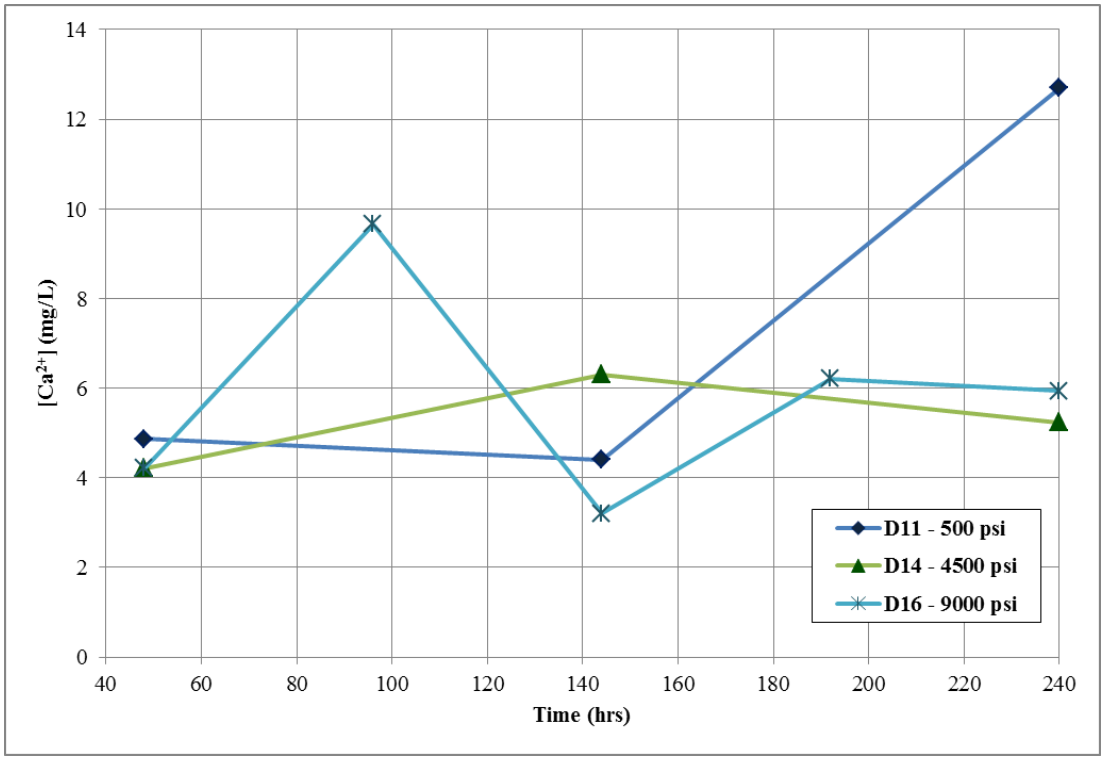

Figure 5.12. Water analysis: [Ca2+] for the dolomite samples.

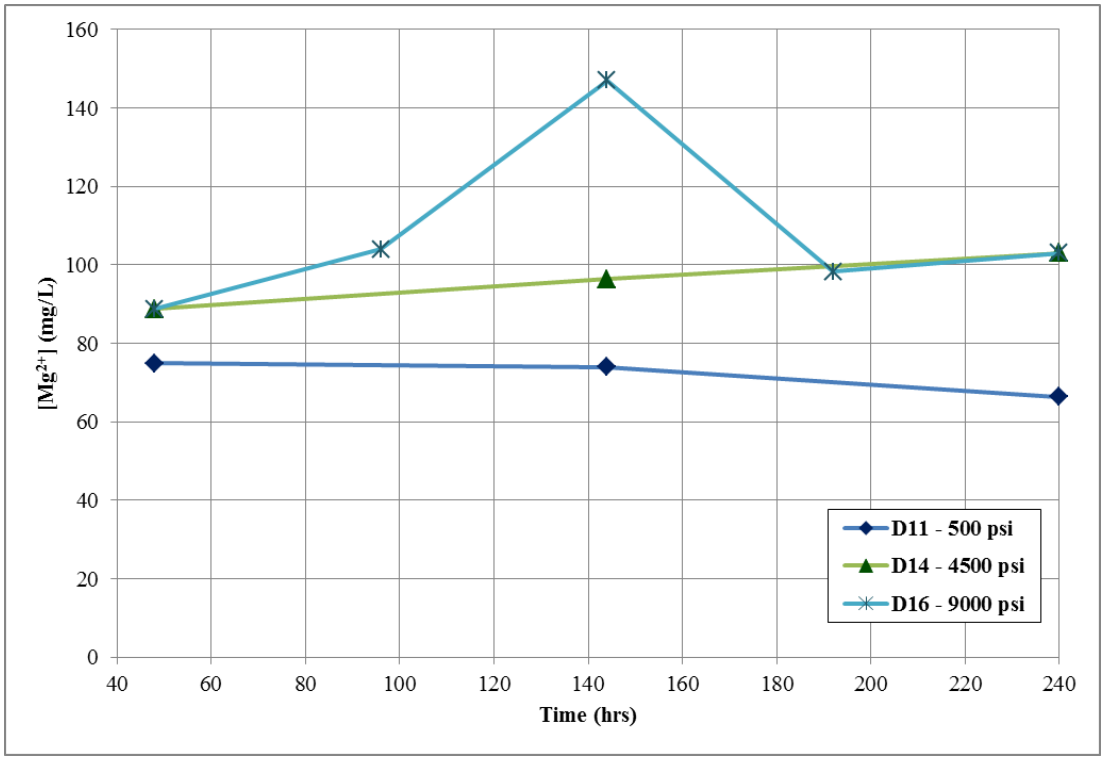

Figure 5.13. Water analysis: [Mg2+] for the dolomite samples.

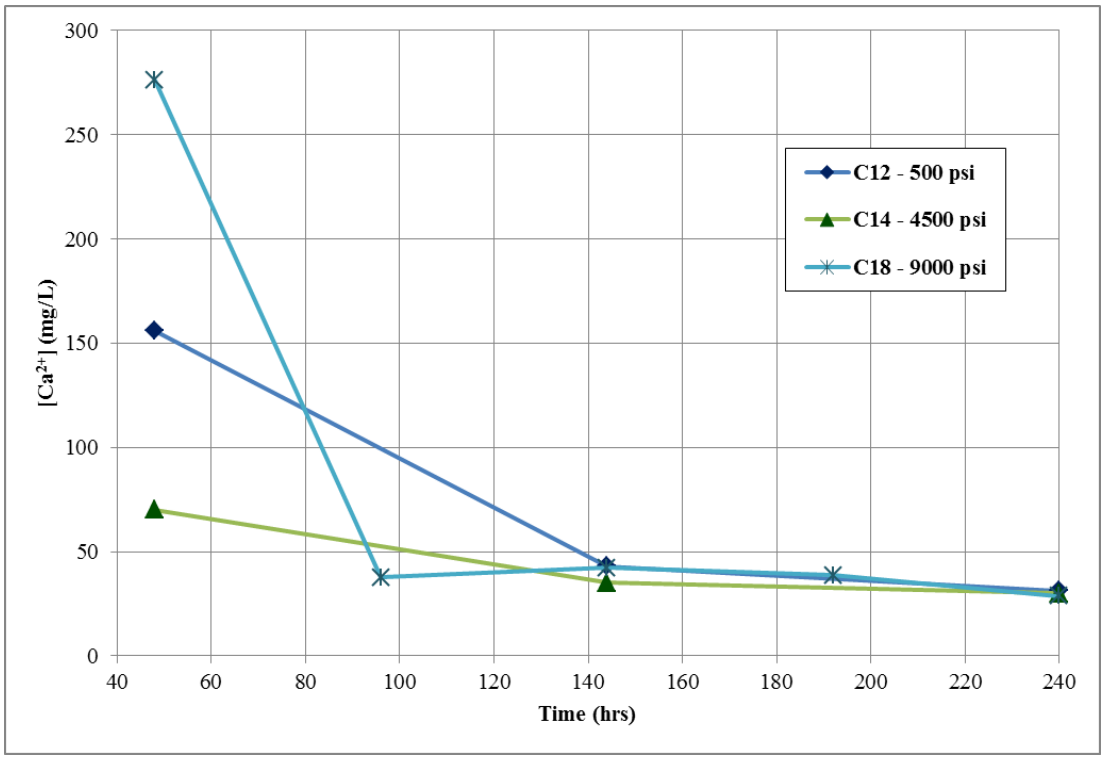

Figure 5.14. Water analysis: [Ca2+] for the coquina samples.

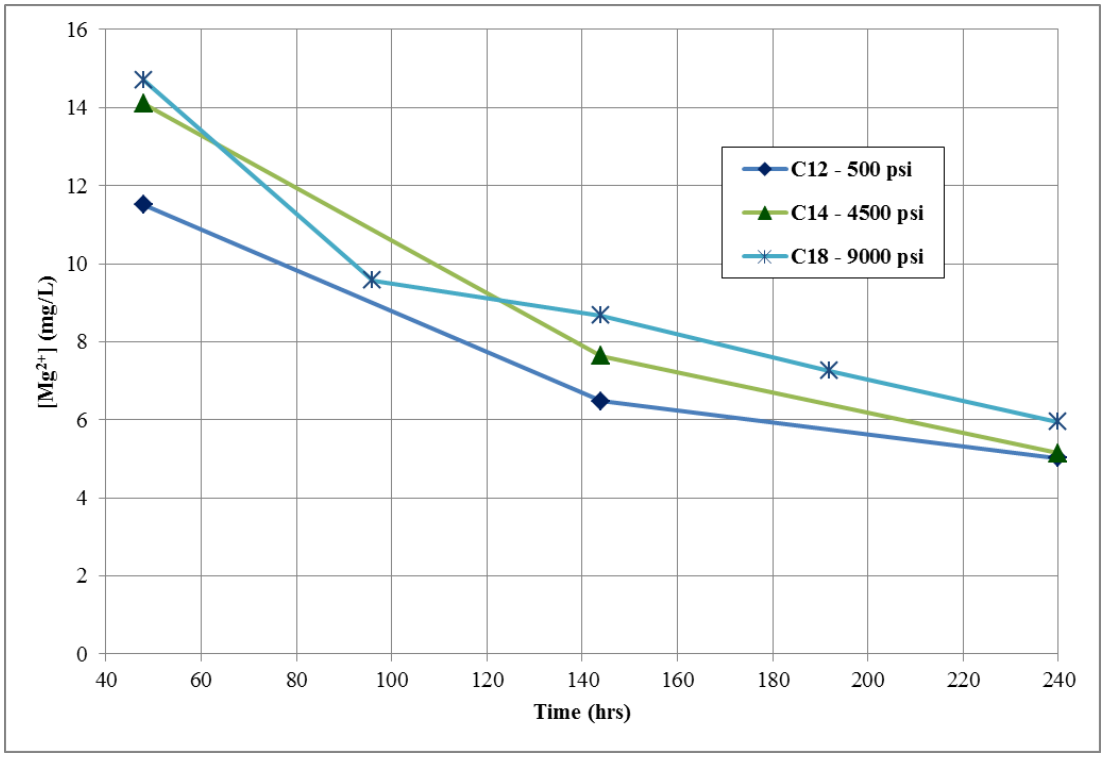

Figure 5.15. Water analysis: [Mg2+] for the coquina samples.

5.3.Discussions

Chapter 5 reports a series of experiments designed to study how permeability and porosity of coquina and dolomite change in presence of CO_2 and water at the pre-salt reservoir conditions. It was seen that dissolution rate decreases with time, it increases with pressure and initial porosity. Coquina's dissolution rate is higher than Dolomite's. In general, dissolution of carbonate rocks causes increases in permeability and porosity of the rock. In the experimental results, decreases of these properties were also found. These decreases were attributed to the deposition caused by the depressurization after the dissolution experiment.

The depressurization effect was more pronounced in the dolomite samples which presented an overall decrease in permeability and little change in porosity. Coquina samples showed higher dissolution rates, and an overall increase in porosity and permeability.

6. DISSOLUTION OF CARBONATE ROCKS: EFFECTS OF SALINITY

This chapter also addresses the main objective of this work, which is to evaluate the permeability and porosity changes of carbonate rocks due to the injection of CO_2 and water at conditions close to that of the pre-salt reservoirs. Here the focus is on how different water salinities affect the rock properties. The experiments performed herein were repeated with two different salinities and at 9,000 psi. One more step was added before starting the experiment, which involved cleaning the samples with toluene before starting the tests to remove any organic components left. Also, before the permeability and porosity measurements, the samples were cleaned with distilled water to try and decrease the effects of the depressurization.

6.1.Materials and Methods

For the experiments, 2 samples of dolomite (Silurian formation, USA) and 2 samples of coquina (Morro do Chaves, BR) measuring 1" in diameter by 1" in height were used. First, the samples were cleaned using a Soxhlet apparatus. For that 400 mL of toluene were loaded in the heating flask, and three samples at a time were cleaned until the solvent was clear in the extraction tube. After that, the toluene was exchanged for 400 mL of alcohol and again the cleaning lasted until the alcohol was clear in the extraction tube. The effects of the cleaning were evaluated by performing the rock characterization before and after the cleaning took place.

Here again, the rock characterization procedure performed on these samples consisted of: mass measurement using, this time, an analytical scale, permeability measurement with the Ultra-Perm 500 (Figure 3.2) connected with a filtered air source and porosity measurement with the Ultra-Pore 300 (Figure 3.3) connected with a pure N_2 source. For each sample, three different pressure differences were used for the permeability measurements and those differences were not changed in the entire experiment. Again, the permeability error was calculated as explained in APENDIX B. The porosity measurement was performed five times for each sample so that a standard deviation could be calculated.

Tests were carried out at the temperature of 64^{o}c and at the working pressure of 9,000 psi. Each of the 2 samples of dolomite and 2 samples of coquina, was assigned a

different brine with a salinity of 35,000 ppm or 200,000 ppm. The brines were prepared with distilled water and NaCl at the two concentrations.

After rock cleaning and characterization, each sample was loaded in a dedicated high pressure vessel (Figure 5.1) with 20 ml of the assigned brine for that sample. Each vessel was then connected to the vacuum pump shown in Figure 3.5 until the pressure inside was below 1.0e-1 bar to ensure that the brine filled every pore of the sample. After that, the vessel was disconnected form the vacuum pump and, together with a high pressure transfer cylinder (Figure 5.2) filled with CO_2. The container was put inside an air bath heater (Figure 5.3) at the temperature of 64^{o}C. The same experimental set up shown in Figure 5.5 was used to inject CO_2 in the high pressure container until it reached 9,000 psi.

The high pressure vessels were left in the air bath heater during the time period defined for that time-step. In the end, the samples were depressurized and washed-out with distilled water using a desiccator connected to the vacuum pump. The rocks were then dried for at least 16 hours in the air bath heater at 80oC. The procedure was repeated 5 times for every sample. Before and after each experiment cycle, the rock characterization procedure was performed.

Each time the procedure was repeated, a different time-step (the duration of the dissolution reaction) was used. They were: 24h, 24h, 48h, 72h and 72h, in the sequence order, totaling 240h.

6.2. Results

Figure 6.1 to Figure 6.3 show the cleaning effects in the coquina samples in terms of mass variation, permeability variation and porosity variation, respectively. It can be seen in the plot of mass variation that there were organic impurities in the coquina samples that were removed after cleaning. For most samples this implicated in increases in permeability and decreases in porosity. Figure 6.4 to Figure 6.6 show the cleaning effects in the dolomite samples in the same order as it was shown for the coquina samples. Here again, some impurities were removed, although in a lesser proportion than from the coquina samples. It also implied in increases in permeability and decreases in porosity. The occurrence can be explained by the blockage and release of pore throats by the impurities. Therefore, it is possible to have a decrease in porosity if blockage of pore throats leaves some pores inaccessible.

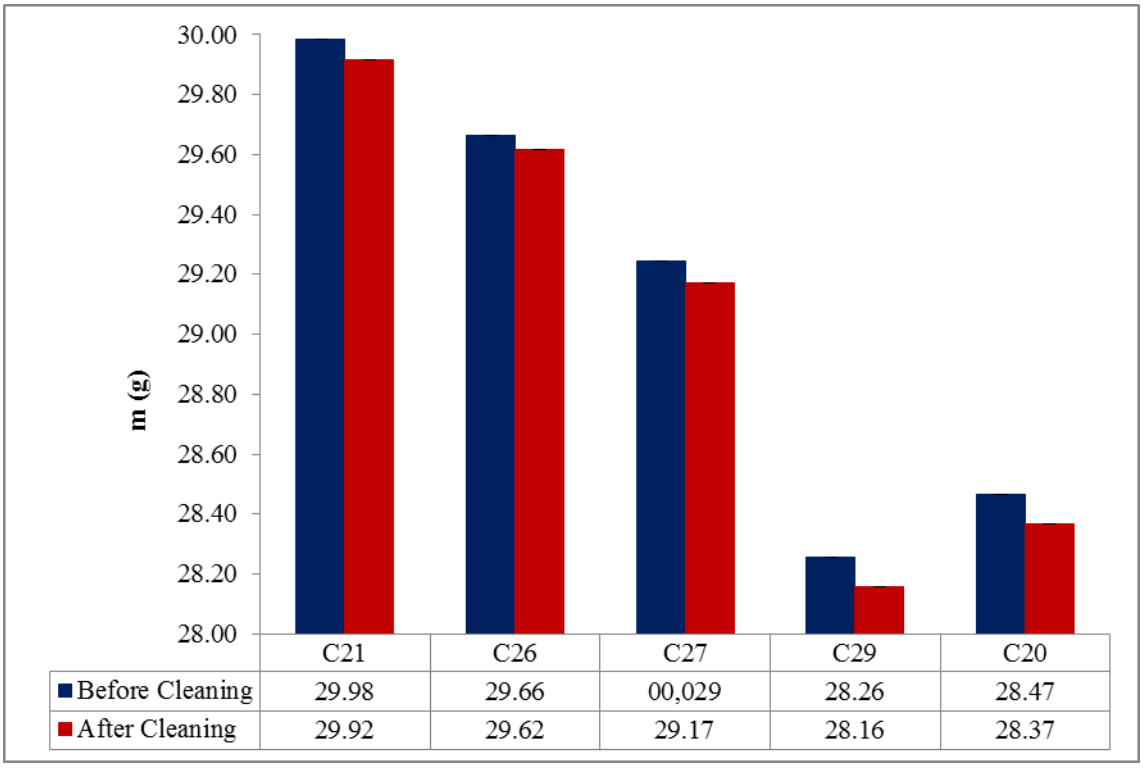

	C21	C26	C27	C29	C20
Before Cleaning	29.98	29.66	00,029	28.26	28.47
After Cleaning	29.92	29.62	29.17	28.16	28.37

Figure 6.1. Cleaning effects on coquina: mass variation.

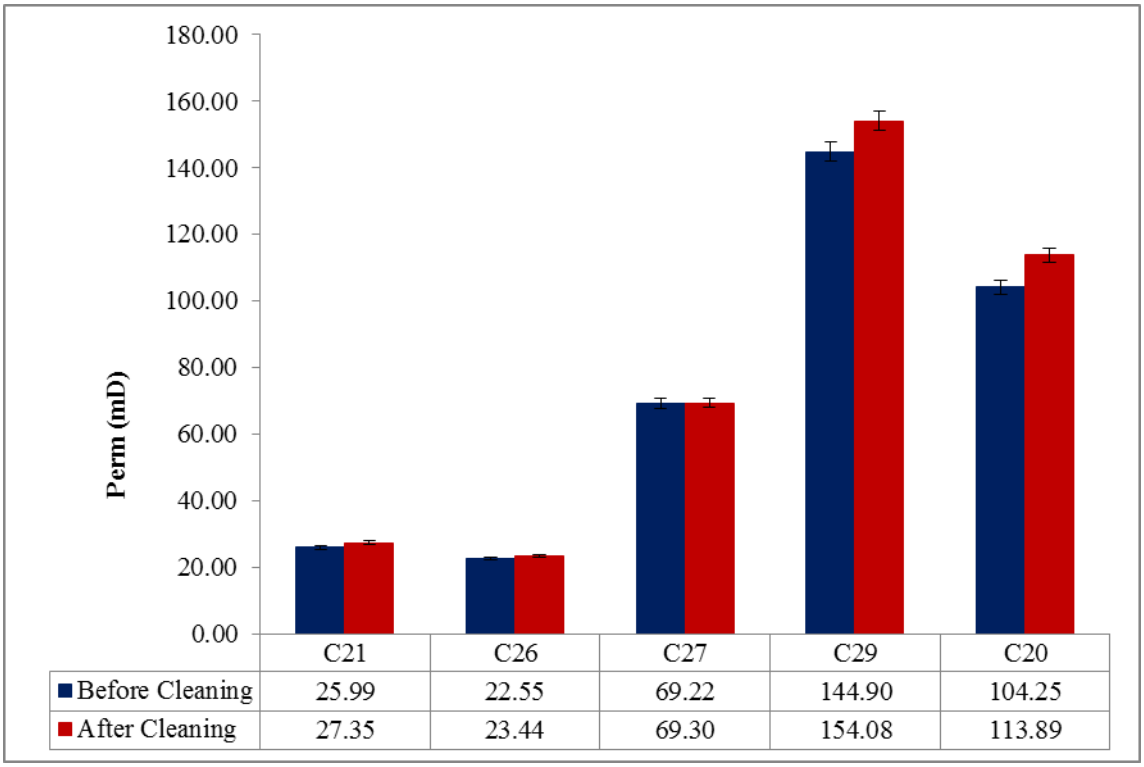

	C21	C26	C27	C29	C20
Before Cleaning	25.99	22.55	69.22	144.90	104.25
After Cleaning	27.35	23.44	69.30	154.08	113.89

Figure 6.2. Cleaning effects on coquina: permeability variation

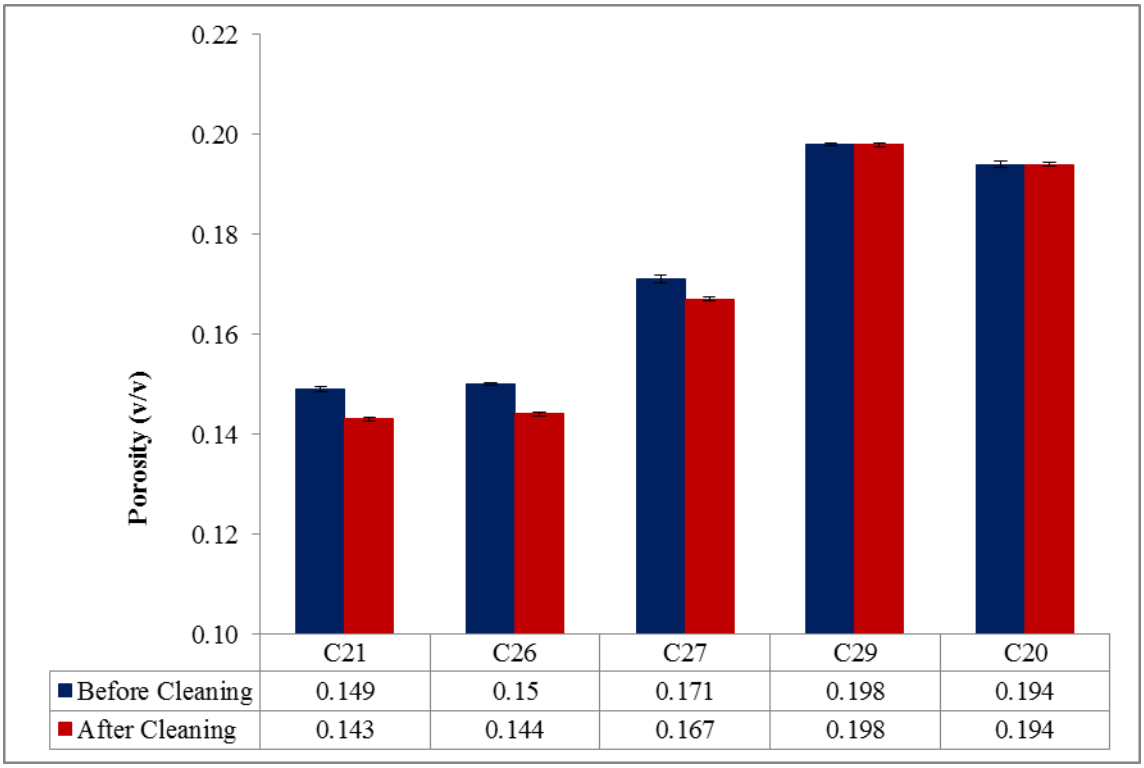

	C21	C26	C27	C29	C20
Before Cleaning	0.149	0.15	0.171	0.198	0.194
After Cleaning	0.143	0.144	0.167	0.198	0.194

Figure 6.3. Cleaning effects on coquina: porosity variation.

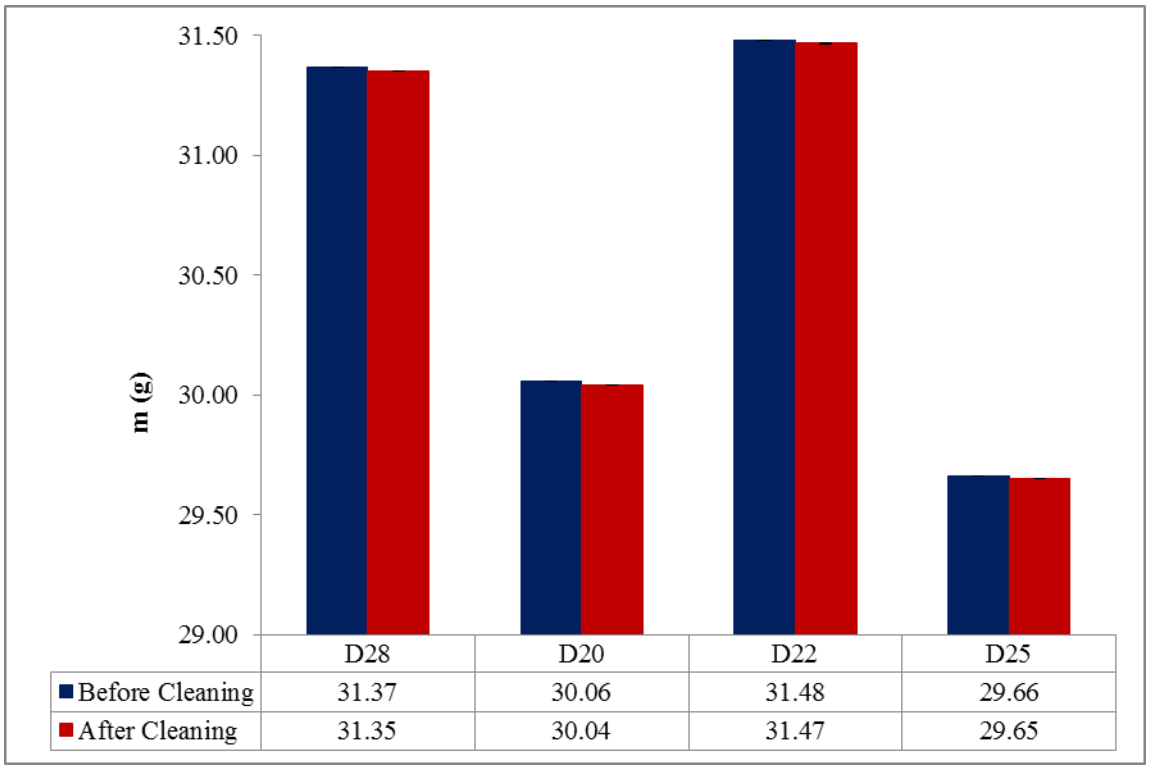

	D28	D20	D22	D25
Before Cleaning	31.37	30.06	31.48	29.66
After Cleaning	31.35	30.04	31.47	29.65

Figure 6.4. Cleaning effects on dolomite: mass variation.

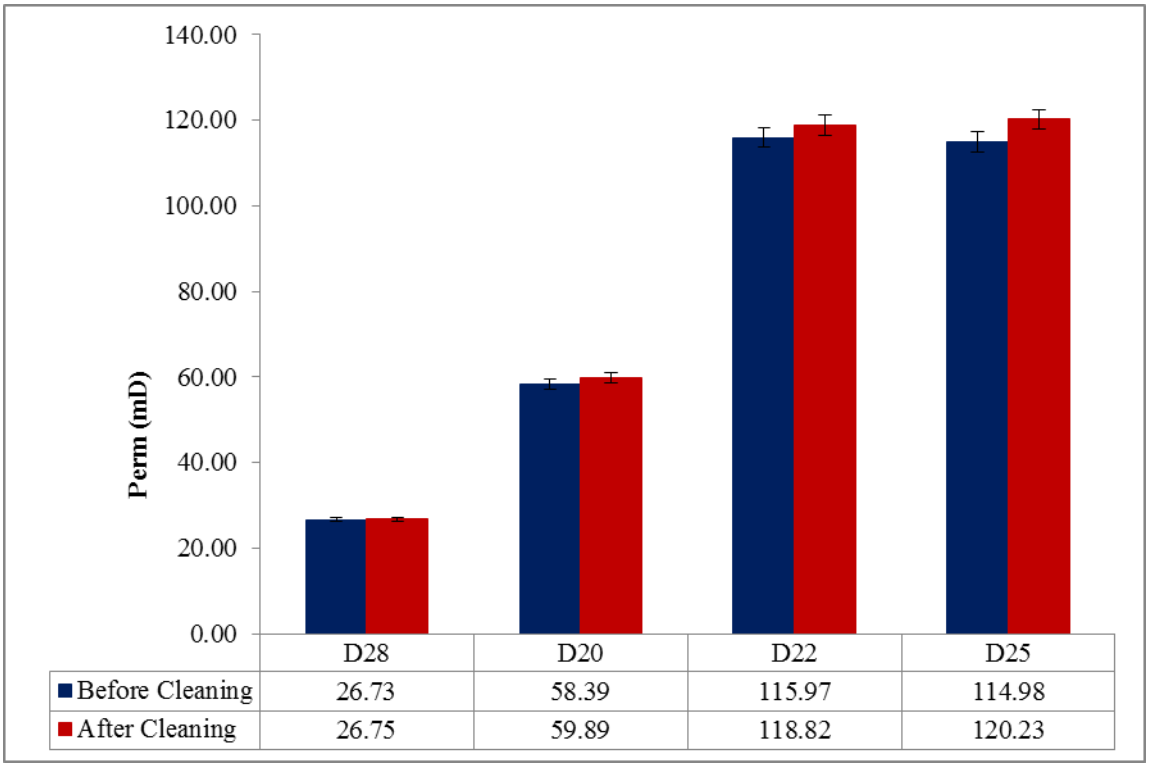

	D28	D20	D22	D25
Before Cleaning	26.73	58.39	115.97	114.98
After Cleaning	26.75	59.89	118.82	120.23

Figure 6.5. Cleaning effects on dolomite: permeability variation.

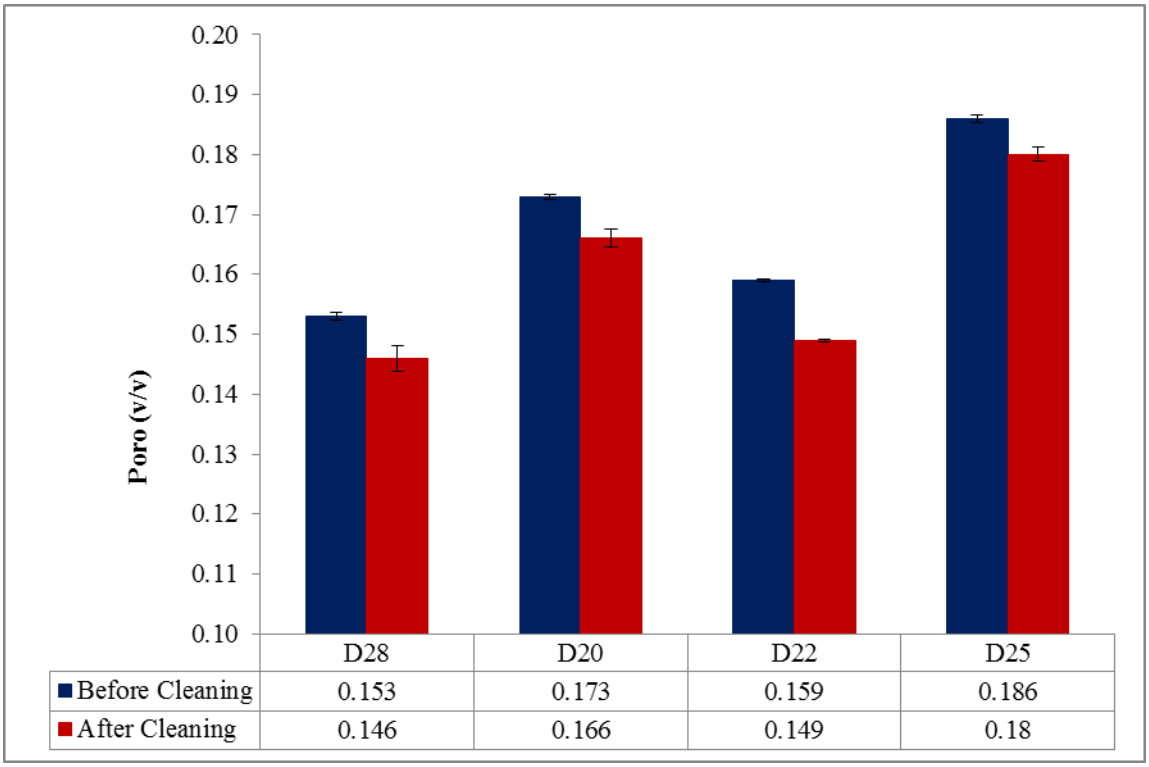

	D28	D20	D22	D25
Before Cleaning	0.153	0.173	0.159	0.186
After Cleaning	0.146	0.166	0.149	0.18

Figure 6.6. Cleaning effects on dolomite: porosity variation.

Values of mass, permeability and porosity after the cleaning are the starting values for the experiment. By comparing these values, two samples of coquina and two of dolomite were chosen for the experiment as the ones having similar permeabilities. Table 6.1. Samples names and assigned brine salinities. shows the samples names and its assigned brine salinities.

Table 6.1. Samples names and assigned brine salinities.

Sample	Salinity (ppm)
D22	35,000
D25	200,000
C29	35,000
C20	200,000

Mass variation results are shown in Figure 6.7. It is important to note that all samples lost partial integrity at t =96 h, and lose some mass. The mass losses were computed and removed from the analysis.

As it was explained in Chapter 5, the dissolution reaction is controlled by the CO_2 dissolved in water and the availability of minerals indicated by the porosity of the sample. Here, as the salinity of the brine increases, the amount of CO_2 dissolved in water decreases, decreasing the dissolution rate. Therefore, the dissolution rate (or the mass variation of the samples) is inversely proportional to salinity of the brine and directly proportional to the porosity of the samples. That said, for samples from the same outcrop, the higher mass variations were found for the samples that were assigned to brines with 35,000 ppm salinity. Also, such as it was found in the previous experiment, the mass variations of the coquina samples were higher than that of the dolomite samples.

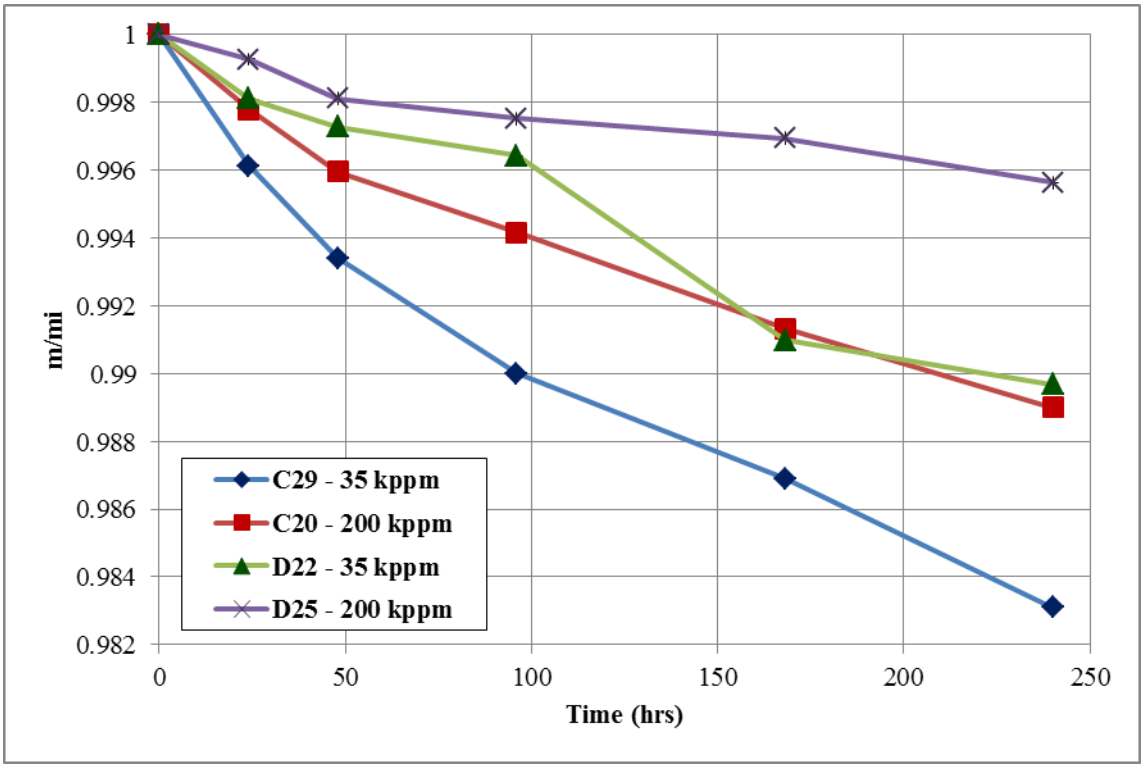

Figure 6.7. Mass variation of all samples

The permeability results can be seen in Figure 6.8. Here, the same reasoning made in Chapter 5 applies: the dissolution reaction translates into increases in porosity and permeability. Decreases in porosity and permeability indicate that deposition is taking place. Since the dissolution experiment takes place in static conditions, only dissolution is taking place during the experiment. The only moment that deposition can occur is during the depressurization of the high pressure vessel. Therefore, any decrease in permeability and porosity of the samples is not occurring during the experiment, but after.

For the permeability results, the samples with the highest salinity brine presented the highest permeability variation to the positive side. This is the contrary that it would be anticipated, since samples with the highest dissolution rates are expected to present the highest permeability variations. The dolomite samples were the ones that suffered the highest permeability variations as it was seen in the previous dissolution study.

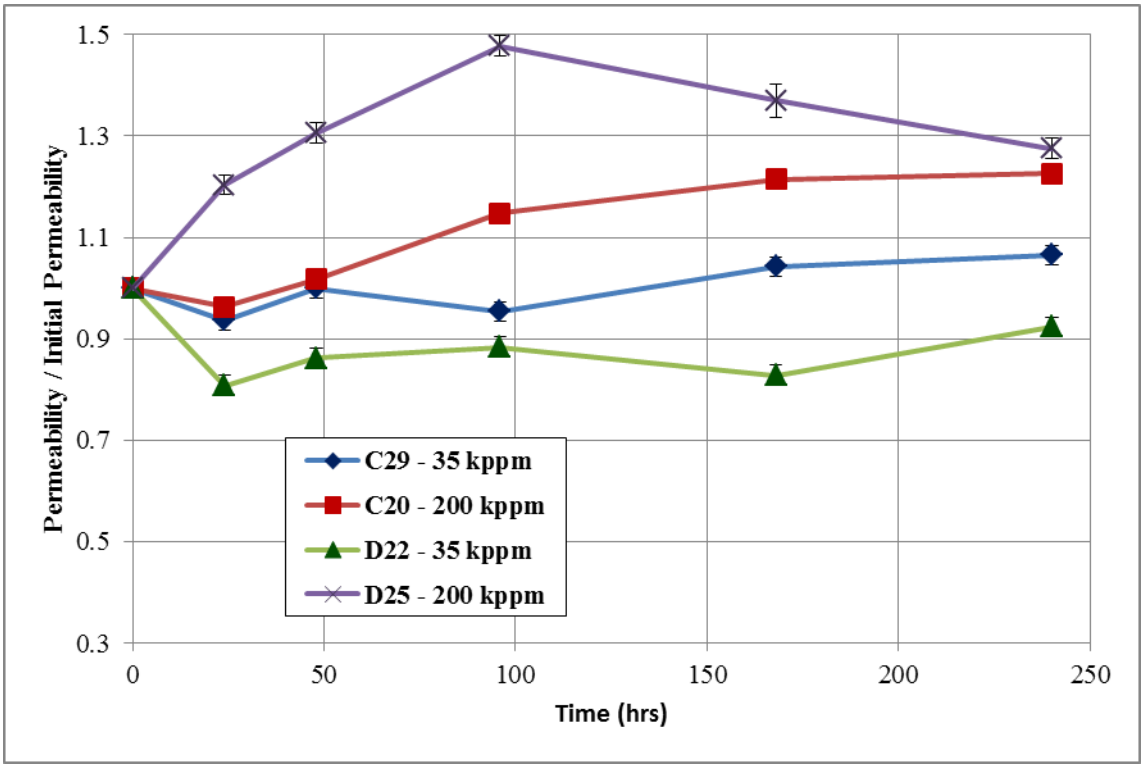

Figure 6.8. Permeability variation of all samples.

The porosity results are shown in Figure 6.9. Porosity varied accordingly tothe mass variation of the samples. Samples under the brine with the 35,000 ppm salinity were the ones with the highest porosity variation to the positive side, while the samples with the 200,000 ppm brine were the ones with the lowest porosity variation to the positive side, if comparing samples with the same type of rock. Also, coquina samples showed higher porosity variation when compared to dolomite samples.

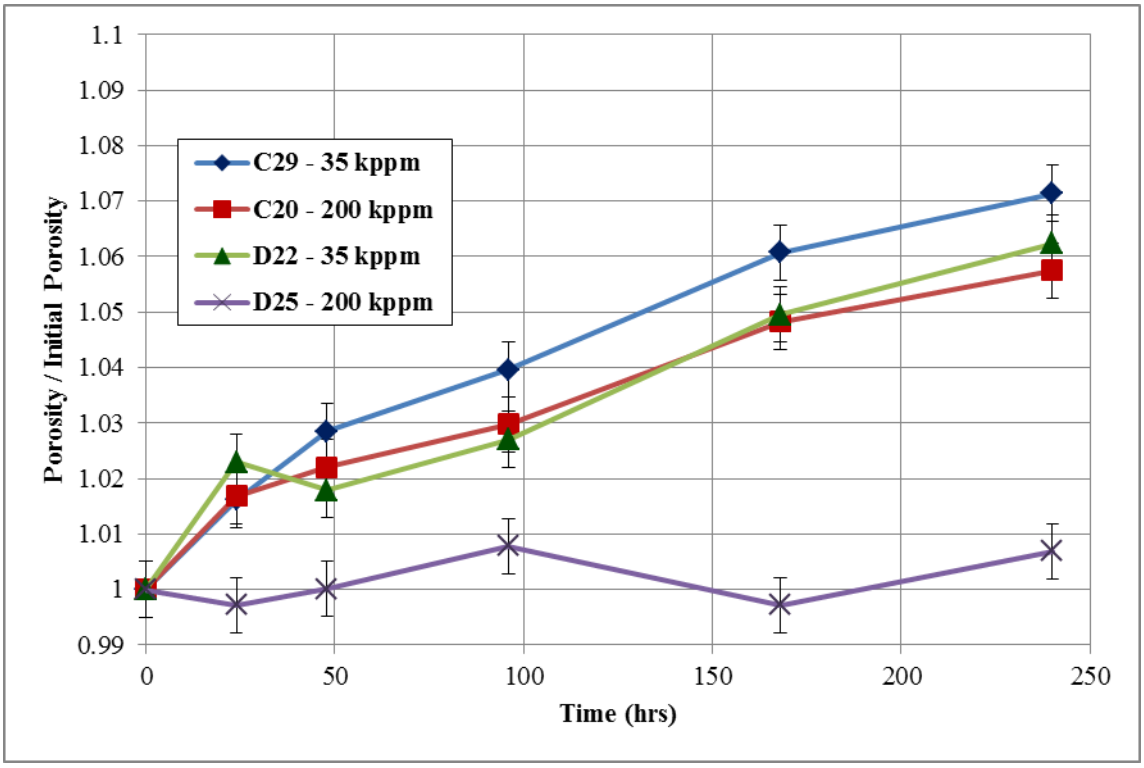

Figure 6.9. Porosity variation of all samples.

Figure 6.10-Figure 6.12 show mass, porosity and permeability variation results, respectively, plotted together with the results for the tests with fresh water at the working pressure of 9,000 psi. As to mass variation, it can be seen that the coquina sample with fresh water showed a dissolution rate higher than all the other samples showed in the graph. Also, mass variation of the dolomite sample with fresh water is higher than the mass variation of the other dolomite samples up to time t =96 h. After this time the dissolution rate for the dolomite sample with the brine of 35,000 ppm salinity surpasses that of the dolomite sample D16.

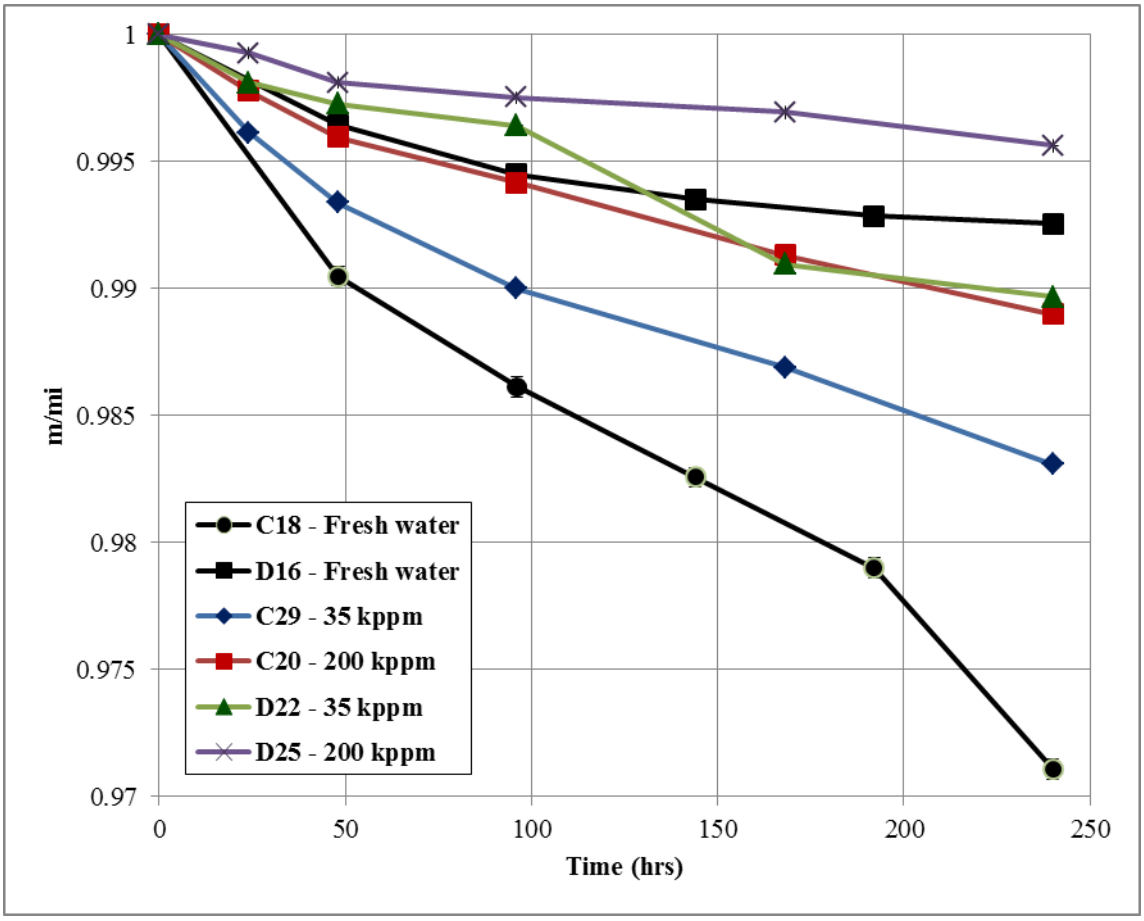

Figure 6.10. Mass variation at 9,000 psi for varying water salinities.

Now, in terms of permeability variation, it can be seen that for D16 the values are very close to those of sample D22 (brine of 35,000 ppm salinity). No conclusions can be drawn for sample C18, since it was considerably affected by the depressurization effects of the system. Regarding porosity (Figure 6.12), sample C18 (fresh water) was the one with the highest porosity variation, as anticipated. From the dolomite samples, sample D16 was expected to have the highest increase in porosity, but it had not.

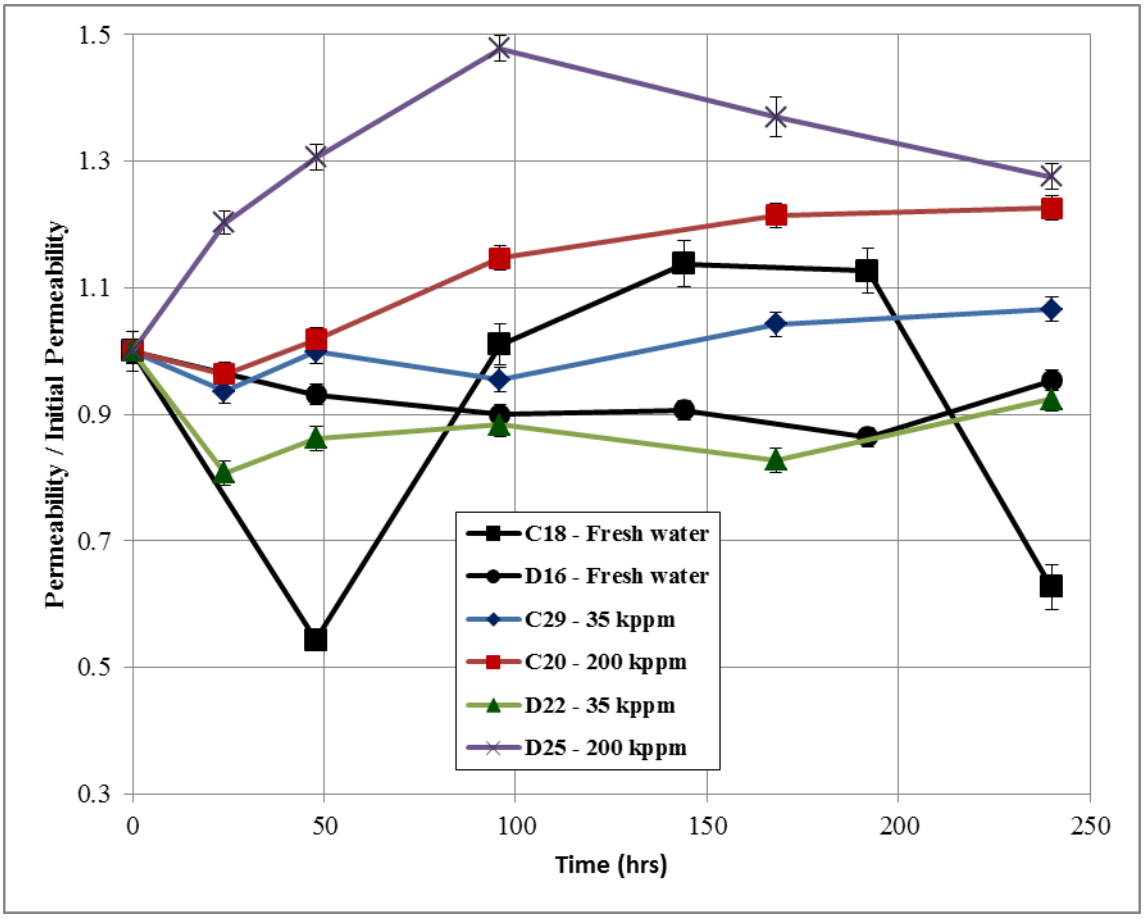

Figure 6.11. Permeability variation at 9,000 psi for varying water salinities.

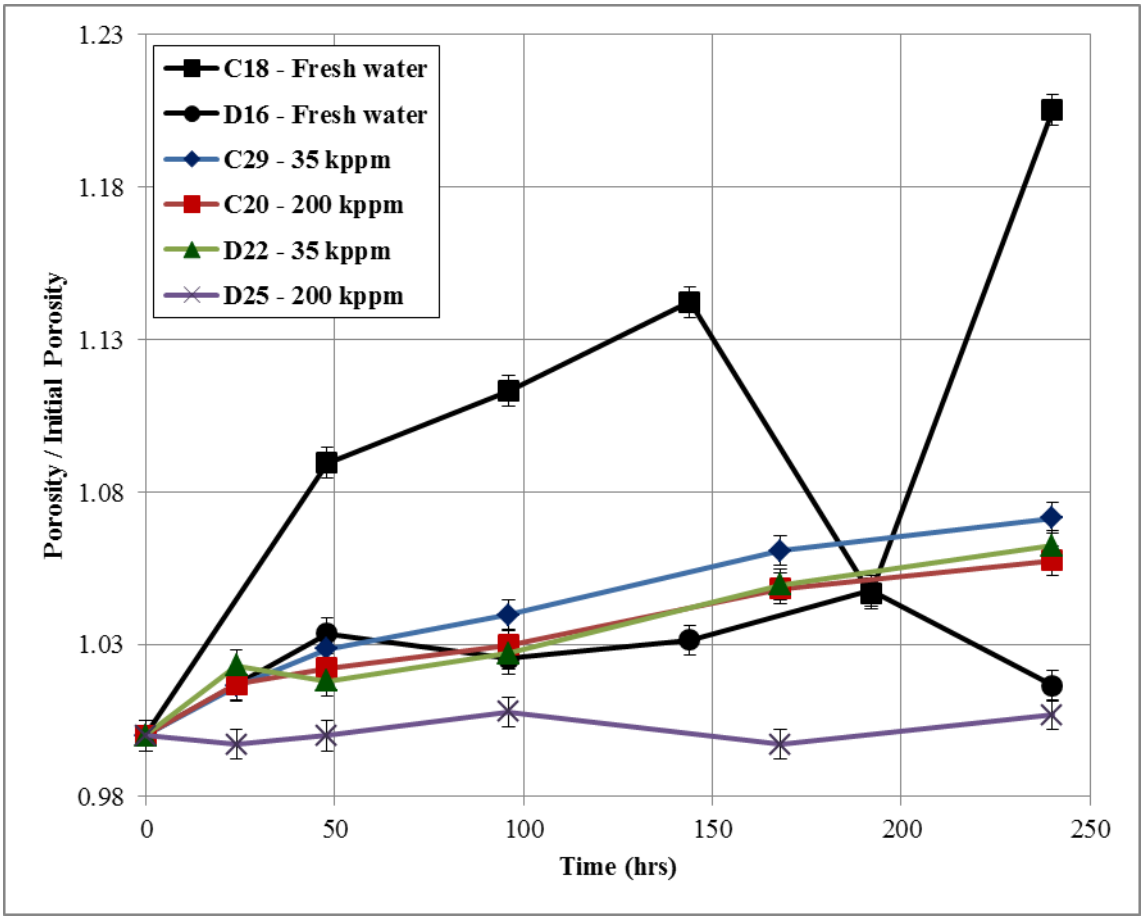

Figure 6.12. Porosity variation at 9,000 psi for varying water salinities.

6.3. Discussions

A set of experiments to study how the dissolution of carbonate rocks varies with salinity is presented in this Chapter. Coquina and dolomite samples were tested in high pressure CO_2/brine systems with two types of brine, one with 35,000 ppm salinity and the other with 200,000 ppm salinity. An additional provision of cleaning the samples of any organic impurities was introduced, prior to the beginning of the experiment.

The cleaning of the samples removed organic impurities of the sample and also changed their porosity and permeability. For the dissolution experiment by itself, in terms of mass, it was possible to see that as salinity increased, there was a decrease in the dissolution rate and a decrease of the mass variation of the sample. Also, as it was seen in previous chapter, the dissolution rates of the dolomite samples were smaller than the ones of the coquina samples, if samples are compared at the same brine salinity.

Porosity changes of the samples were directly proportional to mass variation. Therefore, porosity variation decreased as the brine salinity was increased. The permeability variation of the samples was inversely proportional to brine salinity, meaning that the samples submitted to the highest salinity brine showed the highest increase in permeability.

Again, these conclusions are limited due to the fact that deposition occurred after the experiments due to the depressurization and only the permeability results were affected.

7. CONCLUSION AND RECOMENDATIONS

The main objective of this dissertation was to evaluate how permeability and porosity of carbonate rocks changes due to exposure of CO_2 and water at conditions close to that of the pre-salt reservoirs. The secondary objective was o delineate the best practices for measuring porosity and permeability in laboratory conditions. Chapter 3 and Chapter 4 addressed the secondary objective, while Chapter 5 and Chapter 6 addressed the main objective of the dissertation.

COMPARISONS OF GAS AND LIQUID PERMEABILITY reports the experimental work performed to investigate the issue of converting gas permeability measurements to liquid permeability measurements by applying Klinkenberg analysis. It was shown that it is not possible to calculate liquid permeability with the gas permeability values obtained. Non-Darcy flow regimes can be present in higher mean pressures measurements and for lower mean pressures the error of the permeability value is significant.

The author recommends that a different experimental set up be tested in order to calculate the liquid permeability of rock samples using gas permeability data. The set up should include a back pressure regulator, because it provides improved control of gas flow rate and core differential pressure, as well as it may assist in maintaining viscous flow in higher mean pressures, as it is recommended by McPhee and Arthur (1991).

It was also seen that, as the pressure difference used in the gas permeability measurement increased, the permeability decreased more than it was expected by Klinkenberg's analysis. Therefore, the experimental study in REPEATABILITY ASSESSMENT OF GAS PERMEABILITY AND POROSITY MEASUREMENT was performed in order to evaluate if this variation in permeability is permanent and what is the best procedure for this measurement.

In this Chapter, it was seen that this change in permeability with increase in measurement pressure is not permanent for any of the samples. It was also shown that the average permeability for the same sample, measured in similar conditions (same pressure difference or gas rate), can be used to evaluate changes in a sample's permeability within measurement error. The gas porosity measurement can also be used, with the condition that a calibration is performed after every 5 consecutive porosity measurements. These conclusions were taken into consideration in the following two Chapters.

The experimental study presented in DISSOLUTION OF CARBONATE ROCKS: EFFECTS OF PRESSURE was designed to evaluate how the permeability and porosity of coquina and dolomite outcrop rocks varies in fresh water/CO_2 systems, with increasing pressure (up to 9,000 psi) at constant temperature (64^oC). It was seen that dissolution rate decreases with time, it increases with pressure and initial porosity. Coquina's dissolution rate is higher than Dolomite's. In general, dissolution of carbonate rocks causes increases in permeability and porosity of the rock.

DISSOLUTION OF CARBONATE ROCKS: EFFECTS OF SALINITY presents an experimental study to evaluate the variation of porosity and permeability for coquina and dolomite, in high pressure (9,000 psi) brine/CO_2 systems at constant temperature and varying brine salinity. The results showed that as salinity increased, there was a decrease in the dissolution rate and a decrease of the mass variation of the sample. Porosity variation decreased as the brine salinity was increased and the samples submitted to the highest salinity brine showed the highest increase in permeability.

In the experiments presented in Chapter 5 and 6 it was seen decreases of porosity and permeability. These decreases were attributed to the deposition caused by the depressurization after the dissolution experiment. During the depressurization of the high pressure vessel, some of the ions that were previously dissolved may precipitate on the pore throats decreasing the permeability and effective porosity of the samples. To eliminate this effect, it would be necessary to exchange the water inside the vessel for an inert fluid, before the depressurization. This could be done by changing the experimental apparatus and displacing the pressurized water after the experiment is finished with N_2 for example.

In conclusion, it was seen that it was not possible to obtain liquid permeability values with the gas permeability measured but it was established how the latter should be used together with gas porosity measurement to evaluate the variation of permeability and porosity variation of the samples. Dissolution rate decreases with time, it increases with the pressure and with initial porosity. Finally, in general, as the dissolution rate increases, the permeability and porosity of the rocks increases as well.

REFERÊNCIAS

AMYX, J. W., BASS JR., D. M., WHITING, R.L. Petroleum reservoir engineering: physical properties. United States of America: McGraw-Hill Book Company, Inc, 1960.

DOTSON, B. J., SLOBOD, R. L., MCCREERY, P. N., SPURLOCK, J.W. Porosity-measurement comparisons by five laboratories. Society of Petroleum Engineers, 1951. doi:10.2118/951341-G

BUSTIN, R. M., BUSTIN, A. M. M., CUI, X., ROSS, D. J. K., PATHI, V. S. M. Impact of Shale Properties on Pore Structure and Storage Characteristics. Society of Petroleum Engineers, 2008. doi:10.2118/119892-MS.

LUFFEL, D. L., HOWARD, W. E. Reliability of Laboratory Measurement of Porosity in Tight Gas Sands. Society of Petroleum Engineers, 1987. doi:10.2118/16401-MS

LE BIHAN, A., NICOT, B., MARIE, K., THÉBAULT, V., HAMON, G. Quality Control of Porosity and Saturation Measurements on Source Rocks. Society of Petrophysicists and Well-Log Analysts, sep. 2014.

ROSA, A. J., CARVALHO, R. S., XAVIER, J. A. D. Engenharia de Reservatórios de Petróleo. Editora Interciência Ltda, 2006.

TORSAETER, O., ABTAHI, M.,Experimental Reservoir Engineering Laboratory Workbook", Department of Petroleum engineering and Applied Geophysics, Norwegian University of Science and Technology, 2003.

JOHNSTON, N., BEESON, C. M. Water permeability of reservoir sands. Society of Petroleum Engineers, dec. 1945. doi:10.2118/945043-G.

MUSKAT, M. The flow of homogeneous fluids through porous media. New York: McGraw-Hill, 1937.

FANCHER, G. H., LEWIS, J. A., BARNES, K. B. Some Physical Characteristics of Oil Sands, Pennsylvania State C., Minerals Industries Experiment Station, University Park, 1933.

KLINKENBERG, L. J. The permeability of porous media to liquids and gases. API Drilling and Production Practice, 1941, 200-213.

MCPHEE, C. A., ARTHUR, K. G., Klinkenberg Permeability Measurements: Problems and Practival Solution. Philadelphia. 1991. Advances in Core Evaluation II. Reservoir Appraisal. Proceedings of the 2nd Society of Core Analysis European Core Analysis Symposium. Gordon & Breach Science Publishers. 371-391.

NOMAN, R., KALAM, M. Z. Transition from Laminar to Non-Darcy Flow of Gases in Porous Media. BP Research, Sunbury-on-Thames, UK. 1990.

RUSHING, J. A., NEWSHAM, K. E., LASSWELL, P. M., COX, J. C., BLASINGAME, T. A. Klinkenberg-Corrected Permeability Measurements in Tight Gas Sands.: Steady-State Versus Unsteady-State Techiniques. Society of Petroleum Engineers, jan. 2004. doi:10.2118/89867-MS.

ZHANG, R., HU, S., ZHANG, X., YU, W. Dissolution Kinetics of Dolomite in Water at Elevated Temperatures. Aquatic Geochemistry, dec. 2007. Vol 13, 309-338. Doi:10.1007/s104998-007-9022-z.

FREDD, C. N., FOGLER, H. S. The kinetics of calcite dissolution in acetic acid solutions. Chemical Engineering Science, 1998. Vol 53 (22), 3863-3874.

LIU, Z., YUAN, D., DREYBRODT, W. Comparative study of dissolution rate-determining mechanisms of limestone and dolomite. Environmental Geology, 2005. Vol 49 (2), 274-279.

TAYLOR, K. C., NASR-EL-DIN, H. A. e MEHTA, S. Anomalous Acid Reaction Rates in Carbonate Reservoir Rocks. SPE Journal, 2006. 488-496.

BACCI, G., ET AL., An experimental and numerical investigation in to the impact of dissolution/precipitation mechanisms on CO_2 injectivity in the wellbore and far field regions. International Journal of Greenhouse Gas Control, 2010, doi:10.1016/j.ijggc.2010.05.007.

GRIGG, R. B., SVEC, R. K., LICHTNER, P. C., CAREY, W., LESHER, C. E. CO_2/Brine/Carbonate Rock Interactions: Dissolution and Precipitation. Fourth Annual Conference on Carbon Capture & Sequestration, Alexandria, Virginia, May 2-5, 2005.

IZGEC, O., DEMIRAL, B., BERTIN, H., AKIN, S. CO_2 Injection in Carbonates. Society of Petroleum Engineers, Jan 2005. doi:10.2118/93773-MS.

LUQUOT, L., GOUZE, P. Experimental determination of porosity and permeability changes induced by injection of CO_2 into carbonate rocks. Chemical Geology, 2009. Vol 265, 148–159.

NOIRIEL, C., LUQUOT, L., MADÉ, B., RAIMBAULT, L., GOUZE, P., LEE, J. Changes in reactive surface area during limestone dissolution: An experimental and modeling study. Chemical Geology, 2009. Vol 265, 160-170.

ZEKRI, A. Y., SHEDID, S. A., ALMEHAIDEB, R. A. Investigation of supercritical carbon dioxide, aspheltenic crude oil, and formation brine interactions in carbonate formations. Journal of Petroleum Science and Engineering, 2009. Vol 69, 63-70.

YADAV, S. K., CHAKRAPANI, G. J., GUPTA, M. K. An experimental study of dissolution kinetics of Calcite, Dolomite, Leucogranite and Gneiss in buffered solutions at temperature 25 and 5^{o}C. Environmental Geology, 2008. Vol 53, 1683-1694.

ZANG, P., TWEHEYO, M. T., AUSTAD, T., Wettability alteration and improved oil recovery by spontaneous imbibition of seawater into chalk: Impact of the potentialdetermining ions Ca^{2+}, Mg^{2+}, and SO_4^{2-}, Colloids and Surfaces A: Physicochem. Eng. Aspects, 2007.

U.S. BUREAU OF MINES STAFF, Dictionary of Mining, Mineral, & Related Terms. U.S. Department of Interior, U.S. Bureau of Mines, Washington, D.C., 1996. 3660 p.

NOGUEIRA, M. S., LEMOS, V. B., TERRA, G., J. As “Coquinas” do Membro Morro do Chaves, Cretáceo Inferior da Bacia de Alagoas, e seu Potencial para Reservatório de Petróleo. 2º Congresso Brasileiro de P&D em Petróleo & Gás, 2003.

MUÑOZ, E. R., Estudo da Alteração da Molhabilidade de Carbonatos com Injeção de Água e CO_2, Campinas-SP, 2015. Tese de doutorado, Universidade Estadual de Campinas – Faculdade de Engenria Mecânica e Institudo de Geociências.

KU, H. H., Notes on the use of propagation of error formulas, Journal of Research of the National Bureau of Standards, oct. 1966. Vol 70 (4) 262. doi:10.6028/jres.070c.025. ISSN 0022-4316.

APENDIX A – ADDITIONAL RESULTS

Here is shown the detailed results of the experiments developed in the study presented in COMPARISONS OF GAS AND LIQUID PERMEABILITY but not included in the main text for the sake of objectivity. They are shown here for reference.

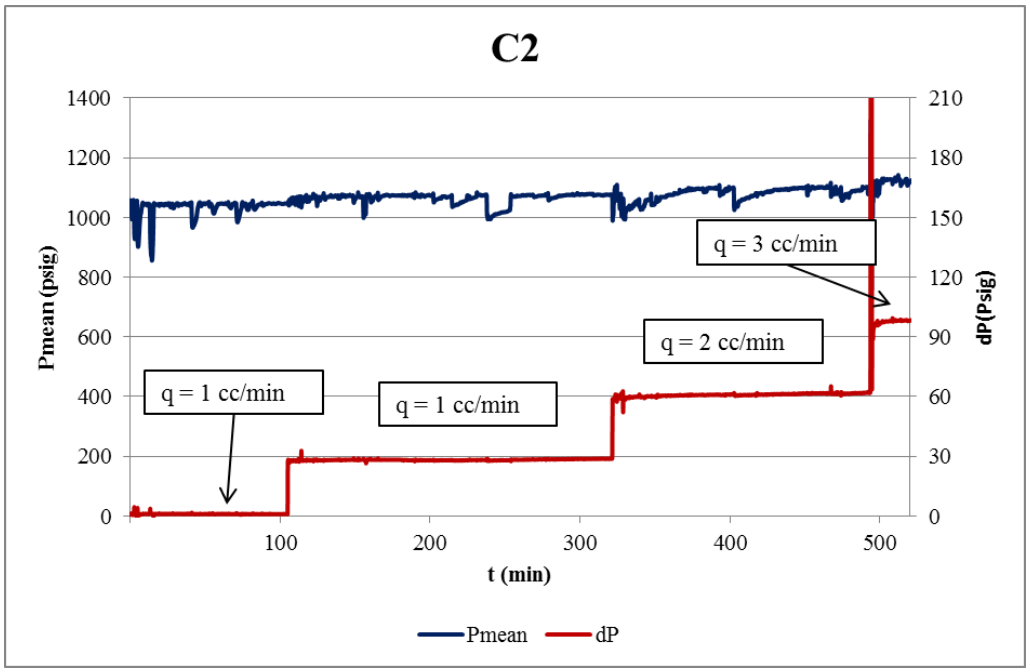

Figure A1. Air to liquid permeability experiment – Pressure results for sample C2.

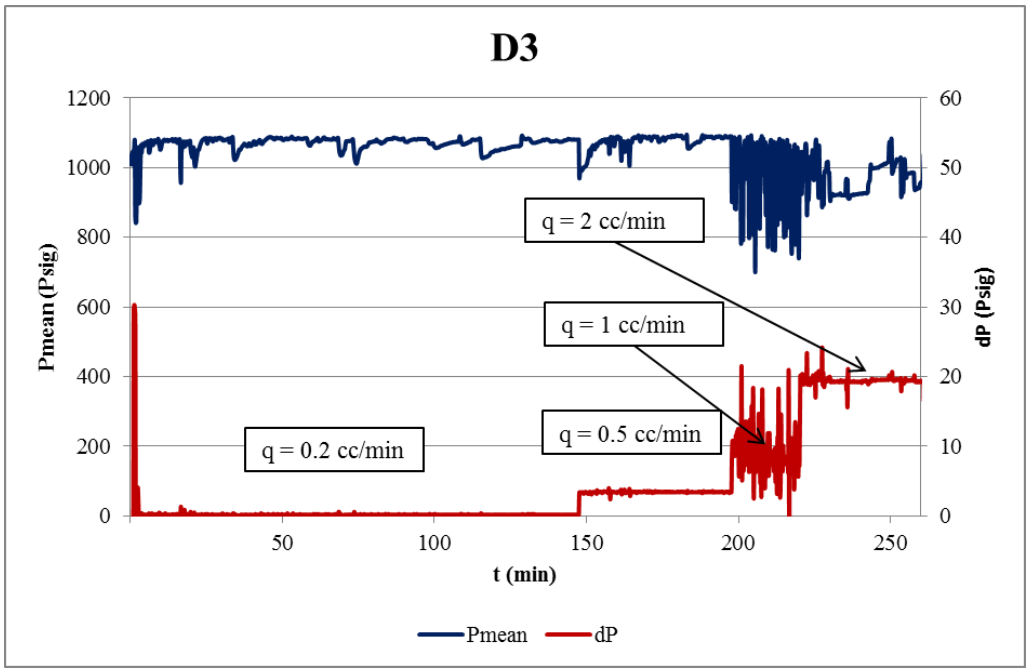

Figure A2. Air to liquid permeability experiment – Pressure results for sample D3.

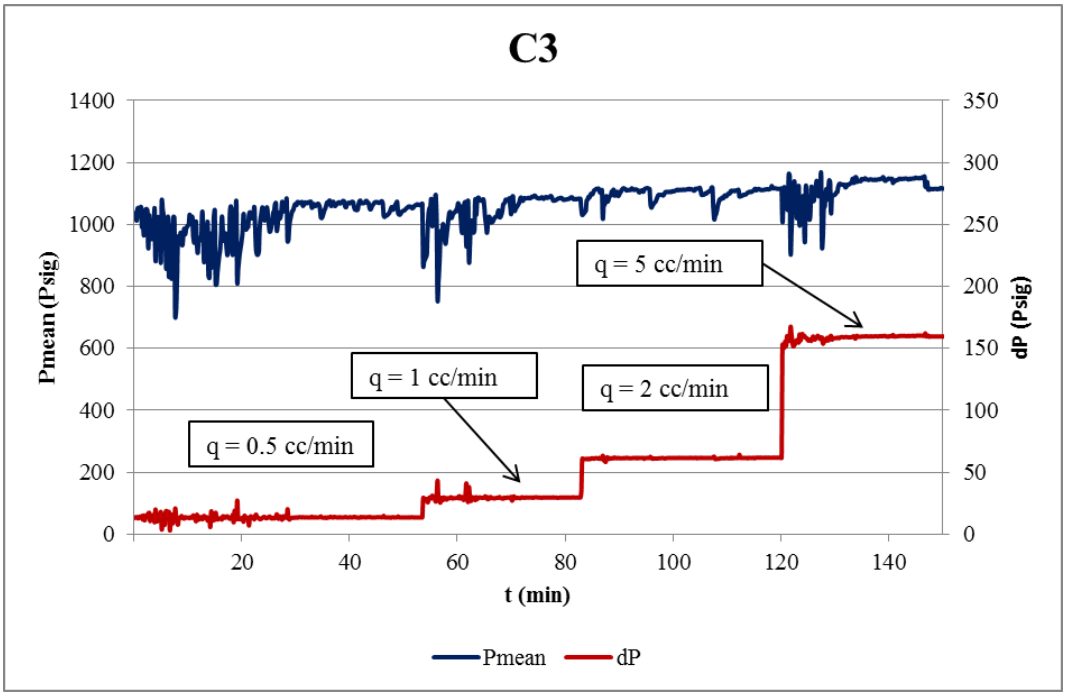

Figure A3. Air to liquid permeability experiment – Pressure results for sample C3.

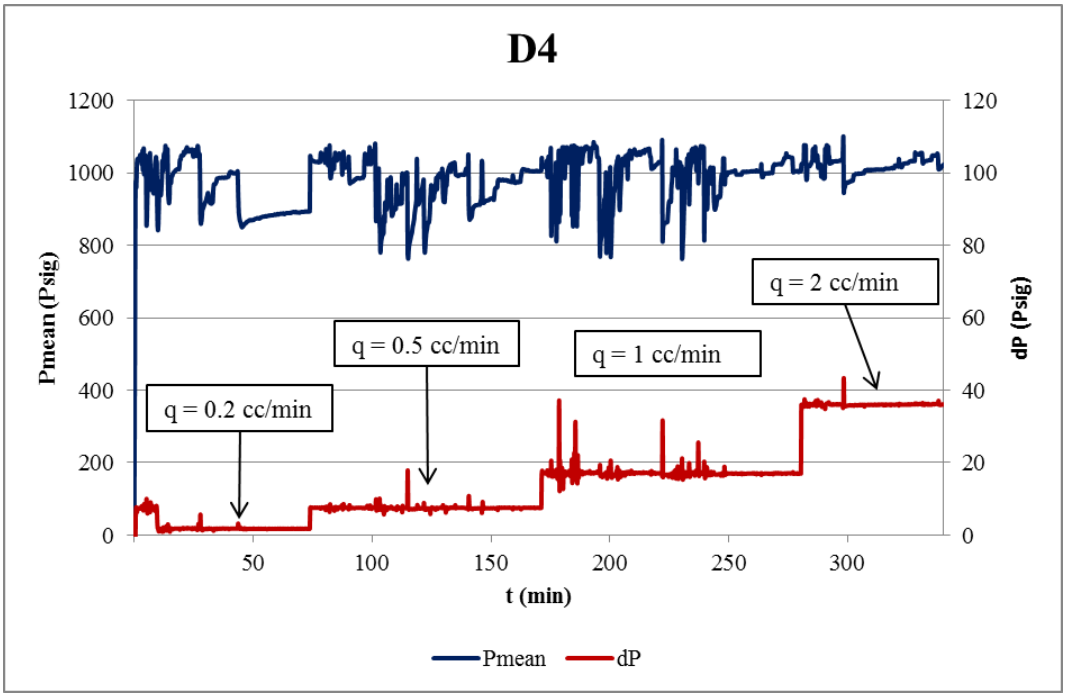

Figure A4. Air to liquid permeability experiment – Pressure results for sample C3.

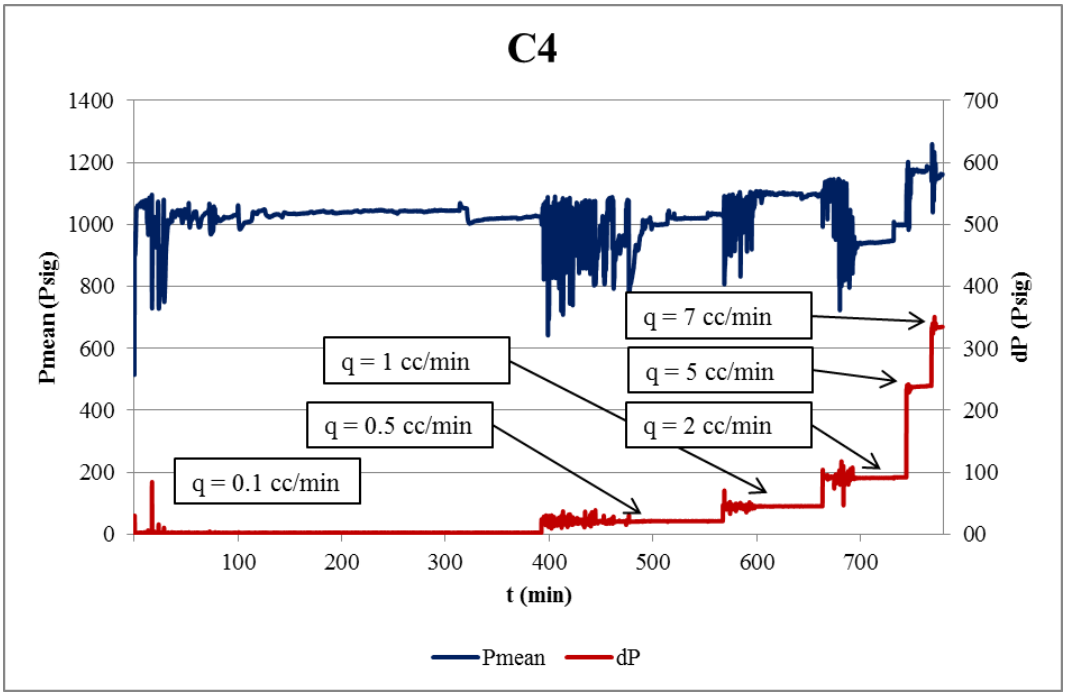

Figure A5. Air to liquid permeability experiment – Pressure results for sample C4.

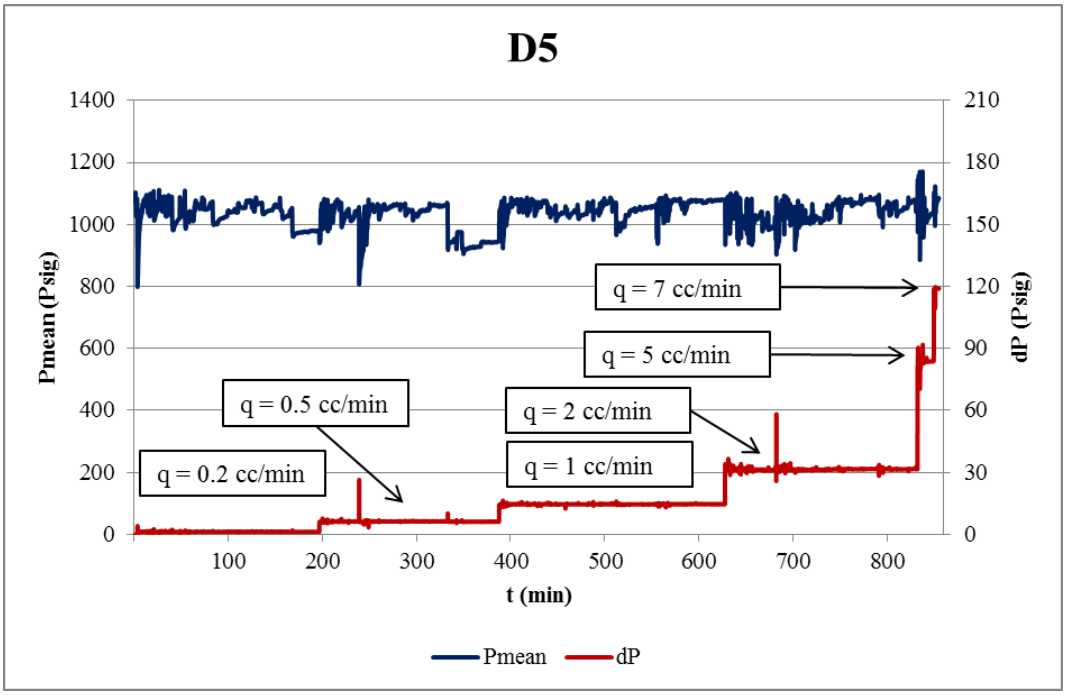

Figure A6. Air to liquid permeability experiment – Pressure results for sample D5.

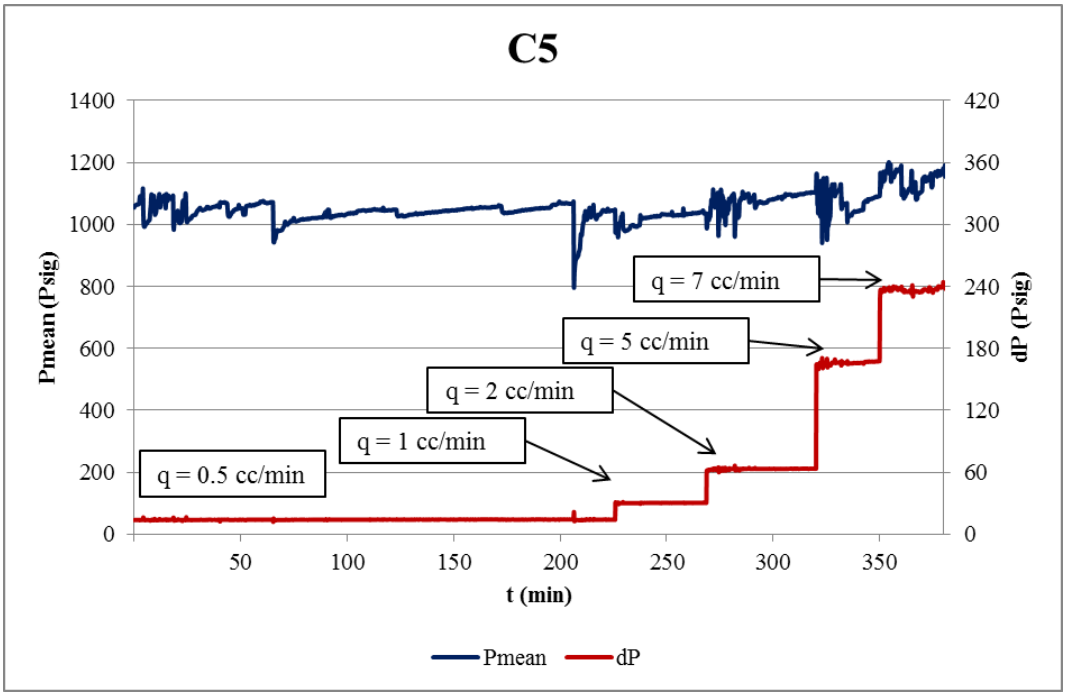

Figure A7. Air to liquid permeability experiment – Pressure results for sample C5.

APENDIX B – MEASUREMENT ERROR CALCULATIONS

In this Appendix the error propagation details are presented. They refer to the Gas permeability measurement using the Ultra Perm 300 and the liquid permeability measurement using the experimental apparatus shown in Figure 3.6. The error calculations for both measurements begin with the variance formula (Ku, 1966):

$$s_f = \sqrt{\left(\frac{\partial f}{\partial x}\right)^2 s_x^2 + \left(\frac{\partial f}{\partial y}\right)^2 s_y^2 + \left(\frac{\partial f}{\partial z}\right)^2 s_z^2 + \cdots} \tag{B.1}$$

where s_f is the standard deviation of the function f, s_x represents the standard deviation of x, s_y represents the standard deviation of y, and so on.

The calculation of the gas permeability measurement error using the Ultra-Perm 500 starts with Equation (2.11), repeated below for completeness.

$$k_a = \frac{2Q\mu LP_2}{A(P_1^2 - P_2^2)} \tag{B.2}$$

where k_a is the air permeability, μ is air viscosity, A is the area of the sample perpendicular to the direction of flow, L is the sample length, Q is flow rate and the inlet and outlet pressures are P_1 and P_2 respectively. In this equipment, the outlet pressure P_2 is maintained constant during measurement and the pressure difference ($\Delta P = P_1 - P_2$) is measured with three different pressure transducers: a low pressure transducer (LP), a medium pressure transducer (MP) and a high pressure transducer (HP). The flow rate is measured with two flow rate transducers: a low flow rate transducer (LF) and a high flow rate transducer (HF). Table B.1 shows the measurement ranges and accuracy of all the aforementioned transducers.

Table B.1. Measurement ranges and accuracy of Ultra-Perm 500's transducers.

Tansducer	**Measurement Range**	**Measurement Accuracy**
LP	0 - 0.9034 psi	0.0007 psi
MP	0 - 5 psi	0.005 psi

HP	0 - 50 psi	0.05 psi
LF	0 - 0.166 cc/s	0.00166
HF	0 - 3.333 cc/s	0.03333

substituting Equation (B.1) into Equation (B.2) and considering the standard deviation of μ, A and L to be negligible:

$$s_{k_a} = \sqrt{\left(\frac{\partial k}{\partial(\Delta P)}\right)^2 s_{\Delta P}^2 + \left(\frac{\partial k}{\partial Q}\right)^2 s_Q^2} \tag{B.3}$$

where s_{k_a} is the standard deviation of the air permeability, $s_{\Delta P}$ represents the standard deviation of the pressure difference and s_Q represents the standard deviation of the flow rate. Therefore:

$$s_{k_a} = \sqrt{\left(\frac{2000 * Q * P_2 * \mu * L}{A} * \frac{-1}{(P_1^2 - P_2^2)^2} * 2P_1\right)^2 * s_{\Delta P}^2 + \left(\frac{2000 * P_2 * \mu * L}{A * (P_1^2 - P_2^2)}\right)^2 * s_Q^2} \tag{B.4}$$

equation (B.4) was used to calculate the accuracy of air permeability measurements taking $s_{\Delta P}$ and s_Q from Table B.1 for the appropriate measurement ranges.

Now, for the liquid permeability measurement using the experimental apparatus shown in Figure 3.6, the calculation of the accuracy of the measured value starts with Equation (**2.10)**, repeated here for completeness:

$$k = \frac{Q\mu L}{A(P_1 - P_2)} \tag{B.5}$$

The flow rate Q is measured by the high pressure pump, $P_1 - P_2 = \Delta P$ is measured by a differential pressure transducer and μ was determined prior to the core-flooding using a high pressure viscosimenter. The accuracy of the equipment is shown in Table B.2.

Substituting Equation (B.**1)** to Equation (B.**5)**, after considering the standard deviation of A and L to be negligible:

$$s_k = \sqrt{\left(\frac{\partial k}{\partial(\Delta P)}\right)^2 s_{\Delta P}^2 + \left(\frac{\partial k}{\partial Q}\right)^2 s_Q^2 + \left(\frac{\partial k}{\partial \mu}\right)^2 s_\mu^2} \quad \text{(B.6)}$$

where s_k is the standard deviation of the air permeability, $s_{\Delta P}$ represents the standard deviation of the pressure difference, s_Q is the standard deviation of the flow rate and s_μ is the standard deviation for the viscosity measurement. Therefore:

$$s_k = \sqrt{\left(\frac{Q\mu L}{A} * \frac{-1}{(P_1 - P_2)^2}\right)^2 s_{\Delta P}^2 + \left(\frac{\mu L}{A(P_1 - P_2)}\right)^2 s_Q^2 + \left(\frac{QL}{A(P_1 - P_2)}\right)^2 s_\mu^2} \quad \text{(B.7)}$$

Eq. B.7 was used to calculate the accuracy of the liquid permeability and $s_{\Delta P}$, s_Q and s_μ were obtained from Table B.2.

Table B.2. Measurement accuracy of the equipment used to measure liquid permeability

Parameter	**Equipment**	**Measurement Accuracy**
Q	High Pressure Pump	0.018 cc/min
$P_1 - P_2 = \Delta P$	Differential Pressure Transducer	2.25 psi
μ	High Pressure Viscosimeter	0.5 cP